MEASUREMENTS OF THE LEAKAGE AND ROTORDYNAMIC PERFORMANCE OF INTERLOCKING LABYRINTH SEALS

A Thesis

by

KEITH WILLIAM GARY

Submitted to the Office of Graduate and Professional Studies of
Texas A&M University
in partial fulfillment of the requirements for the degree of

MASTER OF SCIENCE

Chair of Committee,	Dara W. Childs
Committee Members,	Adolfo Delgado
	Paul Cizmas
Head of Department,	Andreas Polycarpou

December 2017

Major Subject: Mechanical Engineering

ABSTRACT

Annular-labyrinth seals restrict leakage in turbomachinery but may provide unwanted destabilizing forces. This work provides measurements of an interlocking-labyrinth gas seal to further the understanding of leakage characteristics and destabilizing forces. A method using magnetic bearings and differential-pressure transducers is used to measure dynamic forces in the labyrinth seal. Magnetic bearings excite the rotor creating a dynamic pressure wave that is measured and integrated to find the reaction forces. The interlocking seal has 3 teeth on the stator and 2 teeth on the rotor creating 4 cavities. All teeth have a 5 mm height, and the rotor has a 75 mm radius that creates a radial clearance of 0.2 mm with respect to the stator. All tests are conducted at ~ 167 Hz (10 krpm) rotor speed with and without swirl brakes for a range of precession frequencies from 10 – 50 Hz forward and backward. Inlet pressure is varied between 2.75 ~ 4.83 bars, and pressure ratios vary between 0.5 ~ 0.8. Static results are presented for leakage, inlet preswirl, and pressure. Dynamic results are presented for radial and circumferential gas reaction forces on the rotor as well as rotordynamic coefficients. Dynamic results show behavior that is unique to each cavity and are presented for the entire seal as well as for each cavity individually. Cross-coupled stiffness of the entire seal increases with increasing precession frequency, yet all other rotordynamic coefficients are frequency independent and show improved stability via increased effective damping with the use of swirl brakes when considering the entire seal. Negative direct damping values are seen in all but the third cavity. These measurements are useful to industry in validating Computational Fluid Dynamics (CFD) codes for interlocking seals.

DEDICATION

To my mother, Christine Huninghake, for enduring everything she has. She is the most selfless person I have ever known.

ACKNOWLEDGEMENTS

I would like to express my sincere gratitude to Dr. Dara Childs for giving me the research opportunity in the Turbomachinery Laboratory. The education I gained while working under Dr. Childs is immeasurable. The patience and dedication he provided to me during this work allowed for me to learn and grow as an engineer and as a person.

I owe much credit of this thesis to my fiancée, Jennifer Johnson, for her incredibly generous support throughout my time as a research assistant. My performance would not have been the same without her.

I would like to show great appreciation to Dr. Adolfo Delgado for serving on my graduate committee as well as for his valuable input on the results of this work. I would also like to thank Dr. Paul Cizmas for serving on my graduate committee.

The work of this thesis would not have been possible without Andrew Crandall. On many occasions, he altruistically helped troubleshoot the test rig and analyze data. It is because of his recommendations that useful data was obtained.

I was very fortunate to have worked with Mauricio Ramirez. He is an exceptionally smart and nice man. He gave me the tools necessary to succeed and he provided continuous support until the completion of this work.

Many thanks to Clay Norrbin for his generous help. His rotordynamic expertise proved useful on many occasions while assessing complications associated with the test rig and data.

To all of the remarkably smart and kind students working in the Turbomachinery Laboratory who helped during my time as a research assistant: thank you.

Finally, to my father, William Gary, who passed away during this work. He was an incredibly loving individual that I learned many lessons from.

CONTRIBUTORS AND FUNDING SOURCES

Contributors

This work was supervised by a thesis committee consisting of Professors Dara Childs and Adolfo Delgado of the Department of Mechanical Engineering and Professor Paul Cizmas of the Department of Aerospace Engineering.

All work for the thesis was completed by the student, under the advisement of Professor Dara Childs of the Department of Mechanical Engineering.

Funding Sources

All work was completed using independent funds provided by the Texas A&M Turbomachinery Laboratory.

NOMENCLATURE

c	Cross-coupled damping [FT/L]
C	Direct damping [FT/L]
e_0	Precession eccentricity [L]
F	Force [F]
k	Cross-coupled stiffness [F/L]
K	Direct stiffness [F/L]
P	Peak pressure in film of air, introduced in Figure 8 [F/L^2]
R	Rotor radius [L]
V_θ, V_r	Circumferential and radial components of gas velocity [L/T]
β	Phase reference between position and pressure, introduced in Figure 8 [-]
ρ	Gas density [M/L^3]
ω	Rotor speed [1/T]
Ω	Precession frequency [1/T]
C_{eff}	Effective Damping, defined in Eq. (4) [FT/L]
L_C	Length of cavity between rotor and stator labyrinth teeth, illustrated in Figure 15 [L]
P_s	Static pressure, introduced in Eq. (22) [F/L^2]
P_t	Total pressure, introduced in Eq. (22) [F/L^2]

Subscripts

r	Radial direction
θ	Circumferential direction
0	Denotes a location immediately upstream of the test seal

Superscripts

+	Forward precession
-	Backward precession

Acronyms

PR	Pressure Ratio
PSR	Pre Swirl Ratio
TOR	Tooth-On-Rotor
TOS	Tooth-On-Stator

TABLE OF CONTENTS

LIST OF FIGURES

Page

LIST OF TABLES

1. INTRODUCTION

Efficiency of turbomachines is affected by leakage of the working fluid into pathways that do not produce useful energy. Leakage is inevitable due to clearances between rotating and stationary parts. Annular-labyrinth seals aim to minimize leakage with tight clearances and a difficult path for the fluid to escape. Two common seal configurations are see-through and interlocking. Figures 1(A) and (B) show, respectively, a tooth-on-rotor (TOR) and tooth-on-stator (TOS) see-though configuration, while Fig. 1(C) shows an interlocking configuration.

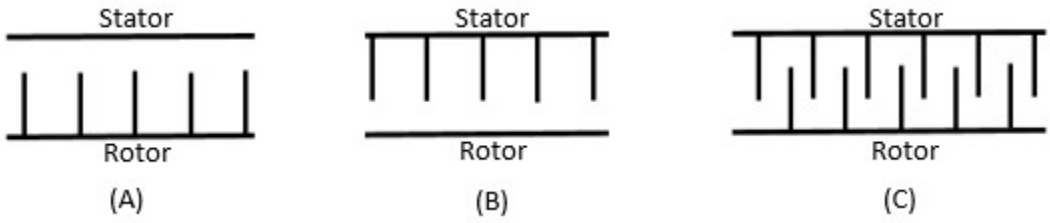

Figure 1. Cross section schematic of tooth-on-rotor (A), tooth-on-stator (B), and interlocking (C) labyrinth seal configurations from Ramirez [1].

Figure 2 illustrates the use of TOS see-through and interlocking seals on the final two stages of a straight through compressor. The intended fluid flow path starts at the large U-shaped entrance at the top left of the figure and exits out the last impeller. The rotor and impeller rotate while the remaining parts of the figure are stationary. The shaft and eye labyrinths are TOS see-through seals that act to prevent leakage between the rotor and stator and the impeller and stator, respectively. Due to the pressure differential, the fluid leaks back into previous stages depicted by flow arrows in the figure. The balance piston labyrinth is an interlocking labyrinth that acts to seal the largest pressure differential in the compressor.

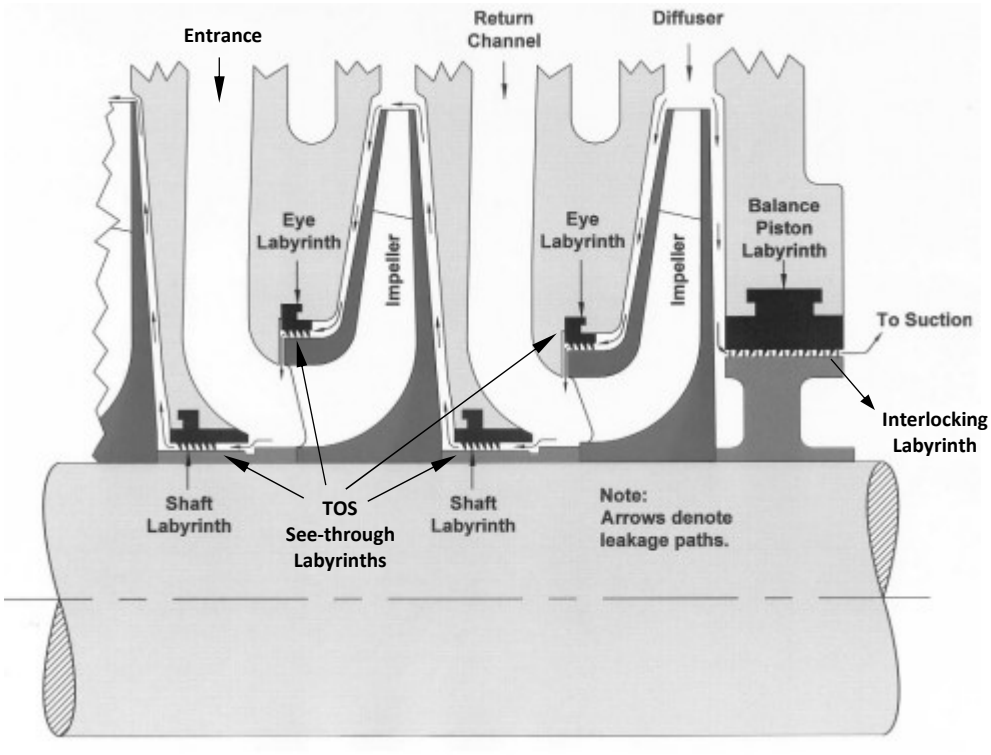

Figure 2. Annular gas seal locations in the final stages of a straight-through centrifugal compressor from Whalen et al. [2].

This thesis focuses on an interlocking labyrinth similar to the balance piston seal of Fig. 2. The radial clearance is the minimum distance between the rotor and stator or the impeller and stator seen in Fig. 1(C). The clearance-to-radius ratio is the radial clearance divided by the rotor radius and is 0.0027 for the interlocking seal of this thesis.

Understanding the rotordynamic characteristics of gas annular seals is important to model and design turbomachinery. Numerical predictions via computer codes [3] as well as measured results [4] are available for see-through TOS and TOR seals, but such predictions and data are limited for interlocking seals. Reliable data from measured results will help validate current predictions from CFD codes.

Dynamic reaction forces of a labyrinth seal cavity are modeled using spring and dampers in parallel as seen in Fig. 3. The x and y reaction forces in the figure are defined

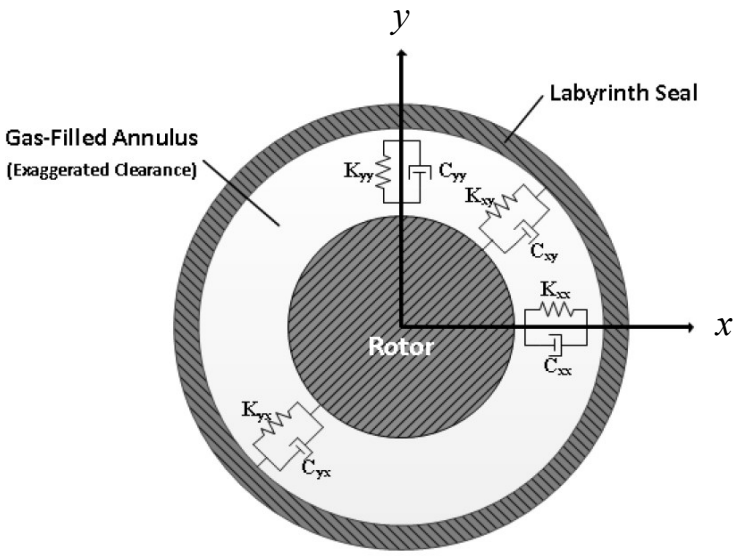

Figure 3. Dynamic model of a gas labyrinth seal with a centered rotor from Arthur [5].

by

$$-\begin{Bmatrix} F_x \\ F_y \end{Bmatrix} = \begin{bmatrix} K_{xx} & K_{xy} \\ K_{yx} & K_{yy} \end{bmatrix} \begin{Bmatrix} x \\ y \end{Bmatrix} + \begin{bmatrix} C_{xx} & C_{xy} \\ C_{yx} & C_{yy} \end{bmatrix} \begin{Bmatrix} \dot{x} \\ \dot{y} \end{Bmatrix} \tag{1}$$

F_x and F_y represent the seal forces. Terms x and y represent relative rotor-to-stator displacement, while $\dot{x}$ and $\dot{y}$ represent relative rotor velocity in the x and y directions. K_{xx}, K_{yy}, C_{xx}, and C_{yy} are the direct stiffness and damping terms, respectively, and K_{xy}, K_{yx}, C_{xy}, and C_{yx} are the cross-coupled stiffness and damping terms, respectively. Direct terms produce reaction forces in the direction of rotor displacement, and the cross-coupled terms produce reaction forces that are orthogonal to rotor displacement. Cross-coupled terms result from circumferential fluid rotation.

Equation (1) is simplified with the assumption of small rotor motion about a centered position, and using $K_{xx} = K_{yy} = K$, $C_{xx} = C_{yy} = C$, $K_{xy} = -K_{yx} = k$, and $C_{xy} = -C_{yx} = c$ gives

$$-\begin{Bmatrix} F_x \\ F_y \end{Bmatrix} = \begin{bmatrix} K & k \\ -k & K \end{bmatrix} \begin{Bmatrix} x \\ y \end{Bmatrix} + \begin{bmatrix} C & c \\ -c & C \end{bmatrix} \begin{Bmatrix} \dot{x} \\ \dot{y} \end{Bmatrix} \quad (2)$$

Figure 4 shows the rotating radial F_r and circumferential F_θ seal force components and the stationary F_x and F_y force components for a rotor with a precession rate Ω in the same direction as rotor spin ω and a precession eccentricity e_0. This condition is referred to as forward precession.

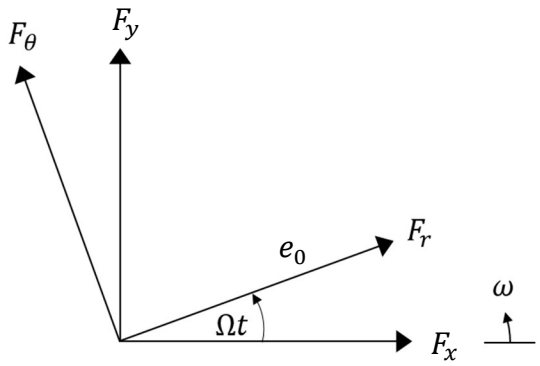

Figure 4. Direct and cross forces relative to *x* and *y* forces for forward precession.

Figure 5 shows the reaction force components in the radial and circumferential directions that account for the direct and cross-coupled reaction forces. For forward precession, a positive *K* and *c* act to center the rotor. A positive *k* acts in the direction of precession and is destabilizing while a positive *C* acts in opposition to rotor precession and is stabilizing.

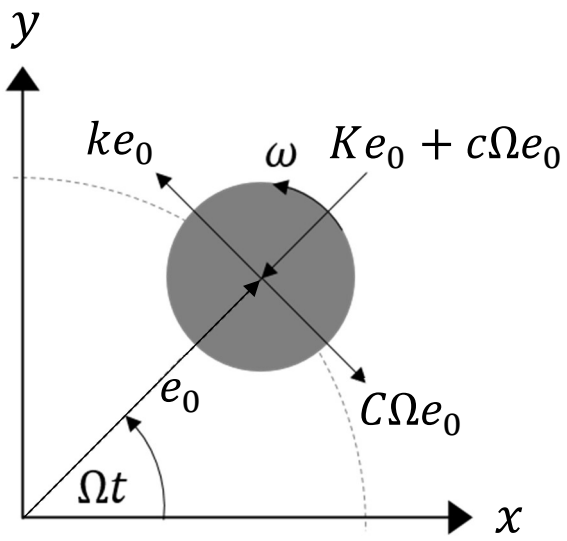

Figure 5. Force components for forward precession.

For backward precession, ω remains counterclockwise and Eq. (2) is unchanged; however, Ω reverses direction and the rotating radial and circumferential components relative to the *x* and *y* forces are seen in Fig. 6. The resulting radial and circumferential force components

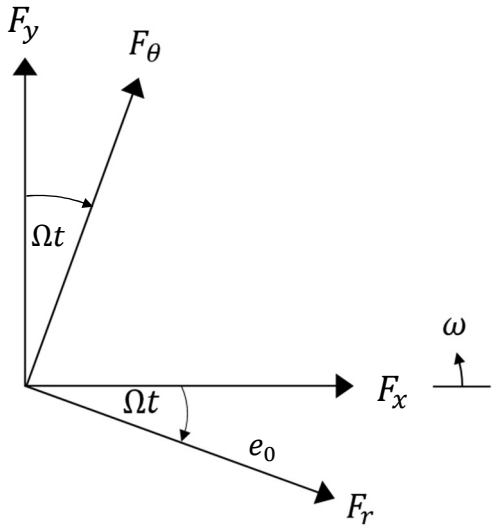

Figure 6. Direct and cross forces relative to *x* and *y* forces for backward precession.

are seen in Fig.7. The direct Ke_0 and cross-coupled stiffness ke_0 terms do not depend on rotor-precession direction. Figure 7 shows the terms $C\Omega e_0$ and $c\Omega e_0$ reversing directions as Ω changes sign from positive to negative.

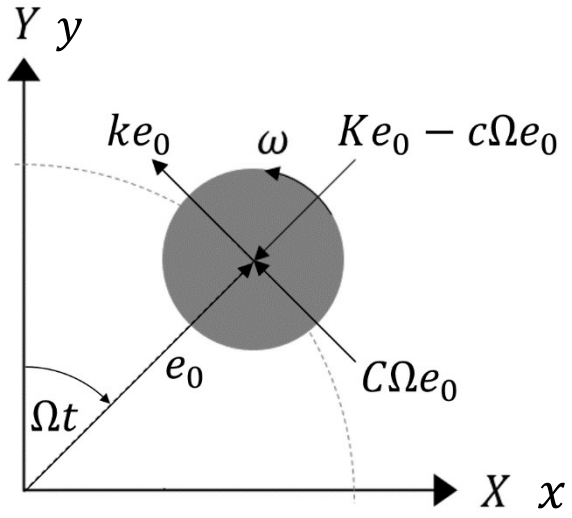

Figure 7. Force components for backward precession.

The destabilizing force ke_0 in the direction of rotor rotation is caused by fluid rotation in the seal cavities. The fluid rotation entering the seal arises from rotor spin and/or turbomachinery components attached to the rotor such as impellers and turbines and is termed preswirl. The preswirl velocity $V_{\theta 0}$, rotor radius R, and ω are used to define the preswirl ratio as

$$PSR = \frac{V_{\theta 0}}{R\omega} \tag{3}$$

A positive preswirl ratio is defined to be in the direction of ω, and it can be reduced by adding swirl brakes upstream of the entrance to the seal. Swirl brakes are devices used to slow or reverse *PSR* using circumferential obstructions in the path of $V_{\theta 0}$. Absent rotor precession, direct damping is not generated, and $F_\theta / e_0 = k$, where k is purely destabilizing. In the case of forward rotor precession, C acts against k to stabilize the rotor, and a useful relation identified as effective damping is used to describe stability as

$$C_{eff} = C - \frac{k}{\Omega} \tag{4}$$

If rotor precession and thus damping terms are absent, only K and k can be measured. In 1980, Benckert and Wachter [6] first accomplished this for see-through and interlocking seals by displacing their rotor with respect to their stator, measuring the static pressure distribution, and calculating the static reaction force. Their findings showed the destabilizing force arising from k was purely due to fluid rotation in the seal. Using swirl brakes to control *PSR*, their results also showed destabilizing k values were reduced by the swirl brakes.

The first dynamic tests of gas interlocking seals to obtain measured damping results was performed by Childs and Elrod [7] in 1988. They conducted tests for varying pressure ratios, excitation frequencies, and rotor speeds. They present normalized direct stiffness, cross-coupled stiffness, and direct damping rotordynamic coefficients versus absolute pressure ratio for three excitation frequencies. Their results showed coefficients that varied for each excitation frequency, with repeatable results, that the authors state as "disturbing to the extent that they conflict with the generally-held view that rotordynamic coefficients provide a frequency-independent relation between reaction-forces and motion."

By using an external shaker, in 1999 Baumann [8] tested a high-pressure radial compressor that used interlocking seals. He provides damping using logarithmic decrement and natural frequencies of his entire machine. His tests are conducted with a maximum discharge pressure reaching 400 bar and show a significant decrease in the rotor natural frequency with increasing discharge pressure for cases using swirl brakes. These results indicate a large negative direct stiffness coefficient that is not characteristic of measured results for see-through seals. His damping results show positive values decreasing with increasing discharge pressure. Baumann defines the threshold of stability where damping becomes negative and it occurs near a maximum discharge pressure of 250 bar for cases with swirl brakes, and 400 bar for cases without swirl brakes.

2. THEORY

An extension of test methods used by Millsaps [9], Wagner et al. [10], and Ramirez [1] on see-through labyrinth seals is used on the interlocking labyrinths for this work. In 1994 Millsaps used a shaft-in-shaft test rig to test a single-cavity TOS seal. Differential pressure sensors were used to measure the precessing pressure field in the labyrinth cavity and identify rotordynamic coefficients. In 2009 Wagner et al. used magnetic bearings to support and excite their rotor. They also used dynamic pressure measurements to identify rotordynamic coefficients. In 2017 Ramirez followed Wagner et al.'s procedure and used magnetic bearings and differential pressure sensors to validate the test rig that is used for the work of this thesis. Figure 8 shows a schematic of a forward precessing rotor. Peak pressure P is assumed to build behind the rotor's rotating position vector e_0 by the angle β due to fluid rotation and is defined as

$$\beta = \angle e_0 - \angle P \tag{5}$$

where $\angle e_0$ is the phase angle of rotor position and $\angle P$ is the phase angle of the peak dynamic air pressure. The + and – symbols in Fig. 8 identify positive and negative precessing pressure waves.

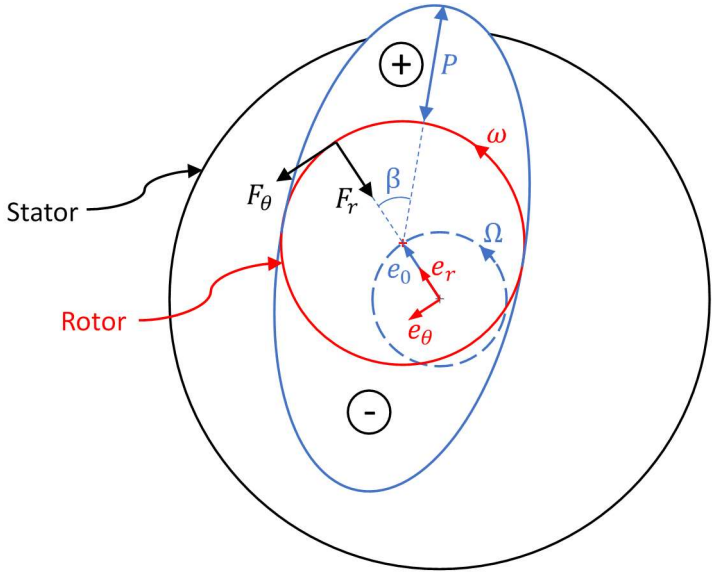

Figure 8. Schematic of seal reaction forces due to rotor displacement for forward precession.

The figure shows the radial (F_r) and circumferential (F_θ) reaction force components imparted on the rotor by the pressure distribution for the assumed angle β. A positive radial force is defined as centering, and radial and circumferential reaction forces in terms of rotordynamic coefficients for forward precession are defined by

$$F_r^+ = e_0(K + c\Omega) \tag{6}$$

$$F_\theta^+ = e_0(k - C\Omega) \tag{7}$$

where the superscript (+) indicates forward precession.

Equations for forward precession that decompose the dynamic pressure into radial and circumferential components to relate with rotordynamic coefficients are defined by

$$F_r^+ = L_c R\pi P \cos\beta = e_0(K + c\Omega) \tag{8}$$

$$F_\theta^+ = L_c R\pi P \sin\beta = e_0(k - C\Omega) \tag{9}$$

Similarly, for backward precession Fig. 9 shows a schematic locating the pressure wave relative to rotor position and shows reaction forces. Radial and circumferential reaction forces in terms of rotordynamic coefficients for backward precession are defined by

$$F_r^- = e_0(K - c\Omega) \tag{10}$$

$$F_\theta^- = e_0(k + C\Omega) \tag{11}$$

where the superscript (-) indicates backward precession.

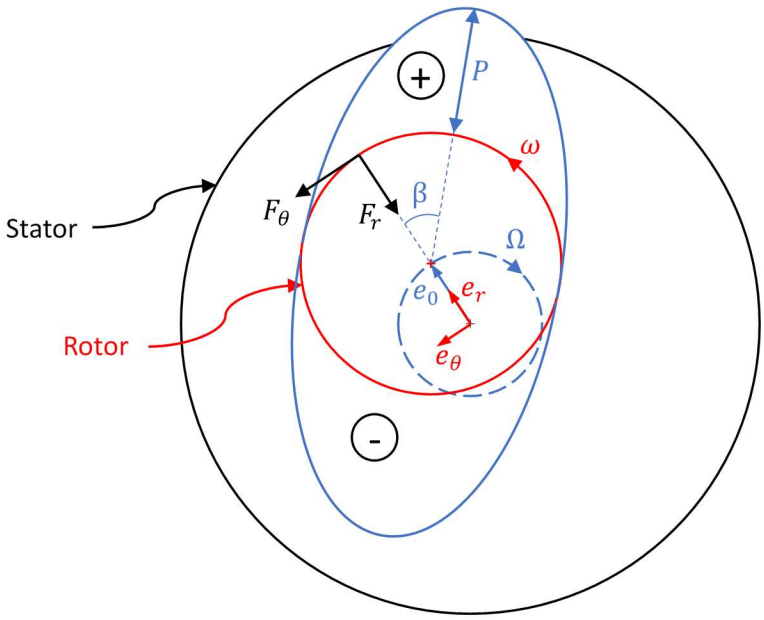

Figure 9. Schematic of seal reaction forces due to rotor displacement for backward precession.

Through Eq. (5), the change in direction of Ω causes β to become negative, and the equations decomposing the dynamic pressure into radial and circumferential forces are defined by

$$F_r^- = L_c R\pi P \cos\beta = e_0(K - c\Omega) \tag{12}$$

$$F_\theta^- = L_c R\pi P \sin\beta = e_0(k + C\Omega) \tag{13}$$

Note that the Ω values in Eqs. (12-13) are positive. Figures 10(A) and (B), respectively, show the predicted normalized radial and circumferential reaction forces combining forward (Ω) and backward ($-\Omega$) precession. K is represented by the vertical axis intercept of Fig. 10(A), and k is represented by the vertical axis intercept of Fig. 10(B). For both figures, forward and backward precession results are expected to meet at the vertical axis without a discontinuity.

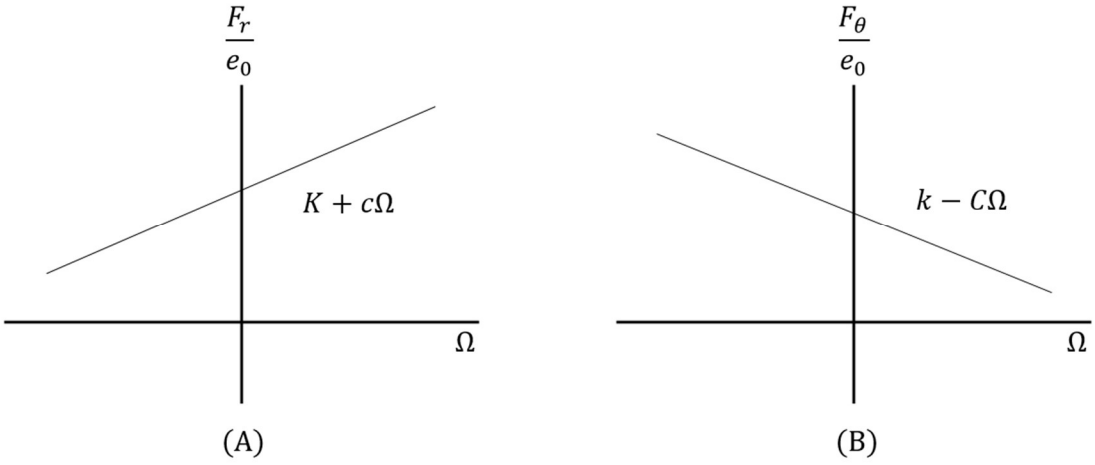

Figure 10. Predicted normalized radial (A) and circumferential (B) forces.

Combining forward and backward precession equations at the same frequency values allows for each rotordynamic coefficient to be solved for explicitly. Combining radial reaction forces gives

$$K = \frac{-(F_r^+ + F_r^-)}{2e_0} \tag{14}$$

$$c = \frac{F_r^- - F_r^+}{2e_0\Omega} \ , \Omega > 0 \tag{15}$$

Similarly, combining circumferential reaction forces gives

$$k = \frac{F_\theta^+ + F_\theta^-}{2e_0} \tag{16}$$

$$C = \frac{F_\theta^- - F_\theta^+}{2e_0\Omega} \ , \Omega > 0 \tag{17}$$

The interlocking seal of this thesis has four cavities each with two differential pressure sensors located 180 degrees apart. Peak pressure amplitudes P of the two sensors inside a single cavity are averaged, and the phase angle β that the peak pressure P lags the rotor

position e_0 seen by each sensor is also averaged to find reaction force components for each cavity. The cavity forces are summed to generate the total seal reaction forces as

$$\sum_{n=1}^{4} F_r^+ = \sum_{n=1}^{4} L_c \, R\pi P_n \cos\beta_n = e_0(K + c\Omega) \tag{18}$$

$$\sum_{n=1}^{4} F_\theta^+ = \sum_{n=1}^{4} L_c \, R\pi P_n \sin\beta_n = e_0(k - C\Omega) \tag{19}$$

$$\sum_{n=1}^{4} F_r^- = \sum_{n=1}^{4} L_c \, R\pi P_n \cos\beta_n = e_0(K - c\Omega) \tag{20}$$

$$\sum_{n=1}^{4} F_\theta^- = \sum_{n=1}^{4} L_c \, R\pi P_n \sin\beta_n = e_0(k + c\Omega) \tag{21}$$

3. TEST APPARATUS

3.1 Test Rig

The interlocking labyrinth seals are tested in a rig located at Texas A&M University's Turbomachinery Laboratory. The rig was used by Ramirez [1] in 2017 to test see-through labyrinth seals. Figure 11 shows the test rig. The magnetic bearings on each end of the figure act to radially support and excite the rotor into circular precession orbits. Air enters the test rig through hoses on top and bottom of the seal housing located at the center of the figure. The seals are located within the housing in a back-to-back configuration to minimize thrust from the incoming air. To modify the rig for interlocking seal tests, a TOR shaft was installed, and the existing stator seals were replaced. The remaining parts of Figure 11 remain unchanged.

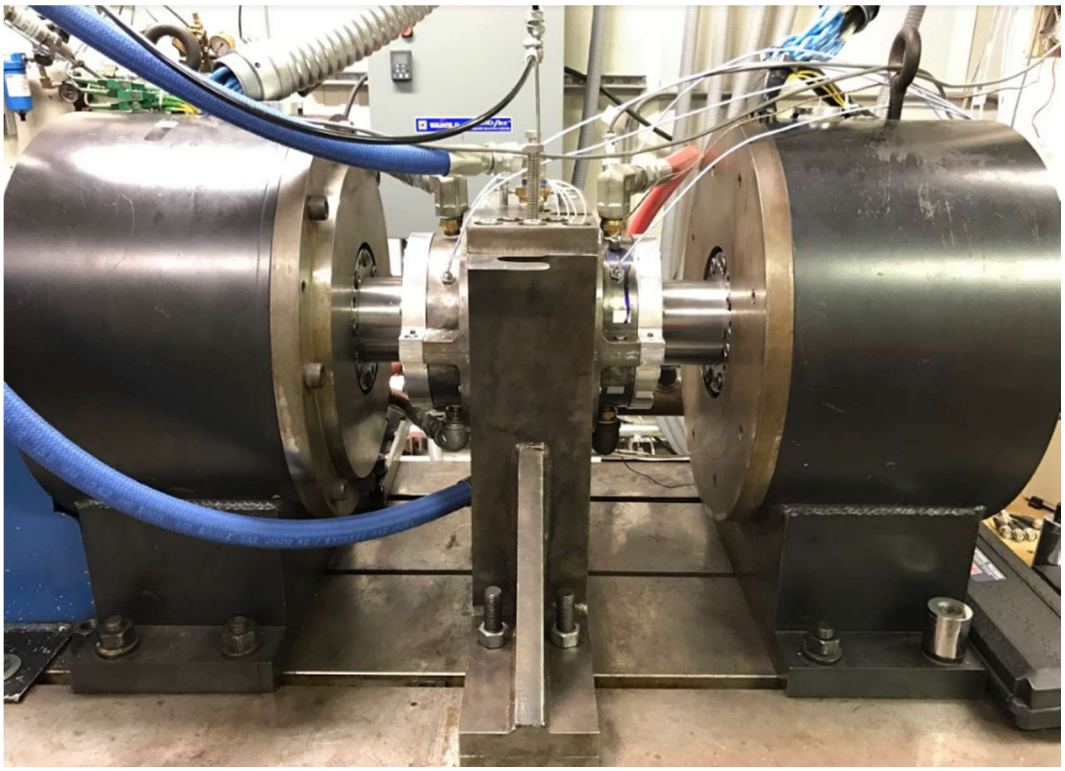

Figure 11. Test rig used by Mauricio Ramirez for master's thesis work in 2017.

Figure 12 shows a cross section view of the test rig assembly. The rig is symmetric about the axis of rotation. Air enters the test rig through ports located at (1) and is forced through a swirl vane (2) and swirl brakes (3) before entering identical back-to-back interlocking seals. The seals are comprised of tooth-on-stator seals (4) and a tooth-on-rotor seal (5) shrunk fit onto the rotor (6). Air escapes from exit ports (7) and exit labyrinth seals (8). The test rig pressure ratio (PR) is controlled downstream of the exit ports using a back-pressure valve located in piping that exits at (7). All instrumentation and data acquisition are identical to Ramirez's [1] work with the exception of six additional differential pressure sensors due to three additional test cavities on this work's seal.

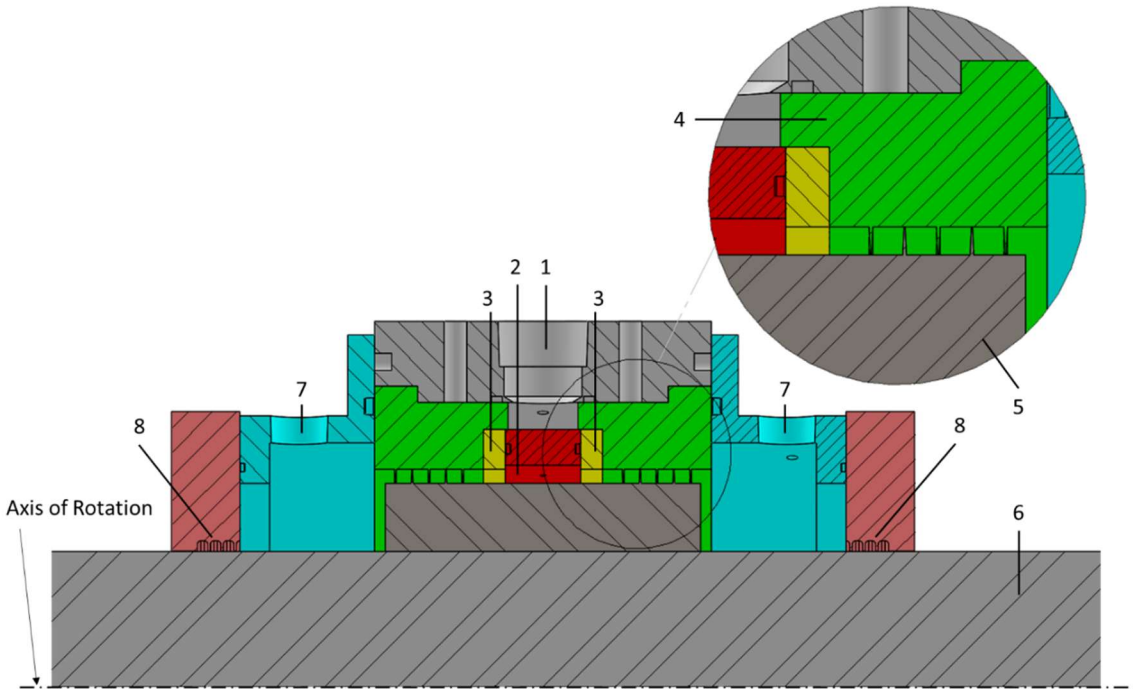

Figure 12. Cross section of test rig assembly.

Due to interlocking rotor and stator seals, a split housing is necessary for assembly and disassembly of the rig. Figure 13 shows a computer animated model of the fully assembled rig (A) and an exploded view (B) showing the split faces that provide air a potential exit. Liquid sealant is used on all split faces of the rig to prevent unwanted leakage.

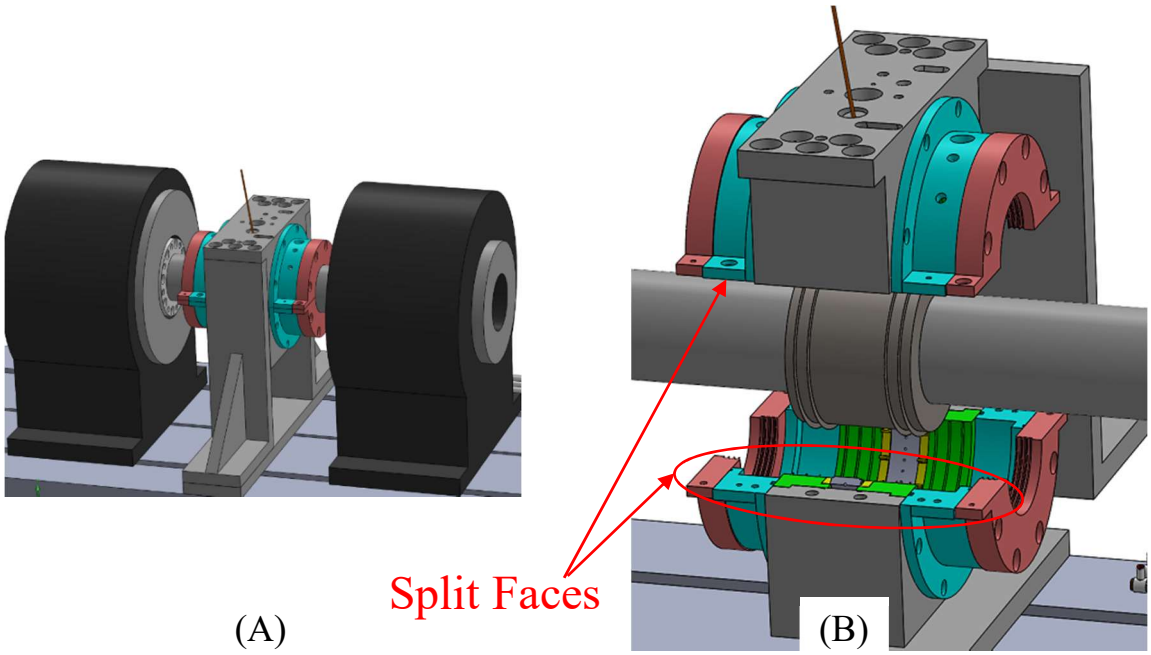

Figure 13. Computer animated model of the fully assembled test rig (A), and an exploded view of the test rig showing the split faces (B).

The test rig's maximum inlet pressure is 21 bars, yet a maximum inlet pressure of 4.83 bars was used for this thesis due to centering and alignment issues caused by higher inlet pressures. At inlet pressures higher than 4.83 bars, the rotor is displaced off-center with respect to the stator, and the dynamic pressure wave no longer travels at a uniform rate circumferentially. The model used to obtain dynamic reaction forces for this work relies on dynamic pressure phase which is only reliable if the dynamic pressure wave travels at a uniform rate circumferentially.

3.2 Alignment

Prior to alignment, the rotor is installed inside the magnetic bearings on rolling element "catcher" bearings that are used to support the rotor when an electromagnetic force is not levitating the rotor. Once levitated, the rotor is pushed laterally by an output voltage via LabVIEW software. Position sensors located inside the magnetic bearings are used to monitor a proportional plot of magnetic bearing current versus position of the rotor as it is pushed toward the stator. When the rotor has reached the stator, an inflection point is seen in which the position no longer increases and current reverses direction. The

voltage and position at the inflection point are recorded and the rotor is pushed in the opposite direction until an inflection point is seen on the opposite side. A centering voltage found from the inflection points is then input to the magnetic bearings. This process is repeated on the *x* and *y* axes until the centering voltages cease fluctuating.

To align the stator onto the rotor, a radially oversized imitation rotor known as a mandrel is used. The axially length of the mandrel is just long enough to contain the test seal and exit labyrinths of Figure 12. The test seal, stator housing, and exit labyrinths are tightened around the mandrel in a vertical position while unrestricted movement of the mandrel is regularly checked to confirm alignment. The horizontally split parts are taken apart while retaining axial assembly. The horizontally split parts are then assembled around the rotor while using feeler gages to obtain an initial alignment. After the stator has been fully assembled around the rotor, the rotor is again pushed laterally using the magnetic bearings to measure the exit labyrinth clearance.

Care must be taken to ensure the rotor makes contact with the exit labyrinths, and not the catcher bearings, in each direction that the rotor is pushed. If this outcome is not confirmed, alignment is compromised, and the stator must be moved into a position where contact with the exit labyrinth seals occurs. When confident the exit labyrinths are concentric with the catcher bearings, the rotor is centered within the exit labyrinths and thus the test seal.

3.3 Test Seal

Figures 14(A) and (B) show, respectively, the interlocking stator and rotor seal drawings. There are 3 teeth on the stator and 2 teeth on the rotor, creating four cavities. The axially distance between teeth is 12.5 mm, the radial clearance C_r is 0.2 mm, the cavity length L_c is 6 mm, and the tooth height is 5 mm.

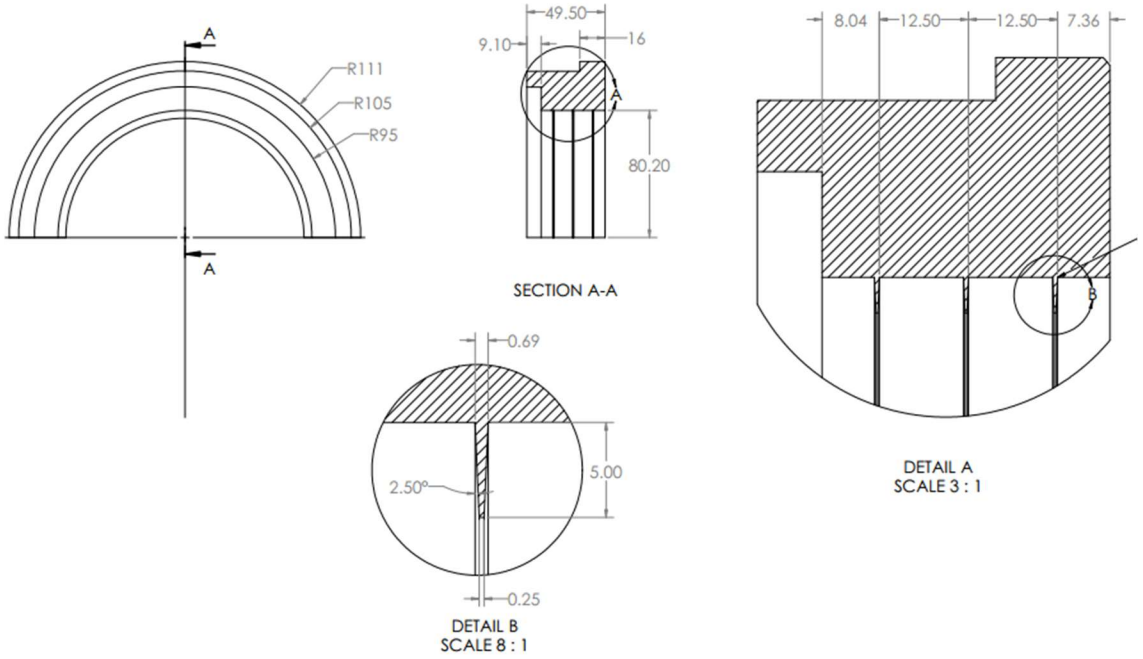

(A)

NOTE: All dimensions in mm

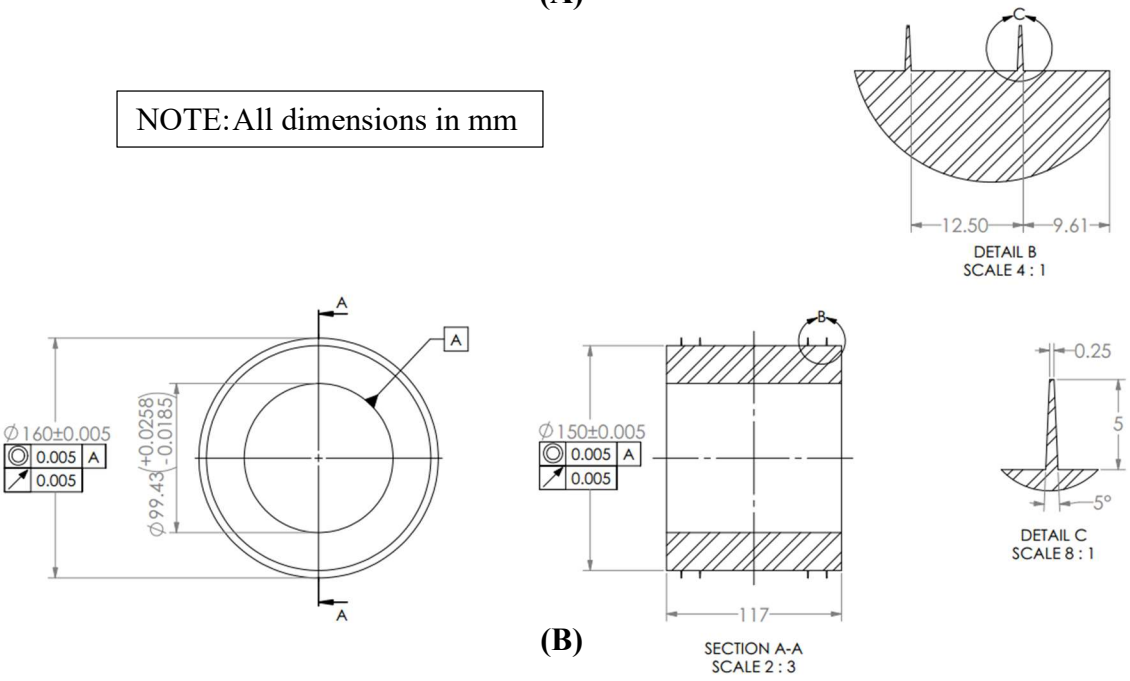

(B)

Figure 14. Seal-on-stator (A) and seal-on-rotor (B) drawings.

Figure 15 shows the axial location of pressure ports to be used for the differential pressure sensors. Cavities are numbered 1-4 beginning nearest the entrance of the seal.

Cavities 1 – 4 each have two sensors located 180 degrees apart to assess phase and amplitude fidelity from measured results.

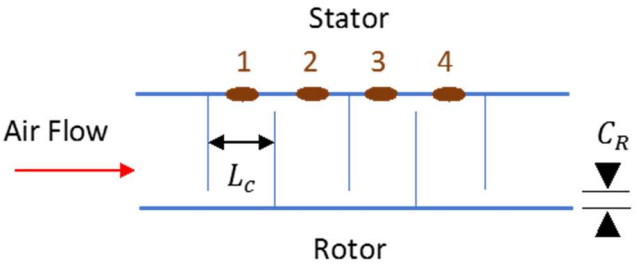

Figure 15. Pressure tap axial locations.

Figure 16 shows the circumferential location of differential pressure sensors with respect to the positive *x* and *y* axes. Sensors 1 and 2 are located in cavity 1, sensors 3 and 4 in cavity 2, sensors 5 and 6 in cavity 3, and sensors 7 and 8 in cavity 4.

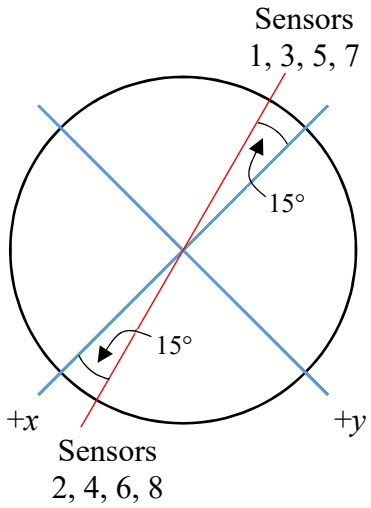

Figure 16. Circumferential location of differential pressure sensors.

3.4 Swirl Brakes

Figure 17 shows a drawing of the swirl brakes used. There are 20 equally spaced teeth around the full circumference of the swirl brakes (10 per half). The radial clearance

of the swirl brakes and the rotor is 0.48 mm. For tests conducted without swirl brakes, a spacer that is identical to the swirl brakes is used with the exception of the teeth.

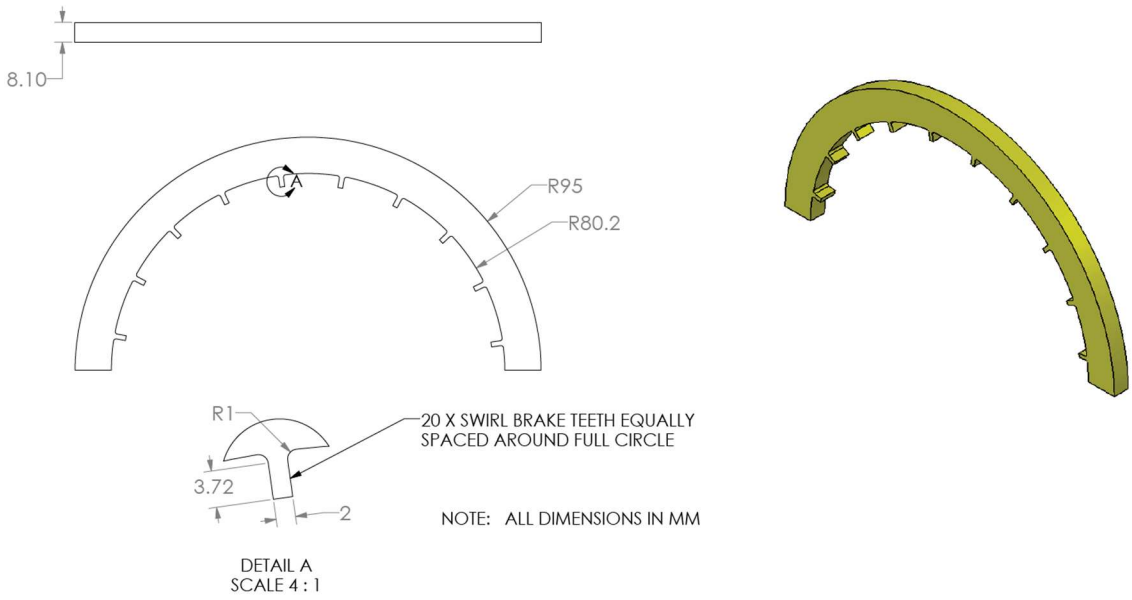

Figure 17. Swirl brake drawing.

Proximity sensors that are used to measure the rotor's dynamic position during testing are seen in Figure 18. These are the proximity probes used in the process of measuring the angle β that peak dynamic pressure P lags the rotor's rotating vector e_0. They are circumferentially located on the x and y axes seen in Fig. 16, and they are axially located 30 mm from the exit of each stator seal. The stator seals seen in Fig. 18 were not used for this work but they have identical dimensions as the stator seals of this thesis with exception of the teeth dimensions and number of teeth.

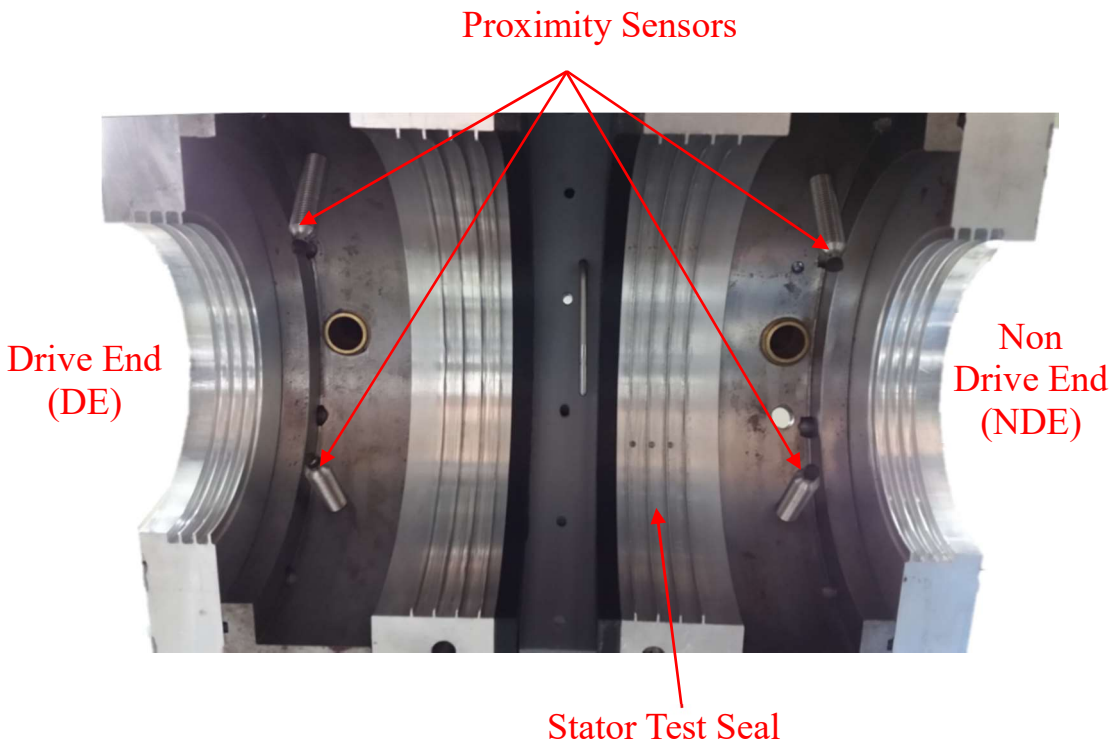

Figure 18. Bottom view of stator housing and test seal showing proximity probe locations.

3.5 Test Procedure

The test matrix used for the interlocking seal is seen in Table 1. Tests are conducted with a range of target inlet pressures from 2.75 – 4.83 bar (40 – 70 psia), target pressure ratios from 0.5 – 0.8 for each inlet pressure, and a rotor speed of ~ 167 Hz. The rotor is excited through a range of precession frequencies from 10 – 60 Hz forward and backward at an amplitude that is ~ 13% of C_r. A modal impact test was conducted to determine the rotor's first bending natural frequency and it occurs at approximately 440 Hz which is well above the highest precession frequency. A target PSR of 0.5 is used with and without swirl brakes. Proximity sensors are used to measure the rotor's dynamic position, and the dynamic pressures are measured using differential pressure sensors. Information regarding test rig instrumentation is found in Table 2.

Table 1. Interlocking labyrinth seal test matrix.

Configuration	Inlet Pressure (bar (psia))	Pressure Ratio*	Preswirl Ratio**	Rotor Speed (krpm)	Precession Frequency*** (Hz)
Without Swirl Brakes	2.75 (40)	0.5, 0.6, 0.7, 0.8	0.5	10	10, 15, 20, 25, 30, 35, 40, 45, 50
	3.79 (55)				
	4.83 (70)				
With Swirl Brakes	2.75 (40)				
	3.79 (55)				
	4.83 (70)				

*All pressure ratios are tested for each inlet pressure
**Target preswirl is not adjusted with the addition of swirl brakes
***All frequencies apply to forward and backward precession

Table 2. Instrumentation information.

Measurement	Number of Sensors	Brand	Model	Range	Error
Position	5	Bently Nevada	3300 XL NSv	2.54 mm (100 mils)	± 2.54 µm ± (0.1 mil)
Differential Pressure	8	Omega	MMDDB005BI V5P4B0T1	0.34 bar (5 psi)	± 0.0007 bar (± 0.01 psi)
Static Pressure	2	Omega	PX329-300	20.7 bar (300 psi)	± 0.25%
Volumetric Flow	1	Flow Technology	FT20NEE1-GEH-5	8.8 - 101.5 ACFM	± 0.25%
Swirl Differential Pressure	1	Emerson	3051CD4M22A 1AM5B4DFQ4	20.7 bar (300 psi)	± 0.0008 bar (± 0.012 psi)
Temperature	2	Omega	GG2036	-270 - 1372 °C	± 2.2 °C

Each pressure sensor has two ports that measure static pressure and total pressure separately with dynamic pressure as the output. This set-up is particularly advantageous in situations where the desired dynamic pressure is much lower than the static pressure. Total pressure in each cavity is piped directly to a sensor but also into a plenum that

outputs a nominal static pressure that is piped to the remaining port of the sensor. The plenum contains mineral wool insulation that damps oscillation from the total pressure and outputs static pressure.

Air entering the test rig is forced through a swirl vane which redirects flow into a circumferential motion in the direction of rotor rotation inducing a preswirl. The preswirl is measured by means of a Pitot-tube located directly after the swirl vane and before the seal entrance. The Pitot-tube is directed into the fluid flow and measures total pressure as well as static pressure. Figure 19 shows the Pitot-tube location and swirl vane hole dimensions. The holes are angled five degrees from a plane perpendicular to the outside face of the vane in the direction of rotor speed ω. The inlet swirl velocity $V_{\theta 0}$ is determined through the equation of total pressure as

$$V_{\theta 0} = \left[\frac{2(P_t - P_s)}{\rho}\right]^{\frac{1}{2}} \tag{22}$$

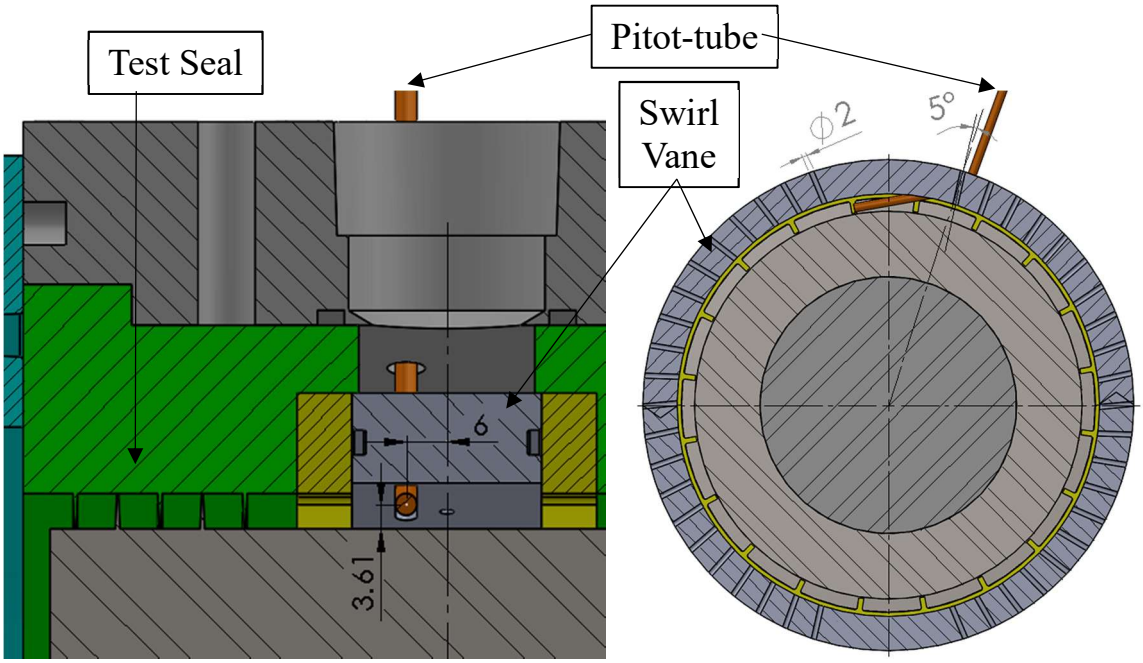

Figure 19. Pitot-tube location and swirl vane side view with hole dimensions in millimeters.

3.6 Repeatability

40,000 samples of data are collected at a sampling rate of 25,000 samples per second over 1.6 seconds for each precession frequency tested. The data are partitioned equally eight times for each precession frequency and are compared for repeatability. The standard deviations of the partitioned data are used as error bars for the results.

4. DISCUSSION OF RESULTS

The results are presented in three sections. First, static results are presented followed by dynamic forces and finally rotordynamic coefficients. Dynamic forces and rotordynamic coefficients are presented for each of the four cavities individually and then together due to the differing behavior of each cavity. Figures are shown with straight lines connecting data points so trends can be visualized.

Many issues were encountered in the process of obtaining measured results for the interlocking-labyrinth-seal. Ramirez's [1] work in 2017 on a see-through-labyrinth seal was completed to benchmark the test rig and was motivated by the issues encountered while attempting to collect interlocking seal data.

4.1 Static Results

40,000 samples of data are taken for each precession frequency tested. The average and standard deviation are calculated from dividing each frequency's data into eight equal sections of 5,000 samples. For static results, the average and standard deviation from each precession frequency are again averaged over all frequencies for a single inlet pressure and pressure ratio. The resulting averages are presented as the static results and one standard deviation from the average for each value as the error.

Table 3 shows inlet pressure, outlet pressure, and pressure ratios (PR) for all tests without swirl brakes. Inlet pressure used for PR is downstream of the swirl vane and upstream of the test seal and swirl brakes. Inlet pressure air is piped to the test rig from a compressor after being filtered and stored in an accumulator. The accumulator helps maintain a steady inlet pressure to the test rig yet small fluctuations are seen. Actual pressure ratio is controlled by a valve downstream of the test rig which allows outlet pressure to be varied to achieve the target pressure ratio. The largest discrepancy from target pressure ratio is the 0.8 case in which the back pressure valve is fully closed, and air escaping from the exit labyrinths prevents any further increase in actual pressure ratio.

Table 3. Inlet and outlet static pressure measurements without swirl brakes.

Configuration	Target PR	Inlet Pressure (bar (psia))	Outlet Pressure (bar (psia))	Actual PR
Without Swirl Brakes	0.5	2.77 ± 0.03 (40.7 ± 0.4)	1.32 ± 0.01 (19.5 ± 0.2)	0.48 ± 0.01
		3.77 ± 0.01 (55.4 ± 0.2)	1.77 ± 0.01 (26.0 ± 0.2)	0.47 ± 0.00
		4.67 ± 0.05 (68.6 ± 0.8)	2.35 ± 0.03 (34.6 ± 0.4)	0.50 ± 0.01
	0.6	2.89 ± 0.03 (42.5 ± 0.4)	1.74 ± 0.01 (25.6 ± 0.2)	0.60 ± 0.01
		3.48 ± 0.01 (51.2 ± 0.2)	2.16 ± 0.02 (31.7 ± 0.3)	0.62 ± 0.01
		4.63 ± 0.03 (68.1 ± 0.4)	2.83 ± 0.02 (41.6 ± 0.3)	0.61 ± 0.01
	0.7	2.91 ± 0.02 (42.8 ± 0.3)	1.98 ± 0.03 (29.1 ± 0.4)	0.68 ± 0.01
		3.83 ± 0.02 (56.3 ± 0.3)	2.68 ± 0.02 (39.4 ± 0.3)	0.70 ± 0.01
		5.2 ± 0.2 (76 ± 3)	3.6 ± 0.1 (53 ± 2)	0.70 ± 0.03
	0.8	2.63 ± 0.01 (38.7 ± 0.1)	2.03 ± 0.01 (29.8 ± 0.2)	0.77 ± 0.01
		3.68 ± 0.03 (54.1 ± 0.4)	2.82 ± 0.03 (41.5 ± 0.4)	0.77 ± 0.01
		4.63 ± 0.02 (68.0 ± 0.3)	3.53 ± 0.03 (51.9 ± 0.4)	0.76 ± 0.01

To install swirl brakes, the test rig is disassembled, re-assembled, and aligned before tests continue. Each assembly and alignment setup is slightly different, and results reflect this. Table 4 shows inlet pressure, outlet pressure, and pressure ratio for all tests

with swirl brakes. An actual pressure ratio of 0.8 is again the most difficult to achieve, and values are lower with swirl brakes than without for this pressure ratio. This result is more likely to arise from the assembly process than a consequence of swirl brakes. Mass flow rate results presented subsequently clearly show lower values with swirl brakes than without for a 0.8 PR probably indicating increased leakage at the split faces as a result of the assembly process for installation of swirl brakes.

Table 4. Inlet and outlet static pressure measurements with swirl brakes.

Configuration	Target PR	Inlet Pressure (bar (psia))	Outlet Pressure (bar (psia))	Actual PR
With Swirl Brakes	0.5	2.86 ± 0.01 (42.1 ± 0.1)	1.49 ± 0.003 (21.9 ± 0.05)	0.52 ± 0.00
		3.67 ± 0.02 (53.9 ± 0.3)	1.82 ± 0.01 (26.7 ± 0.1)	0.49 ± 0.00
		5.0 ± 0.1 (73 ± 2)	2.45 ± 0.05 (36.0 ± 0.7)	0.49 ± 0.01
	0.6	2.89 ± 0.01 (42.5 ± 0.2)	1.78 ± 0.01 (26.1 ± 0.1)	0.61 ± 0.00
		3.61 ± 0.02 (53.1 ± 0.3)	2.20 ± 0.01 (32.3 ± 0.1)	0.61 ± 0.00
		4.9 ± 0.1 (72 ± 2)	2.99 ± 0.07 (44 ± 1)	0.61 ± 0.02
	0.7	2.99 ± 0.01 (44.0 ± 0.2)	2.10 ± 0.01 (30.9 ± 0.1)	0.70 ± 0.00
		3.95 ± 0.07 (58 ± 1)	2.72 ± 0.05 (40.0 ± 0.7)	0.69 ± 0.02
		5.0 ± 0.1 (72 ± 2)	3.44 ± 0.08 (51 ± 1)	0.70 ± 0.02
	0.8	2.89 ± 0.01 (42.5 ± 0.1)	2.17 ± 0.01 (31.9 ± 0.1)	0.75 ± 0.00
		3.70 ± 0.02 (54.4 0.3)	2.74 ± 0.01 (40.3 ± 0.2)	0.74 ± 0.01
		4.85 ± 0.05 (71.3 ± 0.7)	3.55 ± 0.03 (52.1 ± 0.5)	0.73 ± 0.01

Table 5 shows density, mass flow rate, swirl velocity, and preswirl ratio (PSR) for all tests without swirl brakes installed. For a constant inlet pressure, absent choking, a lower pressure ratio has a higher mass flow rate than a higher pressure ratio; yet, this trend

is not observed for each instance in the table. This result is due to small fluctuations of inlet pressure. Density is strongly related to inlet pressure and is the likely cause of witnessing mass flow rate increasing, despite an increase in pressure ratio. PSR is calculated using the rotor surface speed of approximately 78.54 m/s. The actual PSR is within 15% of the target PSR of 0.5 for all cases without swirl brakes.

Table 5. Density, mass flow, and swirl measurements without swirl brakes.

Configuration	Target Inlet Pressure (bar)	Target PR	Density (kg/m^3)	Mass Flow Rate (g/s)	Swirl Velocity (m/s)	PSR
Without Swirl Brakes	2.75	0.5	3.30 ± 0.03	4.18 ± 0.04	38 ± 6	0.49 ± 0.07
		0.6	3.43 ± 0.00	4.32 ± 0.04	35 ± 4	0.44 ± 0.05
		0.7	3.45 ± 0.00	4.27 ± 0.03	34 ± 6	0.44 ± 0.08
		0.8	3.12 ± 0.01	2.49 ± 0.01	34 ± 6	0.43 ± 0.08
	3.79	0.5	4.47 ± 0.00	8.97 ± 0.03	45 ± 3	0.57 ± 0.04
		0.6	4.13 ± 0.02	6.58 ± 0.03	42 ± 3	0.54 ± 0.04
		0.7	4.55 ± 0.00	7.12 ± 0.03	39 ± 4	0.50 ± 0.06
		0.8	4.37 ± 0.03	5.73 ± 0.04	34 ± 5	0.43 ± 0.07
	4.83	0.5	5.56 ± 0.00	12.6 ± 0.1	43 ± 3	0.55 ± 0.04
		0.6	5.51 ± 0.03	12.4 ± 0.1	38 ± 4	0.48 ± 0.05
		0.7	6.2 ± 0.2	12 ± 0	37 ± 3	0.47 ± 0.04
		0.8	5.48 ± 0.03	8.69 ± 0.04	36 ± 5	0.46 ± 0.06

Table 6 shows density, mass flow rate, swirl velocity, and PSR for all tests with swirl brakes installed. Fluctuations of inlet pressure, and thus density, again break the trend of increasing mass flow rate with decreasing pressure ratio on a single occasion. Swirl velocity and PSR decrease with increasing pressure ratio but a relation with inlet

pressure is not seen. Swirl velocities and PSRs decrease an average of 37% with swirl brakes installed.

Table 6. Density, mass flow, and swirl measurements with swirl brakes.

Configuration	Target Inlet Pressure (bar)	Target PR	Density (kg/m^3)	Mass Flow Rate (g/s)	Swirl Velocity (m/s)	PSR
With Swirl Brakes	2.75	0.5	3.39 ± 0.01	4.38 ± 0.02	31 ± 3	0.40 ± 0.04
		0.6	3.41 ± 0.01	4.31 ± 0.02	28 ± 5	0.36 ± 0.06
		0.7	3.53 ± 0.02	4.08 ± 0.02	27 ± 5	0.34 ± 0.06
		0.8	3.41 ± 0.01	3.67 ± 0.01	25 ± 6	0.32 ± 0.07
	3.79	0.5	4.35 ± 0.02	7.58 ± 0.04	26 ± 3	0.33 ± 0.04
		0.6	4.26 ± 0.02	6.87 ± 0.03	22 ± 5	0.28 ± 0.06
		0.7	4.65 ± 0.09	7.4 ± 0.1	21 ± 6	0.27 ± 0.08
		0.8	4.38 ± 0.02	6.21 ± 0.03	19 ± 6	0.24 ± 0.07
	4.83	0.5	5.9 ± 0.1	14 ± 0	25 ± 6	0.31 ± 0.07
		0.6	5.8 ± 0.1	13 ± 0	22 ± 4	0.29 ± 0.05
		0.7	5.8 ± 0.1	11 ± 0	22 ± 4	0.27 ± 0.05
		0.8	5.72 ± 0.06	10.9 ± 0.1	19 ± 6	0.24 ± 0.08

Figure 20 shows preswirl ratio versus pressure ratio with and without swirl brakes. The legend entries indicate inlet pressure first, followed by whether swirl brakes were installed (w/SB) or they were not (wo/SB). The figure visually illustrates the drop in PSR with swirl brakes and the lack of correlation to inlet pressure.

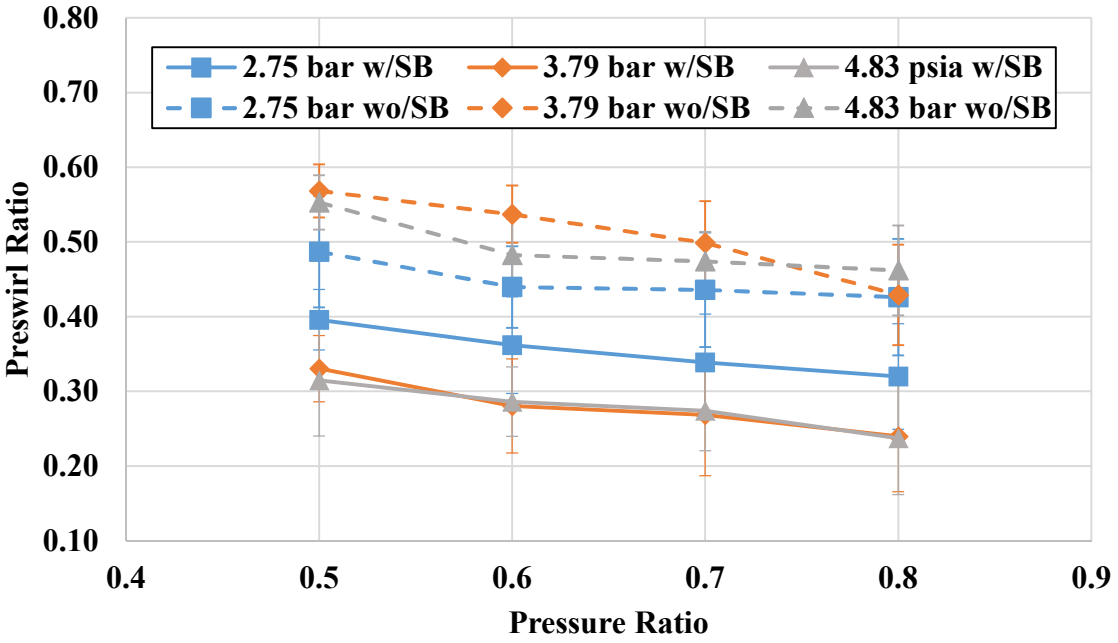

Figure 20. Preswirl ratio versus pressure ratio with and without swirl brakes.

Figure 21 shows mass flow rate versus pressure ratio with and without swirl brakes. Despite the small drop in mass flow rate with swirl brakes at 0.8 PR, the figure shows little difference with

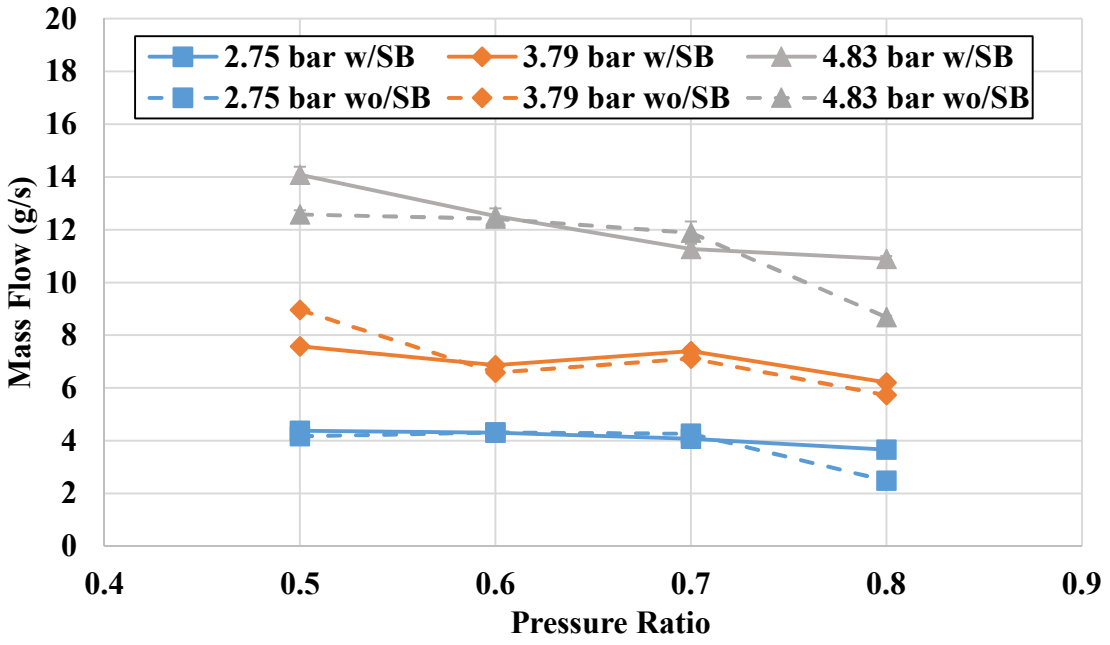

Figure 21. Mass flow rate versus pressure ratio with and without swirl brakes.

and without swirl brakes. Comparing the effect of inlet pressure to pressure ratio on mass flow rate, inlet pressure clearly dominates the behavior of mass flow.

Figure 22 shows the static pressure for each cavity versus cavity number including inlet (Pin) and outlet (Pout) pressures without swirl brakes (Fig. 22(A)) and with (Fig. 22(B)) for an inlet pressure of 4.83 bar. The figure is representative of each inlet pressure, and data for each test condition are provided in Appendix A. Figure 22(A) shows a small pressure drop across the first tooth and a linear drop across subsequent cavities until reaching the last tooth where the largest pressure drop is seen. The static pressure per cavity increases with increasing pressure ratio due to back-pressure build up. Figure 22(B) shows static pressure for each cavity versus cavity number with swirl brakes. Figure 22(A) and Fig. 22(B) show there is little difference in static pressure drop across each tooth of the seal with or without swirl brakes.

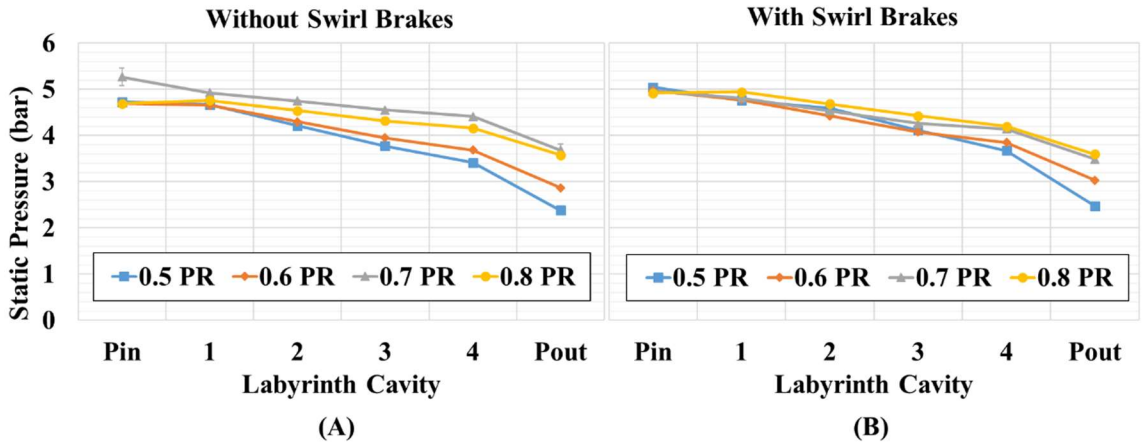

Figure 22. Static pressure versus labyrinth cavity for 4.83 bar inlet pressure without swirl brakes (A) and with swirl brakes (B).

4.2.1 Dynamic Pressures

Dynamic measurements are made by precessing the rotor about the seal center. The precession creates a unique dynamic pressure wave inside each cavity that is integrated over each seal cavity's area to obtain gas reaction forces on the stator. Precession amplitudes are recorded by proximity sensors located on the *x* and *y* axes at the drive end (*DE*) and non-drive end (*NDE*) of the test seal seen in Fig. 18. Figure 23 shows *xDE*, *xNDE*, *yDE*, and *yNDE* vibration amplitude spectrums compiled from each precession frequency at 2.75 bar inlet pressure and a 0.6 PR. An enhanced view of the 10 Hz precession peak shows four distinct peaks for each proximity sensor. Each peak is within 3 microns of any other peak. For each precession frequency a rotor speed peak at approximately 166.67 Hz is seen. Precession amplitudes were between 8 – 12% of the radial clearance for all tests.

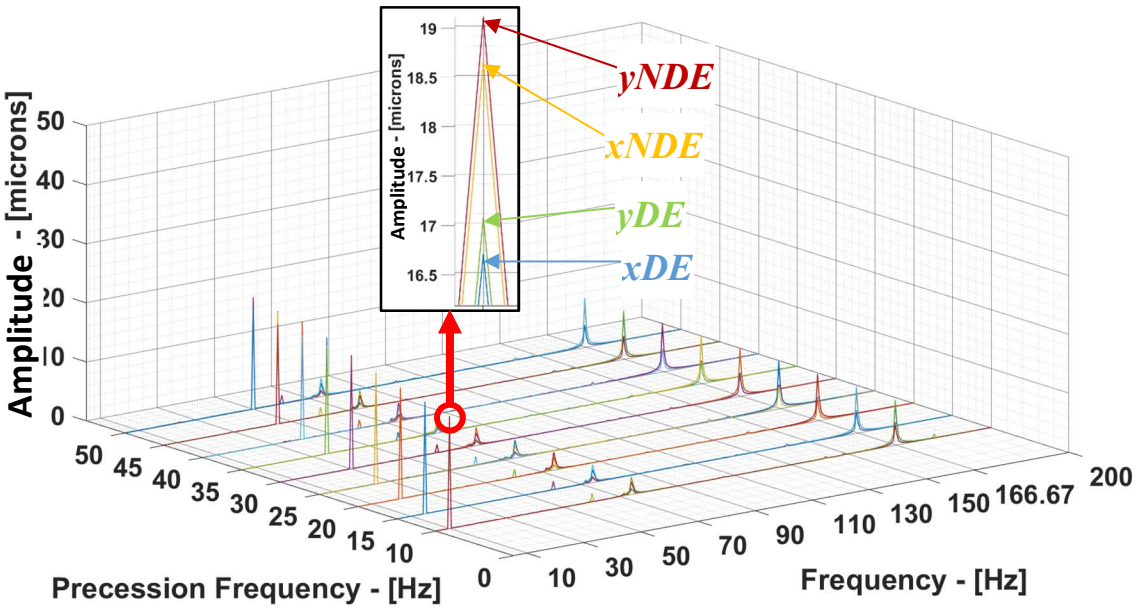

Figure 23. Rotor vibration spectrum from *xDE*, *xNDE*, *yDE*, and *yNDE* proximity probes compiled for all precession frequencies at 2.75 bar inlet pressure and 0.6 PR.

In conjunction with precession amplitude, proximity sensor peak phases are examined to ensure circularity of precession orbits. Figure 24 shows proximity-sensor phase difference versus precession frequency for superimposed forward or backward precession with the *xDE* sensor used as a reference. The phase difference is found by subtracting each sensor's phase from the reference. During forward precession, *x* axis sensors lead *y* axis sensors by 90 degrees, and during backward precession *y* axis sensors lead *x* axis sensors by 90 degrees. For all tests, the *xDE* sensor is less than five degrees out of phase with the *xNDE* sensor, the *yDE* sensor is less than five degrees out of phase with the *yNDE* sensor, and both *x* axis sensors are between 85 to 95 degrees out of phase with both *y* axis sensors.

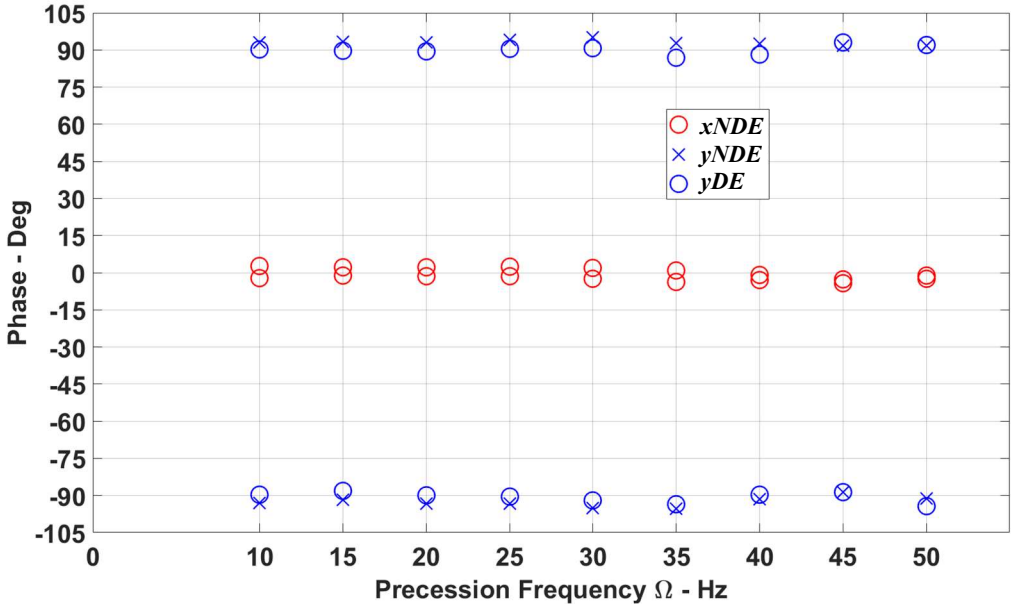

Figure 24. Phase comparison of *xNDE*, *yDE*, and *yNDE* proximity probes with *xDE* used as the reference for forward and backward precession at 3.79 bar inlet pressure and 0.6 PR.

Differential pressure sensors are labeled 1 – 8 starting from the inlet of the seal. Sensors 1 and 2 are located in cavity 1, sensors 3 and 4 in cavity 2, sensors 5 and 6 in cavity 3, and sensors 7 and 8 in cavity 4. Figure 16 shows the circumferential location of the sensors. The dynamic pressure frequency spectrum for sensor number 2 during rotor precession is shown in Fig. 25 for all precession frequencies. A peak at each precession frequency of the test matrix is seen as well as rotor speed for each precession frequency. Dynamic pressure created by rotor speed is commonly higher than the dynamic pressure created by rotor precession, yet Fourier analysis accurately separates the input precession frequency.

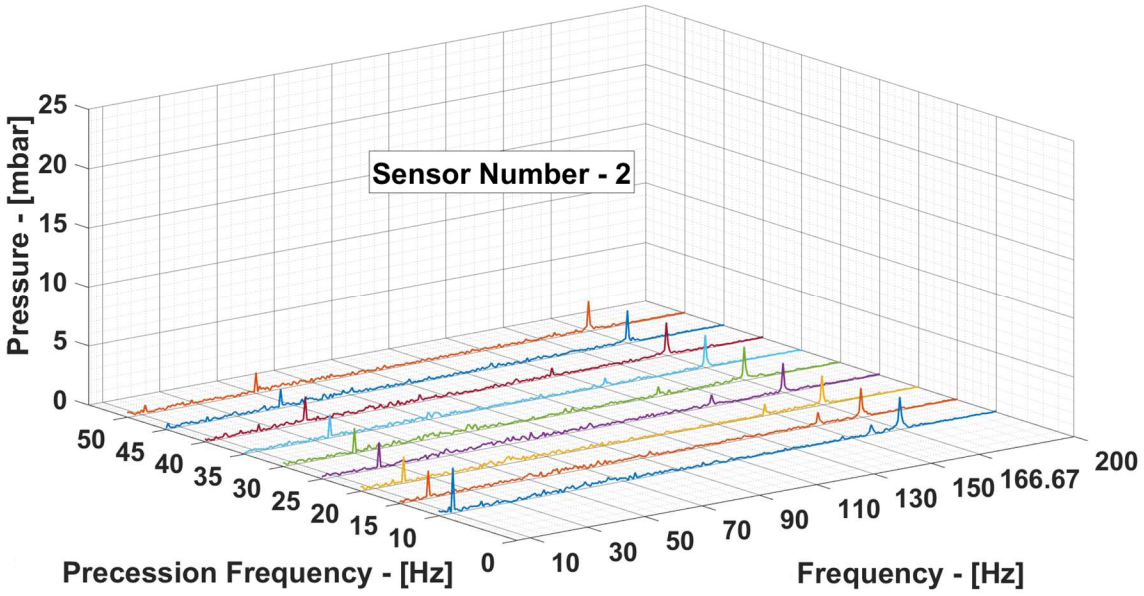

Figure 25. Dynamic pressure spectrum for sensor number 2 over all forward precession frequencies at 2.75 bar inlet pressure and 0.5 PR.

Two differential pressure sensors are installed 180 degrees out of phase in each cavity to ensure the dynamic pressure wave steadily lags the rotating rotor vector e_0. If the pressure wave precesses at a constant circumferential velocity, opposing sensors in each cavity will see a peak dynamic pressure 180 degrees apart in the time domain. Furthermore, if the rotor is centered within the test seal, and precession orbits are circular, dynamic pressure amplitude measurements should be equal for opposing sensors sharing a cavity.

Figure 26 shows the dynamic pressure phase and amplitude versus precession frequency for forward (FWD) and backward (BWD) precession at an inlet pressure of 2.75 bar and a 0.6 pressure ratio after Fourier analysis is used to transform the time domain signal into the frequency domain. Legend entries indicate the differential pressure sensor number. Figure 26(A) and Fig. 26(B) show each sensor's phase versus precession frequency after being corrected to the *xNDE* axis. Equal phase of sensors sharing a cavity in the figure indicates the pressure wave lags e_0 by a constant phase. Figure 26(A) shows that phases of sensors sharing a cavity have reasonable results except for cavity (1) for

forward precession. Figure 26(B) shows phases that are reasonable except for cavity (1) for backward precession. Figure 26(C) and Fig. 26(D) show dynamic pressure amplitude versus precession frequency for each sensor. Figure 26(C) shows cavity (4) is the only cavity with a large discrepancy in amplitude for opposed sensors during forward precession. Figure 26(D) shows cavity (4) to be the only cavity with a large discrepancy in amplitude for opposed sensors during backward precession. Results for each test point are provided in Appendix B.

Figure 26 and Appendix B illustrate large unexpected changes in β when comparing cavities. The figures provide the motivation to present dynamic forces and rotordynamic coefficients by summing the results from each cavity as well as for each cavity individually. All figures of dynamic forces are presented for a 3.79 bar inlet pressure and are representative of remaining inlet pressures.

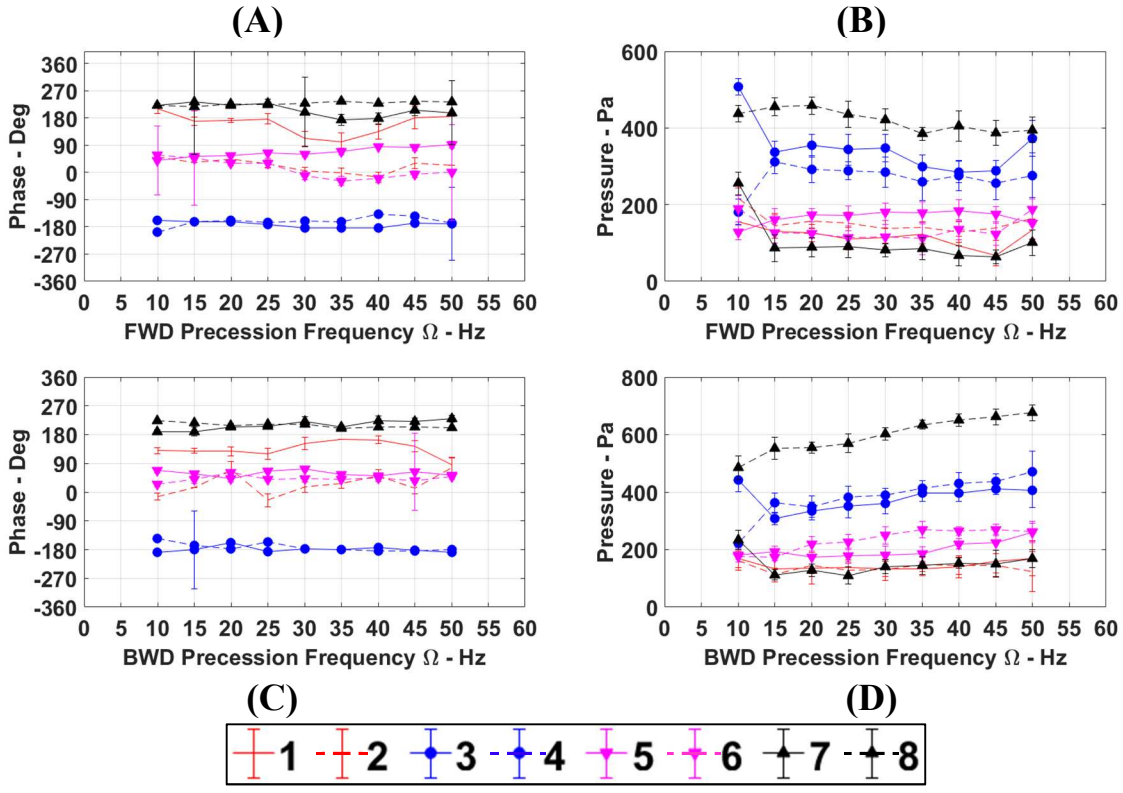

Figure 26. Dynamic pressure phase versus forward (A) and backward (B) precession frequency and dynamic pressure amplitude versus forward (C) and backward (D) precession frequency for each sensor at 2.75 bar inlet pressure and a 0.6 pressure ratio.

4.2.2 Dynamic Force Coefficients

All dynamic force and uncertainty values presented are provided in Appendix C, and legend entries indicate pressure ratios. Ideally, a linear curve fit of measured dynamic forces should appear similar to Figure 10, yet large uncertainties in dynamic pressure phase and amplitude prevent this outcome in many cases. When uncertainties are low in the subsequent dynamic force figures, the results show a linear curve fit represents the data well.

Figure 27 shows F_θ/e_0 versus Ω for the entire seal with and without swirl brakes for each pressure ratio. The slope and intercept of the figures determine, respectively, direct damping *C* and cross-coupled stiffness *k*. Negative slopes indicate positive *C* values, and positive F_θ/e_0 values at zero frequency indicate positive k values. A positive circumferential force indicates the dynamic pressure wave lags the rotating rotor vector e_0 by less than 180 degrees and is pushing the rotor in the same direction as rotor speed ω. Conversely, a negative circumferential force indicates the dynamic pressure wave is pushing the rotor in the opposite direction of ω. Without swirl brakes, linear curve fits of Fig. 27 show negligible values of *C* and slightly negative *k* values for each pressure ratio. With swirl brakes, curve fits show negligible *C* values and negative *k* values for each pressure ratio. Adding swirl brakes has clearly dropped the circumferential reaction force when considering all four cavities.

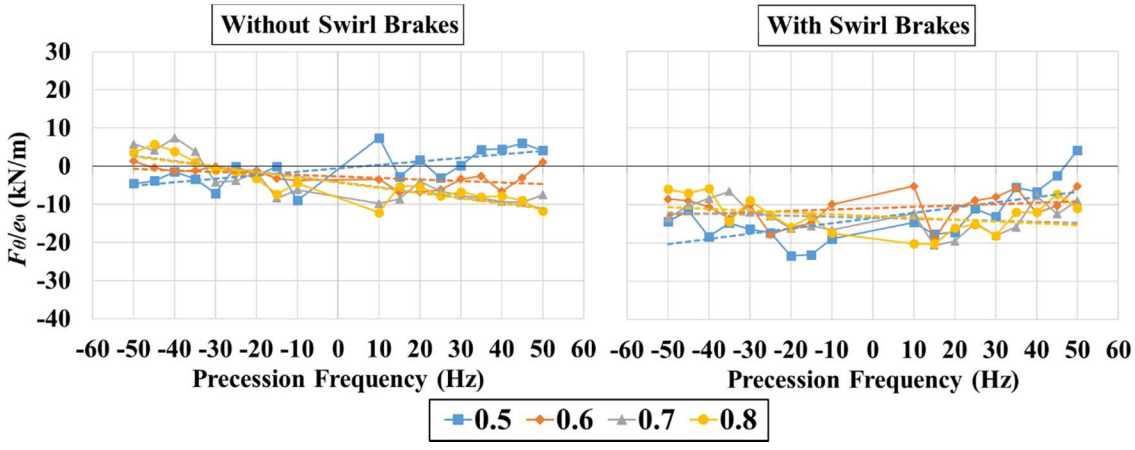

Figure 27. F_θ/e_0 versus Ω for the entire seal at 3.79 bar inlet pressure without and with swirl brakes.

Figure 28 shows F_θ/e_0 versus Ω for each cavity separately with and without swirl brakes for each pressure ratio. The expected trend for F_θ/e_0 is seen in Fig. 10(B). Without swirl brakes, data in Fig. 28(A) show slightly positive forces in cavity (1) and the linear curve fit shows an increasing force as pressure ratio is decreased. With swirl bakes, data in Fig. 28(A) show small forces for each precession frequency in cavity (1) and clearly decreased values compared to without swirl brakes. Without swirl brakes, data in Fig. 28(B) show slightly negative forces in cavity (2), and the curve fit does not show a clear trend as pressure ratio varies. With swirl brakes, data in Fig. 28(B) show negative forces in cavity (2) that are comparable to without swirl brakes with the exception of a 0.5 pressure ratio. Figure 28(C) shows results for cavity (3) and is the first figure that linear curve fits that display appreciable *C* and positive *k* values. Increasing force as pressure ratio is decreased is seen. With swirl brakes, Fig. 28(C) shows positive *C* and *k* values for all pressure ratios and an increasing force with decreasing pressure ratio for cavity (3). Results for *k* are lower in Fig. 28(C) with swirl brakes than without swirl brakes for all pressure ratios. Without swirl brakes, the curve fit of Fig. 28(D) shows a negative *C* for 0.5 pressure ratio and increases for each remaining pressure ratio in cavity (4). The figure also shows negative *k* values for each test. With swirl brakes, Fig. 28(D) shows negative *C* and *k* values for each pressure ratio in cavity (4), and values of *k* are decreased with swirl brakes. Figure 28 shows that each consecutive cavity behaves differently than the previous one.

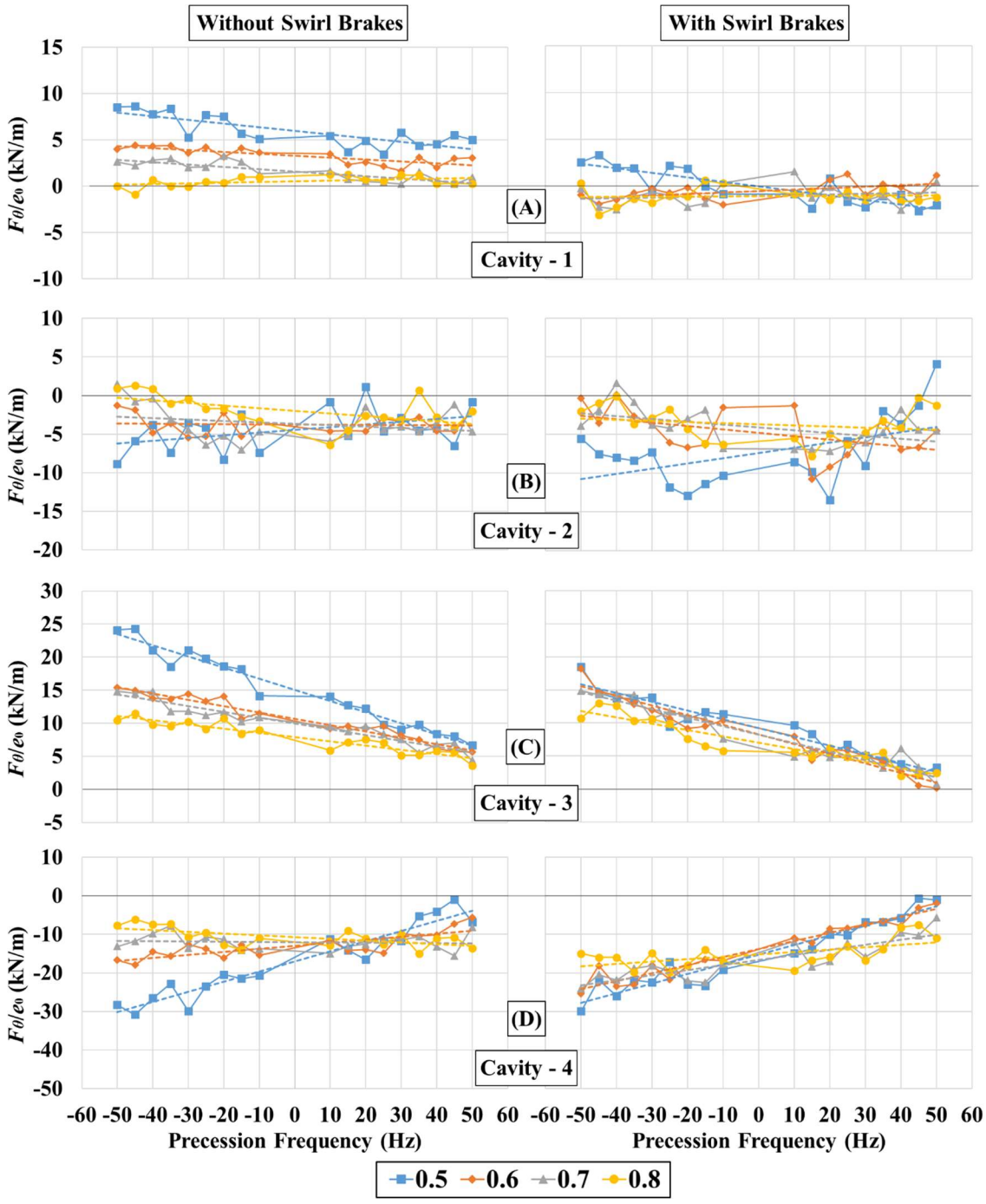

Figure 28. F_θ/e_0 versus Ω at 3.79 bar inlet pressure with and without swirl brakes for (A) cavity – 1, (B) cavity – 2, (C) cavity – 3, and (D) cavity – 4.

The expected trend for F_r/e_0 is seen in Fig. 10(A). Figure 29 shows F_r/e_0 versus Ω for the entire seal with and without swirl brakes for each pressure ratio. The slope and

intercept of the figures determine, respectively, cross-coupled damping c and direct stiffness K. Positive slopes and positive F_r/e_0 values at zero frequency indicate, respectively, positive c and K values. Without swirl brakes, linear curve fits of Fig. 29 show negative K and positive c values for each pressure ratio. With swirl brakes, linear curve fits show negative K and positive c values for each pressure ratio and K values are higher with swirl brakes with the exception of 0.5 pressure ratio.

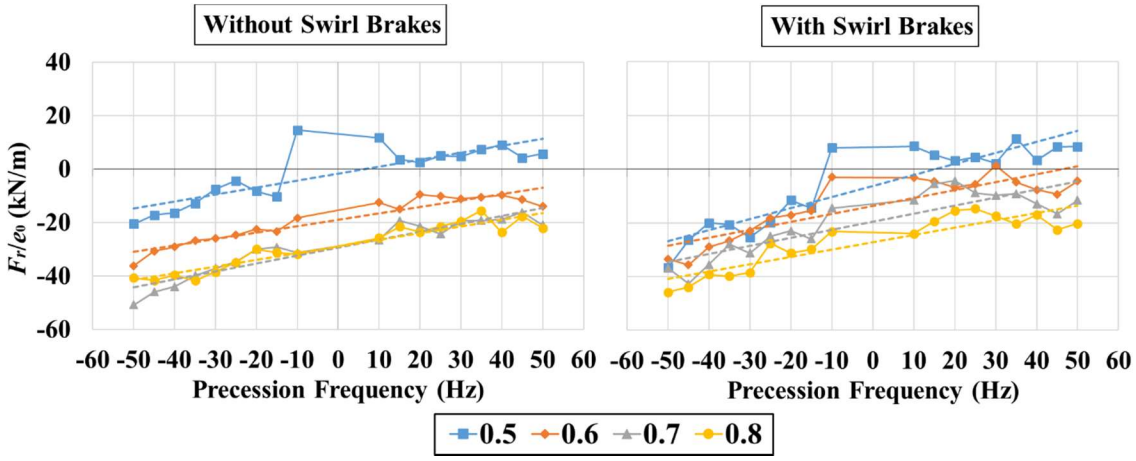

Figure 29. F_r/e_0 versus Ω for the entire seal at 3.79 bar inlet pressure with and without swirl brakes.

With and without swirl brakes, Fig 30 shows F_r/e_0 versus Ω for each cavity separately at each pressure ratio. Without swirl brakes, linear curve fits of Fig. 30(A) show small c and K values in cavity (1). With swirl brakes, Fig. 30(A) shows slightly positive c values and small K values increasing from backward to forward precession in cavity (1). Without swirl brakes, Fig. 30(B) clearly shows positive c and negative K values for cavity (2). With swirl brakes, Fig. 30(B) shows positive c and negative K values for each pressure ratio in cavity (2). Without swirl brakes, Fig. 30(C) shows negative c and positive K values for each pressure ratio in cavity (3) with an increasing force for decreasing pressure ratio trend. With swirl brakes, Fig. 30(C) shows negative c and positive K values in cavity (3) for each pressure ratio. Without swirl brakes, Fig. 30(D) shows positive c and negative K values for each pressure ratio in cavity (4). With swirl brakes, Fig. 30(D) shows positive c and negative K values in cavity (4) for each pressure ratio. Figure 30 further illustrates

the distinctive behavior of each cavity, and the figure does not show a substantial difference with or without swirl brakes.

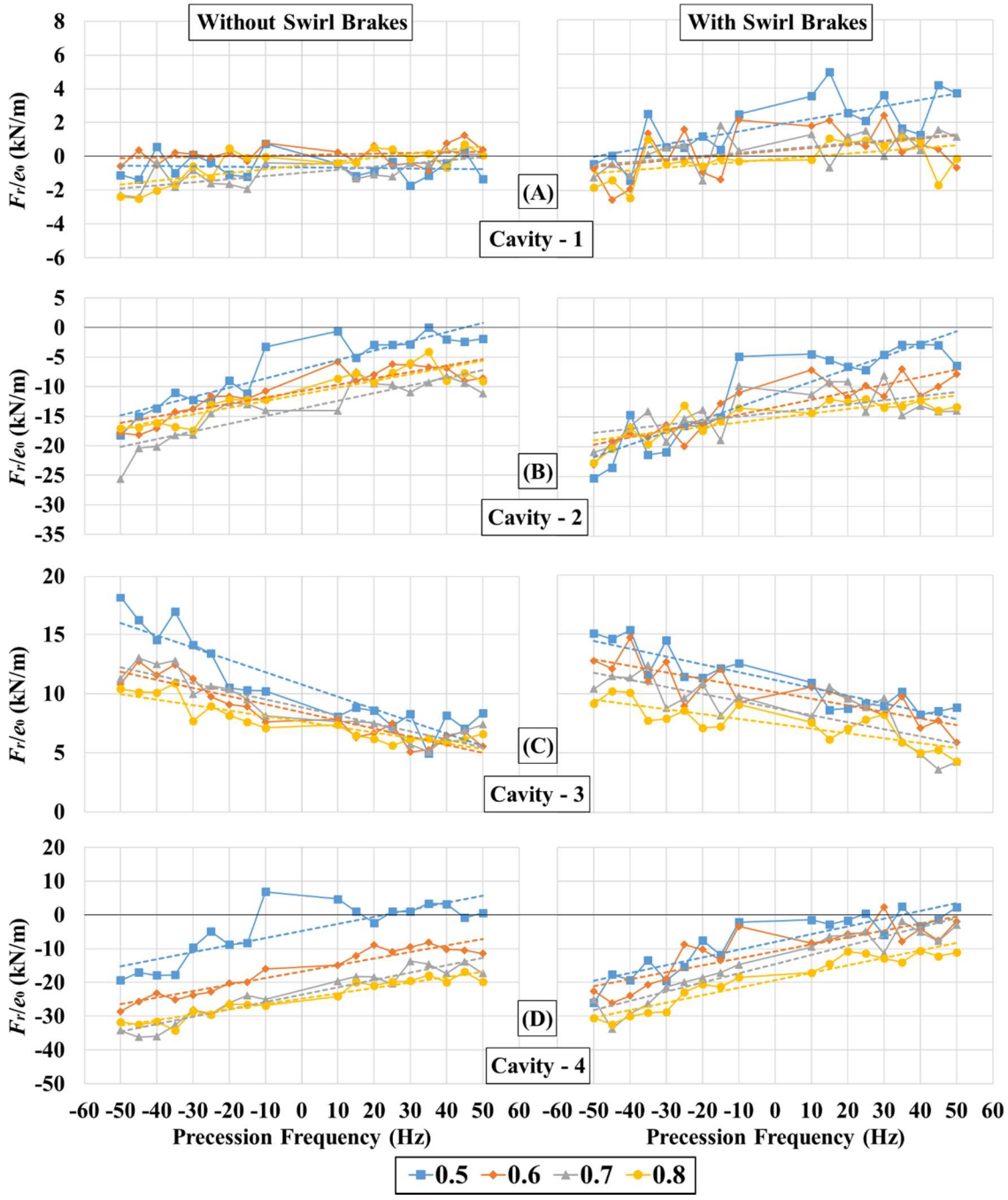

Figure 30. F_r/e_0 versus Ω at 3.79 bar inlet pressure with and without swirl brakes for (A) cavity – 1, (B) cavity – 2, (C) cavity – 3, and (D) cavity – 4.

4.3 Rotordynamic Coefficients

Cross-coupled stiffness *k*, direct damping *C*, direct stiffness *K*, and cross-coupled damping *c* are obtained using the following two methods. (1) From the slope and intercepts of the radial and circumferential reaction force plots, and (2) by combining forward and backward results of radial and circumferential forces at each precession frequency as shown in Eqs. (14-17). The former method produces rotordynamic coefficients for all precession frequencies together based on a best fit line of the data. The latter produces coefficients at each precession frequency. All rotordynamic coefficients produced by the slope and intercept of dynamic force plots are presented for a 3.79 bar inlet pressure and are representative of the remaining data provided in Appendix D.

Table 7 shows coefficients based on slope and intercept without swirl brakes. R^2 values indicate how well the data fits the linear frequency model with a value of one being a perfect fit. Σ(1-4) indicates the summation of cavities (1) through (4). R^2 values for cavity (3) are consistently higher than for any other cavity, including the summation of all four. Odd numbered cavities occur after a tooth on the stator while even numbered cavities occur after a tooth on the rotor. In odd numbered cavities *k* is positive while even numbered cavities produce negative *k* values. Cavity (3) is the only cavity with all positive *C* values. *K* values are negative in all cavities except cavity (3). For most cases, *K* decreases as pressure ratio is increased. Cross-coupled damping *c* does not appear to follow a trend with respect to cavity number or pressure ratio with the exception of cavity (3) in which *c* increases with increasing pressure ratio.

Table 7. *k*, *C*, *K*, and *c* for the entire seal and individual cavities at 3.79 bar inlet pressure without swirl brakes for each test condition using slope and intercept of dynamic forces.

Configuration	Cavity Number	Target PR	k (kN/m)	C (Ns/m)	R^2	K (kN/m)	c (Ns/m)	R^2
Without Swirl Brakes	Σ(1-4)	0.5	-0.55	-14	0.45	-1.7	41	0.66
		0.6	-2.8	6.4	0.27	-19	38	0.88
		0.7	-4.1	22	0.66	-29	47	0.89
		0.8	-4.3	22	0.76	-29	40	0.90
	1	0.5	6.0	-6.3	0.62	-0.7	-0.32	0.01
		0.6	3.3	3.3	0.62	0.085	0.64	0.06
		0.7	1.6	4.0	0.70	-1.0	2.9	0.53
		0.8	0.52	-1.2	0.20	-0.55	3.6	0.56
	2	0.5	-4.5	-5.6	0.19	-7.0	25	0.84
		0.6	-3.8	0.40	0.00	-11	17	0.79
		0.7	-3.6	2.9	0.07	-14	21	0.76
		0.8	-2.0	5.5	0.31	-11	18	0.82
	3	0.5	15	27	0.96	11	-17	0.82
		0.6	11	15	0.95	8.4	-11	0.85
		0.7	10	14	0.92	8.8	-11	0.84
		0.8	7.9	10	0.88	7.6	-7.3	0.80
	4	0.5	-17	-42	0.91	-4.7	33	0.67
		0.6	-13	-12	0.64	-17	31	0.91
		0.7	-12	0.95	0.01	-24	35	0.91
		0.8	-11	7.4	0.38	-25	26	0.92

Table 8 shows coefficients based on the slope and intercept of the radial and circumferential forces with swirl brakes. Cavity (3) has the highest R^2 values for *k* and *C*. With swirl brakes, *k* is positive only in cavity (3). With the exception of a 0.5 pressure ratio in cavity (4), every value of *k* is decreased with the addition of swirl brakes indicating improved stability. Cavity (3) produces positive *C* values decreasing with increasing pressure ratio with the exception of 0.5 pressure ratio. Cavity (4) produces negative values of *C* increasing with increasing pressure ratio. Remaining cavities do not produce values of *C* that are same sign for each case. Values of *C* are small and do not appreciably change with or without swirl brakes. Cavity (1) is the is the only cavity with notably low R^2 values for *K* and *c*. All values of *K* are negative or near zero except in cavity (3) where positive *K* values decrease with increasing pressure ratio. Direct stiffness does not

considerably change with the addition of swirl brakes. Cross-coupled damping does not appear to have a correlation with pressure ratio and is positive for all values except those of cavity (3).

Table 8. *k*, *C*, *K*, and *c* for the entire seal and individual cavities at 3.79 bar inlet pressure with swirl brakes for each test condition using slope and intercept of dynamic forces.

Configuration	Cavity Number	Target PR	k (kN/m)	C (Ns/m)	R^2	K (kN/m)	c (Ns/m)	R^2
With Swirl Brakes	Σ(1-4)	0.5	-13	-22	0.42	-6.2	66	0.81
		0.6	-11	-5.6	0.09	-14	47	0.74
		0.7	-13	4.2	0.05	-20	48	0.74
		0.8	-13	7.5	0.11	-27	43	0.80
	1	0.5	-0.039	7.7	0.71	1.8	5.9	0.51
		0.6	-0.55	-2.5	0.31	0.31	2.9	0.17
		0.7	-1.0	-1.1	0.04	0.38	2.9	0.34
		0.8	-1.1	-0.28	0.00	-0.17	2.6	0.25
	2	0.5	-7.4	-11	0.25	-11	34	0.81
		0.6	-4.8	7.0	0.24	-13	20	0.76
		0.7	-4.1	5.8	0.25	-14	11	0.36
		0.8	-3.7	2.3	0.05	-15	12	0.64
	3	0.5	9.2	21	0.92	11	-10	0.81
		0.6	8.2	23	0.94	10	-8.8	0.70
		0.7	8.2	20	0.92	8.8	-9.4	0.61
		0.8	7.0	15	0.87	7.5	-6.4	0.65
	4	0.5	-15	-40	0.92	-8.0	36	0.79
		0.6	-14	-33	0.94	-11	33	0.70
		0.7	-17	-21	0.75	-15	43	0.88
		0.8	-15	-9.8	0.35	-19	35	0.91

Rotordynamic coefficients produced by combining forward and backward dynamic force results at each precession frequency are presented in the remaining figures for a 3.79 bar inlet pressure. Values for rotordynamic coefficients and uncertainties in the figures are provided in Appendix E. Large error bars are due to large standard deviations in the dynamic pressure phase and amplitude indicating irregular flow. The legend entries w/SB and wo/SB indicate, respectively, with swirl brakes and without swirl brakes. Figure

31 shows k versus Ω for the entire seal at all pressure ratios with, and without, swirl brakes. Clearly, k is decreased with the addition of swirl brakes indicating the decrease in fluid swirl at the entrance of the seal has increased rotor stability. Unexpectedly, k also increases slightly with increasing Ω.

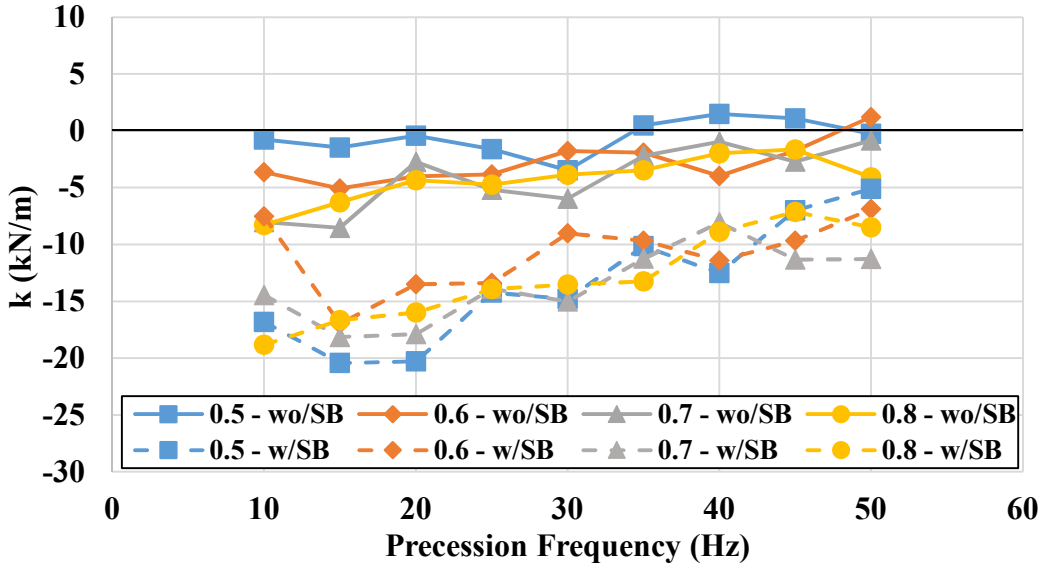

Figure 31. Cross-coupled stiffness k versus Ω for the entire seal at 3.79 bar inlet pressure with and without swirl brakes.

Figure 32 shows k versus Ω in cavity (1) for all pressure ratios with, and without, swirl brakes. Values of k decrease with swirl brakes.

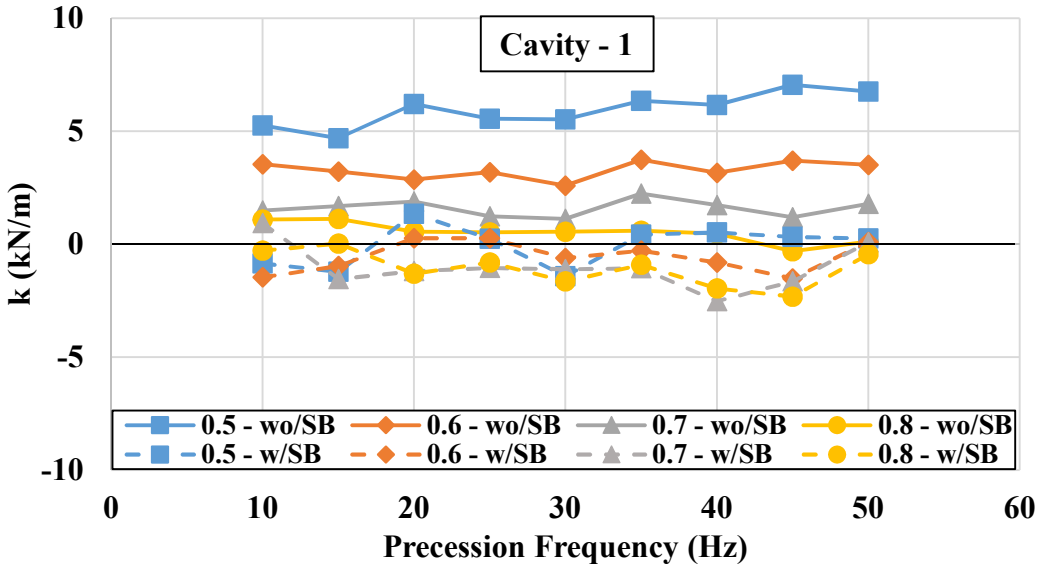

Figure 32. Cross-coupled stiffness *k* versus Ω for cavity (1) at 3.79 bar inlet pressure with and without swirl brakes.

Figure 33 shows *k* versus Ω in cavity (2) for all pressure ratios with, and without, swirl brakes. The addition of swirl brakes decreases *k*, and all values are negative.

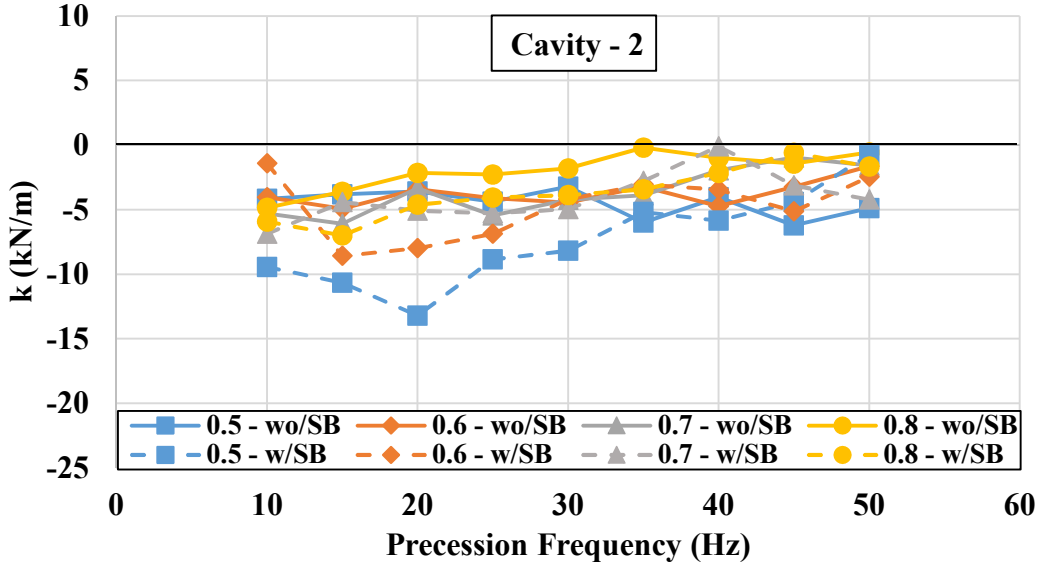

Figure 33. Cross-coupled stiffness *k* versus Ω for cavity (2) at 3.79 bar inlet pressure with and without swirl brakes.

Figure 34 shows *k* versus Ω in cavity (3) for all pressure ratios with, and without, swirl brakes. All values of *k* are positive and decrease with the use of swirl brakes.

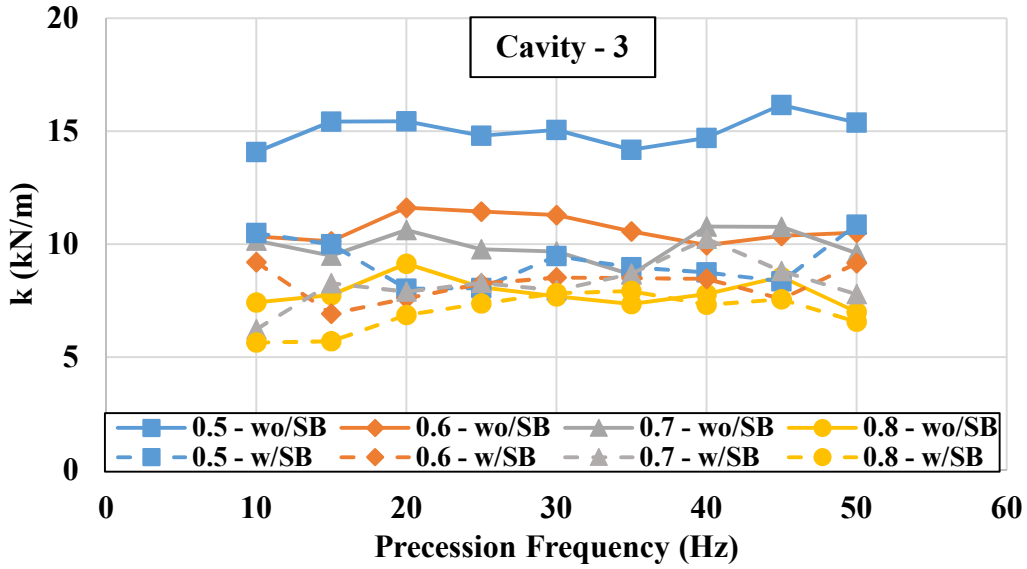

Figure 34. Cross-coupled stiffness *k* versus Ω for cavity (3) at 3.79 bar inlet pressure with and without swirl brakes.

Figure 35 shows *k* versus Ω in cavity (4) for all pressure ratios with, and without, swirl brakes. All values of *k* are negative with the inexplicable exception of 0.8 pressure ratio with swirl brakes. A clear consequence of adding swirl brakes is not seen.

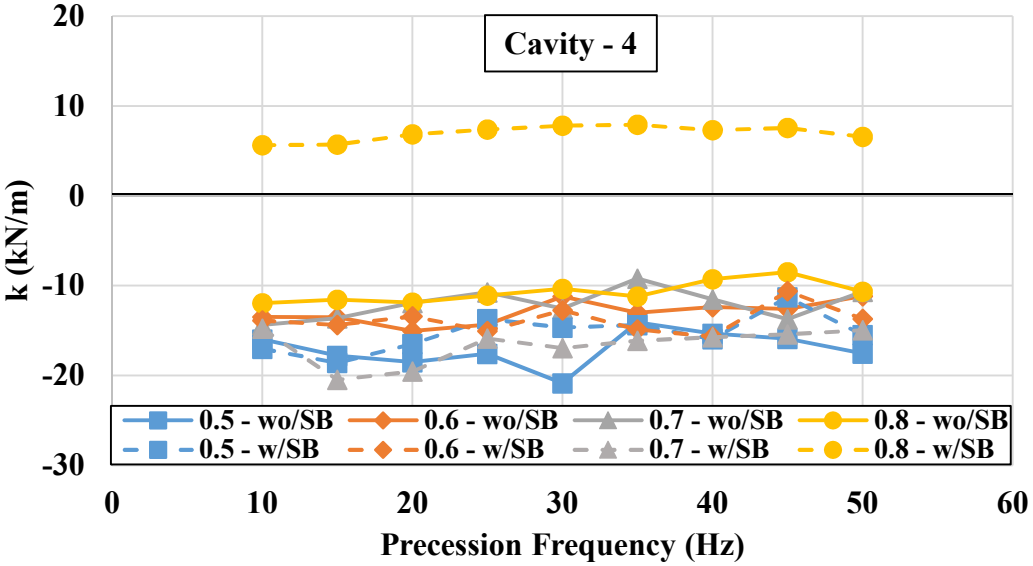

Figure 35. Cross-coupled stiffness *k* versus Ω for cavity (4) at 3.79 bar inlet pressure with and without swirl brakes.

Values of *k* appear to decrease in all cases with the addition of swirl brakes with the exception of cavity (4). Results for *k* produced by the intercept of circumferential force plots in Table 7 and Table 8 are comparable with average values of *k* produced by combining forward and backward circumferential force results for each precession frequency. The results presented for *k* in each cavity generally do not appear to be frequency dependent in contrast with the results presented by Childs and Elrod [7]; however, when considering the entire seal, *k* shows a slight increase with increasing Ω. Linear curves are fit to the data of Fig. 31 to quantify, with R^2 values, the frequency dependency of *k*. Without swirl brakes, R^2 values are, respectively, 0.2, 0.6, 0.7, and 0.7 for pressure ratios of 0.5, 0.6, 0.7, and 0.8 respectively. With swirl brakes, R^2 values are, respectively, 0.8, 0.2, 0.6, and 0.9 for pressure ratios of 0.5, 0.6, 0.7, and 0.8 respectively. With the exception of R^2 values from 0.5 PR without swirl brakes and 0.6 PR with swirl brakes, linear curve fits represent data of Fig. 31 relatively well indicating *k* for the entire seal is frequency dependent.

Figure 36 shows *C* versus Ω for all pressure ratios with, and without, swirl brakes for the entire seal. Values, both with and without swirl brakes, are not consistently positive or negative for varying pressure ratio. A positive *C* is expected based on prior test results for TOS and TOR labyrinth seals.

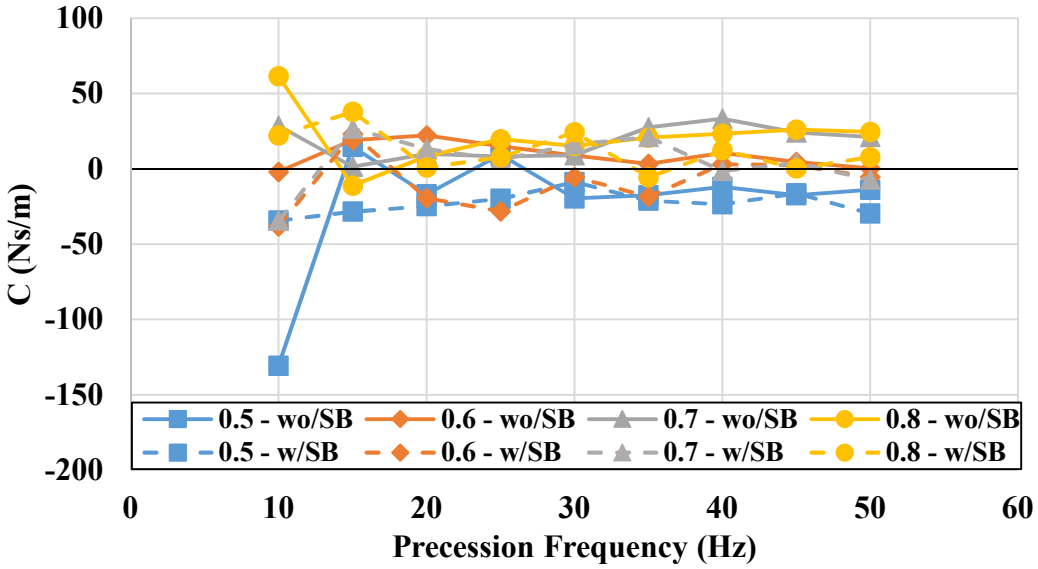

Figure 36. Direct damping *C* versus Ω for the entire seal at 3.79 bar inlet pressure with and without swirl brakes.

Figure 37 shows *C* versus Ω in cavity (1) for all pressure ratios with, and without, swirl brakes. Negative values of *C* are seen at higher pressure ratios, and all values of *C* are small.

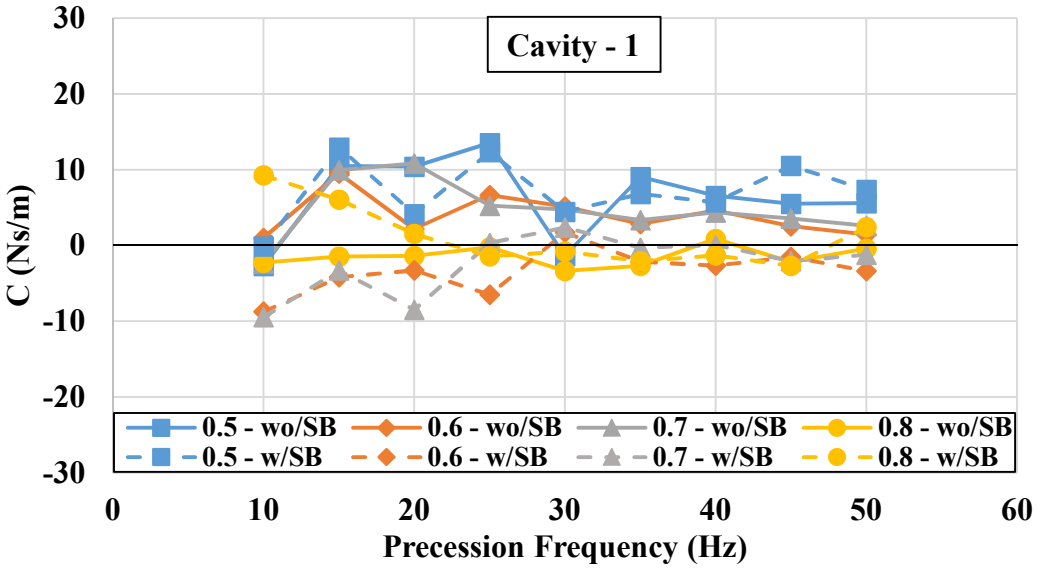

Figure 37. Direct damping *C* versus Ω for cavity (1) at 3.79 bar inlet pressure with and without swirl brakes.

Figure 38 shows *C* versus Ω in cavity (2) for all pressure ratios with, and without, swirl brakes. Adding swirl brakes does not make a noticeable difference and no trend is seen with changing pressure ratio.

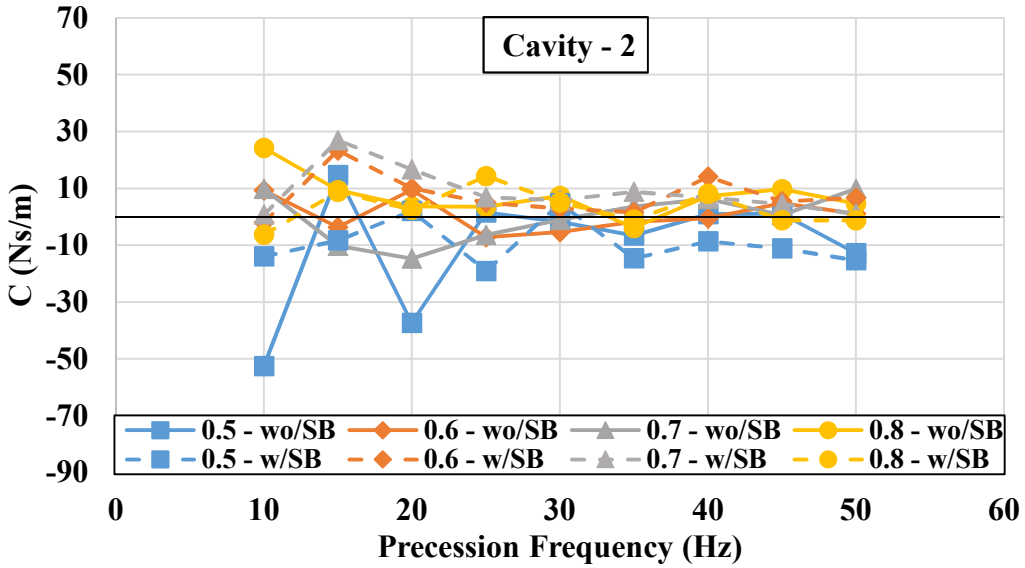

Figure 38. Direct damping *C* versus Ω for cavity (2) at 3.79 bar inlet pressure with and without swirl brakes.

Figure 39 shows *C* versus Ω in cavity (3) for all pressure ratios with, and without, swirl brakes. Values for *C* are distinctly positive when compared with other cavities, but no trend is seen for varying pressure ratio or from adding swirl brakes.

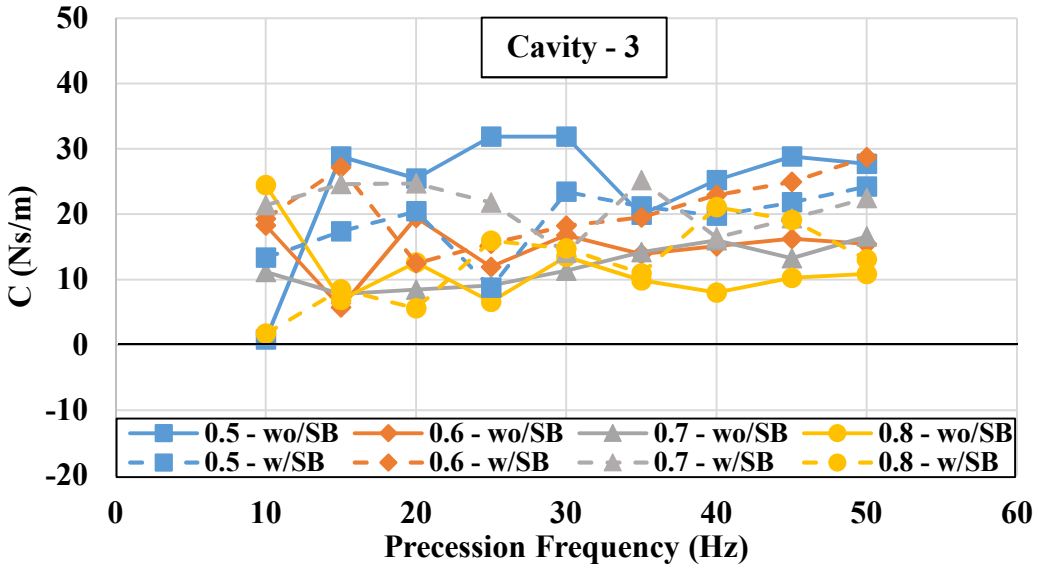

Figure 39. Direct damping *C* versus Ω for cavity (3) at 3.79 bar inlet pressure with and without swirl brakes.

Figure 40 shows *C* versus Ω in cavity (4) for all pressure ratios with, and without, swirl brakes. An effect of swirl brakes is not seen but values of *C* increase with increasing pressure ratio.

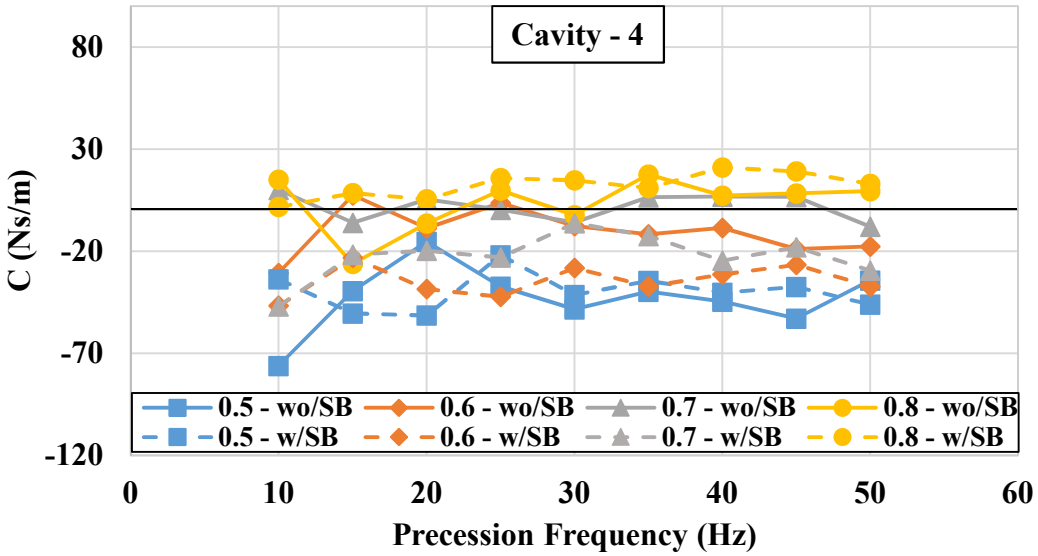

Figure 40. Direct damping *C* versus Ω for cavity (4) at 3.79 bar inlet pressure with and without swirl brakes.

Results for C from the slope of circumferential force plots are comparable to average values of C obtained by combining forward and backward circumferential force results at each precession frequency in the sense that most values are small, and cavity (3) is the only cavity that provides all positive values. The results show relatively frequency independent behavior with large error bars.

Figure 41 shows K versus Ω for all pressure ratios with and without swirl brakes for the entire seal. K decreases with increasing pressure ratio but does not appear to have a tendency to increase or decrease with addition of swirl brakes. Nearly all values for K are negative indicating the pressure wave lags the rotating rotor vector e_0 by more than 90 degrees and pushes the rotor in the direction of the stator.

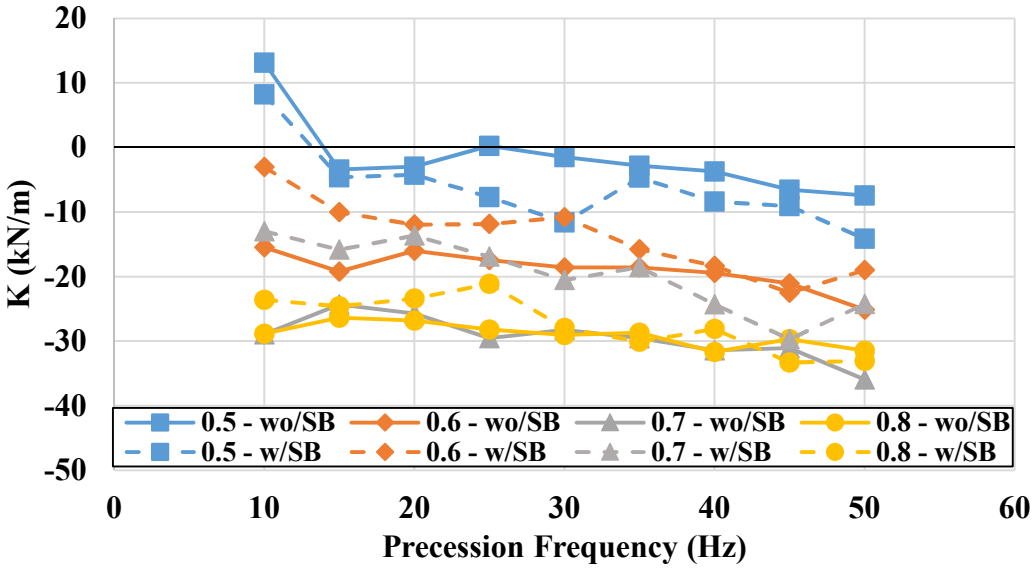

Figure 41. Direct stiffness *K* versus Ω for the entire seal at 3.79 bar inlet pressure with and without swirl brakes.

Figure 42 shows K versus Ω in cavity (1) for all pressure ratios with, and without, swirl brakes. Values of K are negligibly small in magnitude when compared with the entire seal, and slightly higher values are seen with swirl brakes than without.

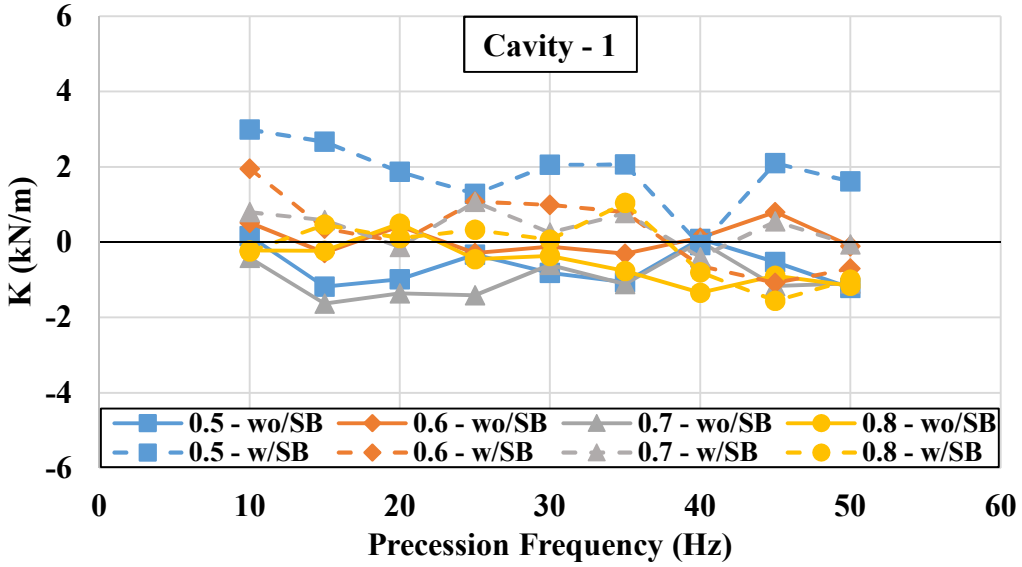

Figure 42. Direct stiffness *K* versus Ω for cavity (1) at 3.79 bar inlet pressure with and without swirl brakes.

Figure 43 shows *K* versus Ω in cavity (2) for all pressure ratios with, and without, swirl brakes. All values are negative with a slight decrease when swirl brakes are added.

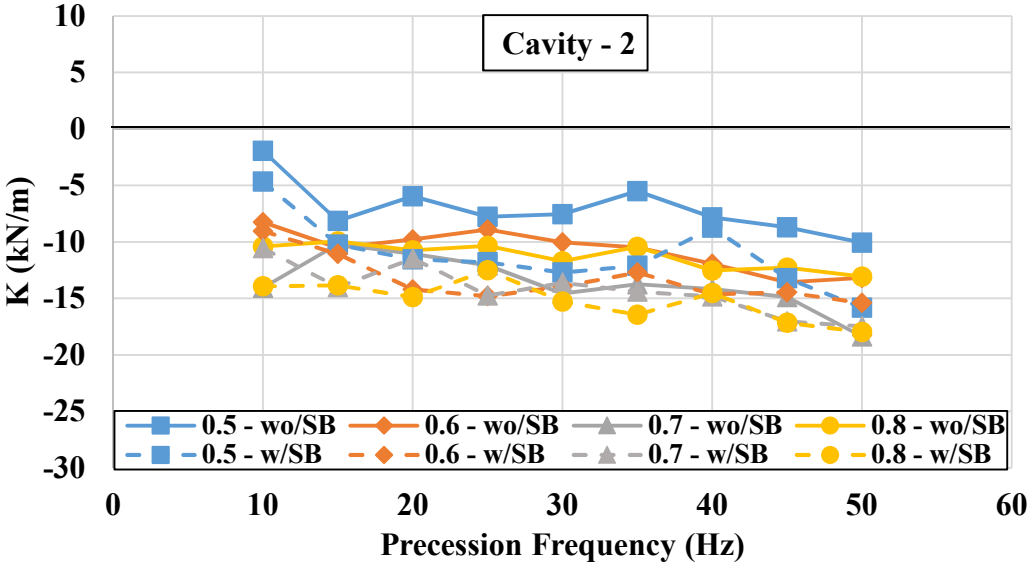

Figure 43. Direct stiffness *K* versus Ω for cavity (2) at 3.79 bar inlet pressure with and without swirl brakes.

Figure 44 shows K versus Ω in cavity (3) for all pressure ratios with, and without, swirl brakes. This is the only cavity to produce all positive values. K decreases with increasing pressure ratio but a clear result from adding swirl brakes is not seen.

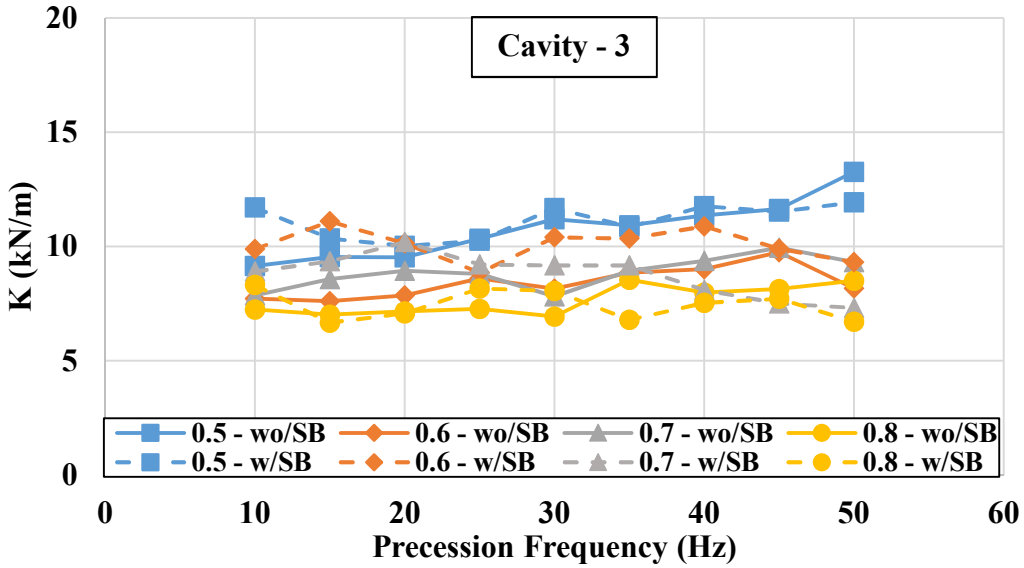

Figure 44. Direct stiffness *K* versus Ω for cavity (3) at 3.79 bar inlet pressure with and without swirl brakes.

Figure 45 shows K versus Ω in cavity (4) for all pressure ratios with, and without, swirl brakes. Nearly all values are negative with the exception of an inexplicable result at 0.8 pressure ratio with swirl brakes. K decreases with increasing pressure ratio (decreasing pressure differential ΔP) and does not have a visible trend with or without swirl brakes.

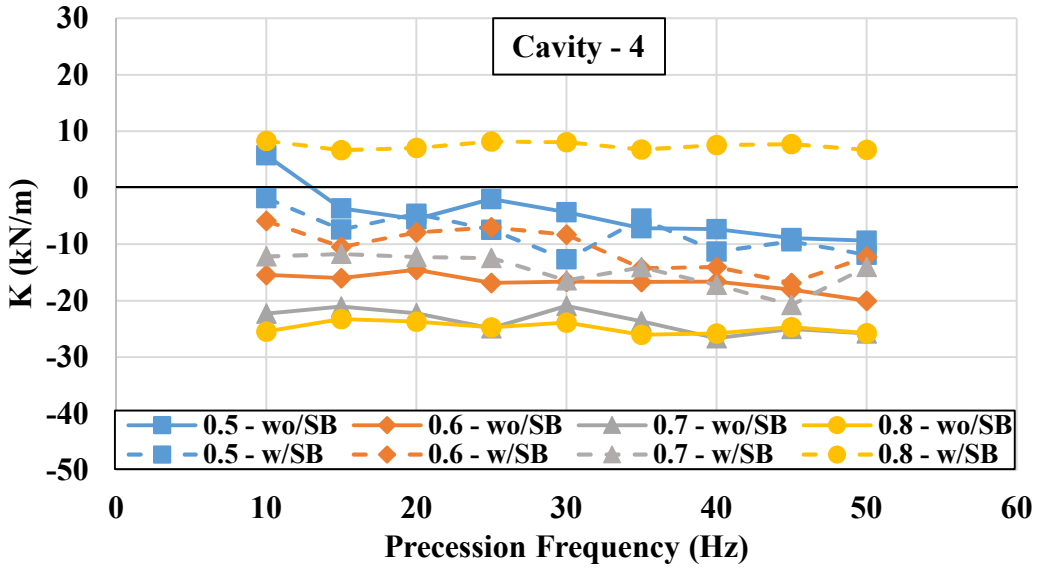

Figure 45. Direct stiffness *K* versus Ω for cavity (4) at 3.79 bar inlet pressure with and without swirl brakes.

Amplitude and sign of K obtained from the intercept of radial force plots are comparable to average values of K obtained by combining forward and backward radial forces at each precession frequency. Clear trends are not present for each cavity with the addition of swirl brakes in either method of obtaining K values. Cavity (3) is the only cavity that produces a positive centering force on the rotor. Results for K generally appear frequency independent.

Before presenting results for effective damping C_{eff}, it is worth restating Eq. (4)

$$C_{eff} = C - \frac{k}{\Omega}$$

Figure 46 shows C_{eff} versus Ω for all pressure ratios with and without swirl brakes for the entire seal. C_{eff} increases with swirl brakes and with increasing pressure ratio (decreasing ΔP). Nearly all values are positive indicating positive net damping. For the entire seal, nearly all values of k are negative which changes the sign of C_{eff} and explains the drop in C_{eff} with increasing Ω.

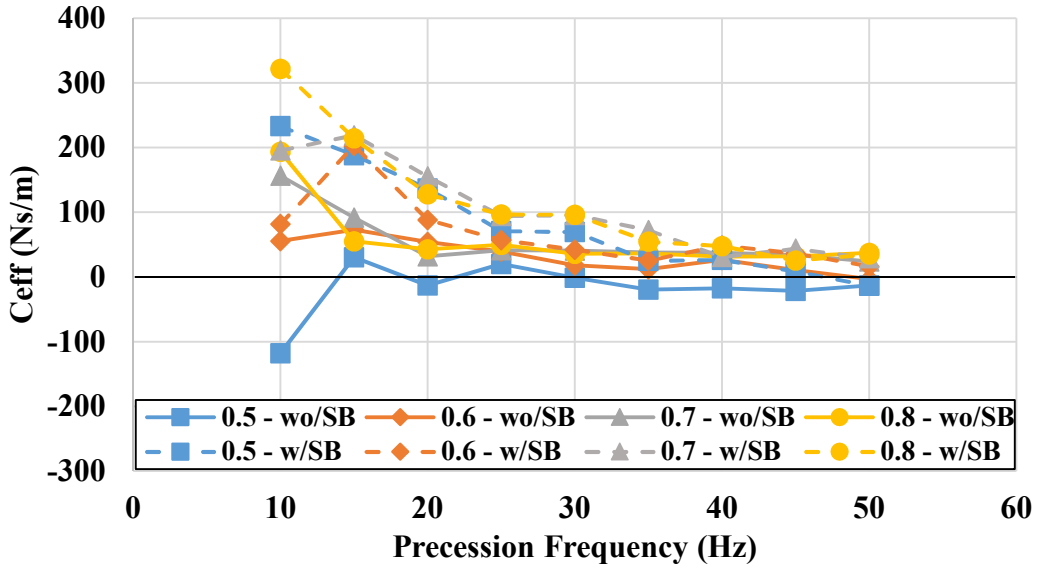

Figure 46. Effective damping C_{eff} versus Ω for the entire seal at 3.79 bar inlet pressure with and without swirl brakes.

Figure 47 shows C_{eff} versus Ω in cavity (1) for all pressure ratios with, and without, swirl brakes. C_{eff} appears to increase with the addition of swirl brakes, and negative values are seen without swirl brakes.

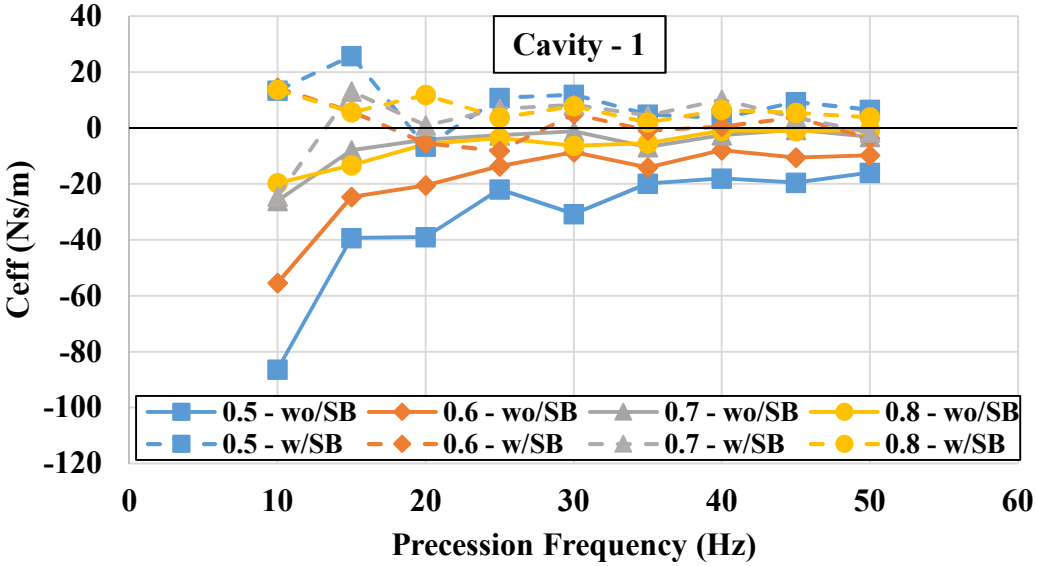

Figure 47. Effective damping C_{eff} versus Ω for cavity (1) at 3.79 bar inlet pressure with and without swirl brakes.

Figure 48 shows C_{eff} versus Ω in cavity (2) for all pressure ratios with, and without, swirl brakes and values are nearly all positive. Swirl brakes appear to provide a slight stability advantage.

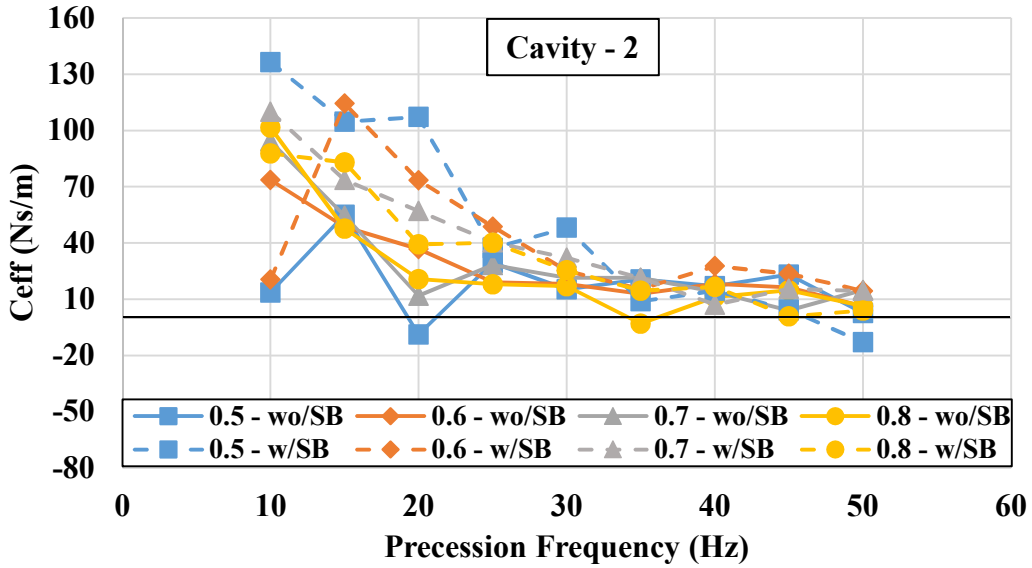

Figure 48. Effective damping C_{eff} versus Ω for cavity (2) at 3.79 bar inlet pressure with and without swirl brakes.

Figure 49 shows C_{eff} versus Ω in cavity (3) for all pressure ratios with, and without, swirl brakes. Swirl brakes provide a stability advantage as well as increasing pressure ratio.

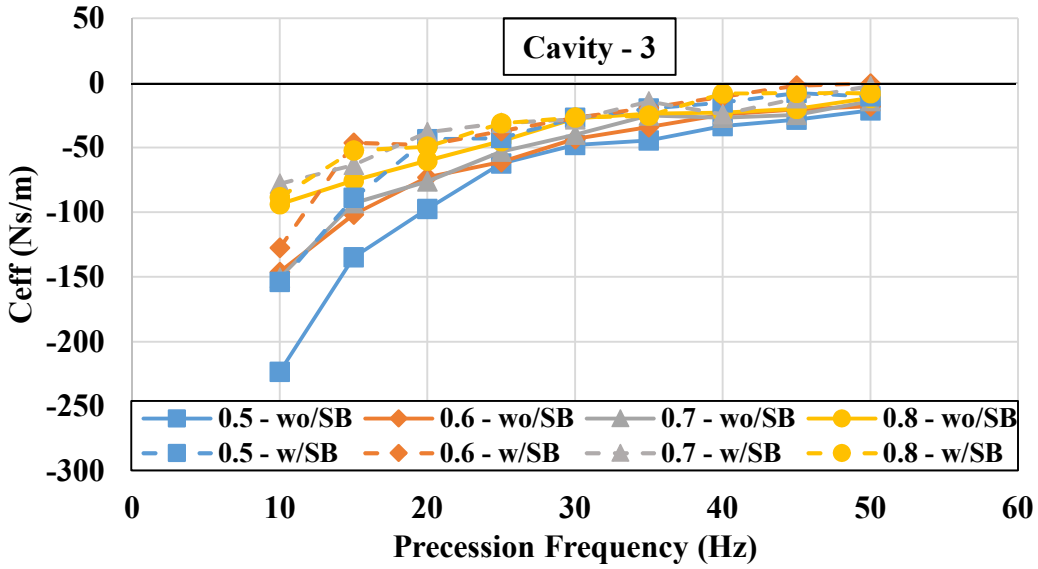

Figure 49. Effective damping C_{eff} versus Ω for cavity (3) at 3.79 bar inlet pressure with and without swirl brakes.

Figure 50 shows C_{eff} versus Ω in cavity (4) for all pressure ratios with, and without, swirl brakes and shows all positive values of C_{eff}. No stability advantage is seen with the addition of swirl brakes or change in pressure ratio.

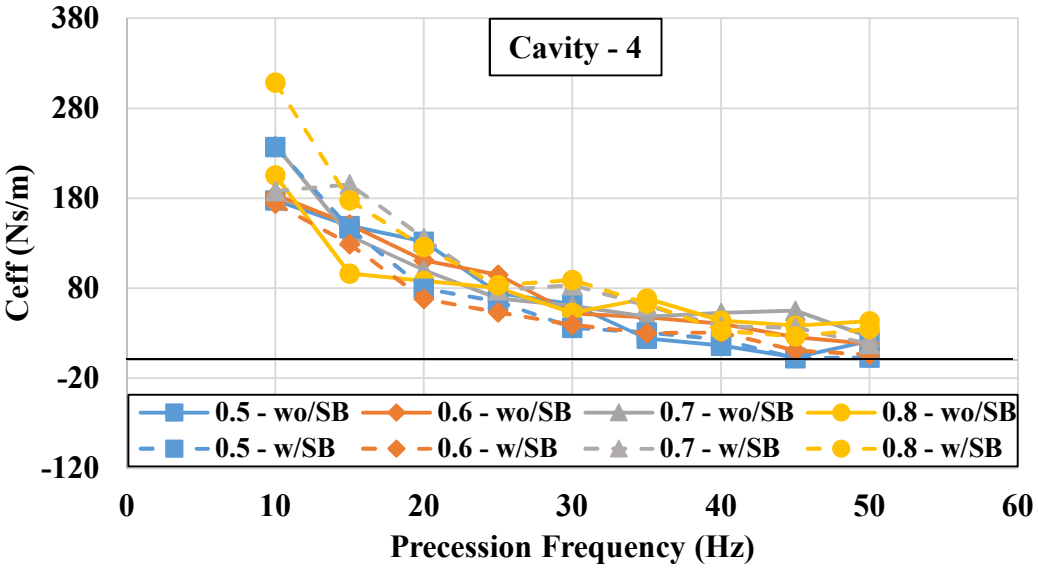

Figure 50. Effective damping C_{eff} versus Ω for cavity (4) at 3.79 bar inlet pressure with and without swirl brakes.

Cavity (3) is the only cavity to provide negative C_{eff} values for each test condition. A cross-over frequency where C_{eff} transitions from negative to positive is not observed for cavity (3) within the frequency range tested. Despite negative C_{eff} values produced by cavity (3), the magnitude of C_{eff} consistently grows with increasing cavity number.

The effect of swirl brakes is more prominent in cavities closer to the entrance of the test seal for k, K, and C_{eff} while an effect is not witnessed for C. In cavities (1-3), results with swirl brakes appear to have a similar effect on k while cavity (4) shows little response. In cavities (1-2), results with swirl brakes for K clearly show distinction from results without swirl brakes, yet cavities (3-4) do not. Results from cavities (1-2) with swirl brakes for C_{eff} show clear separation from those without swirl brakes, cavity (3) shows the effect diminishing, and cavity (4) shows no distinction between results with or without swirl brakes.

5. SUMMARY, CONCLUSIONS, AND EXTENSIONS

Previous difficulties in obtaining interlocking-labyrinth-gas seal measurements from this test rig motivated the work of Ramirez [1] to benchmark the test rig using a see-through tooth-on-stator labyrinth seal. Ramirez's work proved successful, and the process developed to operate the test rig was repeated for the interlocking seal tests of this thesis. Rotordynamic coefficient results for individual cavities are frequency independent and, in this regard, disagree with the results of Childs and Elrod [7]; however, when considering the entire seal, k experiences frequency dependency and increases with increasing Ω.

Tests were conducted at ~ 167 Hz (10 krpm) with and without swirl brakes for a target preswirl ratio of 0.5. Pressure ratios of 0.5, 0.6, 0.7, and 0.8 were tested for forward and backward precession frequencies ranging from 10 – 50 Hz in 5 Hz increments. The target PSR of 0.5 was achieved relatively well, and the addition of swirl brakes decreased PSR to approximately 0.3. Pressure measurements were made in cavities (1-4) and results are presented for the separate cavities as well as net seal force coefficients.

The most notable result from the work of this thesis is the presence of negative C values which are witnessed in every cavity except cavity (3). Baumann [8] shows damping results in the form of logarithmic decrement for a compressor equipped with interlocking seals throughout the machine. His results show initially positive damping values at low discharge pressures and eventually becoming negative but at much higher pressures than the scope of this work (~250 bars with swirl brakes and ~400 bars without swirl brakes).

Values of K are predominantly negative with and without swirl brakes except for cavity (3). A clear difference is not seen in K with the addition of swirl brakes contrary to Baumann's results in which he saw a "remarkable drop of the first bending mode" in configurations with swirl brakes versus without indicating a large drop in K with swirl brakes. Results produced from the summation of reaction forces of all cavities show negative k and positive C_{eff} values indicating stabilizing behavior. The addition of swirl brakes increases stability via increased C_{eff}.

Measurements proved highly dependent on alignment and centering of the test rig. The current process of bolting the rig into place makes alignment difficult and does not allow for adjustments once it is secured in place. Previous work on the test rig was done in 2006 by Zutavern [11] in which “adapters” (jacking screws) were used to center the seal about the rotor. Building on this idea, a system similar to a milling machine in which independent axes could be moved and locked into place would be beneficial for alignment and centering of the current rig.

REFERENCES

[1] Ramirez, A.M. (2017), “Development and Validation of Test Rig for Measurements of Leakage and Rotordynamic Performance of Interlocking Gas Labyrinth Seals” Texas A&M University Turbomachinery Lab, College Station, Tx, Personal Communication.

[2] Whalen, J.K., Alvarez, E., and Palliser, L.P. (2004), "Thermoplastic Labyrinth Seals for Centrifugal Compressors." Proceedings of the Thirty-Third Turbomachinery Symposium, pp. 20-23.

[3] Williams, B.P., and Flack, R.D. (1998), "Calculation of Rotor Dynamic Coefficients for Labyrinth Seals." International Journal of Rotating Machinery 4.4, pp. 257-269.

[4] Picardo, A., and Childs, D.W. (2005), "Rotordynamic Coefficients for a Tooth-on-Stator Labyrinth Seal at 70 Bar Supply Pressures: Measurements Versus Theory and Comparisons to a Hole-Pattern Stator Seal." Journal of Engineering for Gas Turbines and Power 127, pp. 843-855.

[5] Arthur, S.P. (2015), “Measured Rotordynamic Coefficients and Leakage for a Tooth-On-Rotor Labyrinth Seal with Comparisons to a Tooth-On-Stator Labyrinth Seal,” MS Thesis, Department of Mechanical Engineering, Texas A&M University, College Station.

[6] Benckert, H., and Wachter, J. (1980), "Flow Induced Spring Coefficients of Labyrinth Seals for Application in Rotor Dynamics." NASA Conference Publication 2133, pp. 189-212.

[7] Childs, D. W., Elrod, D.A., and Hale, K. (1988), "Rotordynamic Coefficient and Leakage Test Results for Interlock and Tooth-on-Stator Labyrinth Seals." ASME International Gas Turbine Conference, pp. 296-306.

[8] Baumann, U. (1999), "Rotordynamic Stability Tests on High-Pressure Radial Compressors." Proceedings of the 28th Turbomachinery Symposium, pp. 115-122.

[9] Millsaps, K.T., and Martinez-Sanchez, M. (1994), "Dynamic Forces from Single Gland Labyrinth Seals: Part I – Ideal and Viscous Decomposition" Journal of Turbomachinery, ASME, Vol. 116, pp. 686-693.

[10] Wagner, N.G., Steff, K., Gausmann, R., and Schmidt, M. (2009). "Investigations on the Dynamic Coefficients of Impeller Eye Labyrinth Seals." Proceedings of the 38th Turbomachinery Symposium, pp. 53-70.

[11] Zutavern, Z.S. (2006), "Identification of Rotordynamic Forces in a Flexible Rotor System Using Magnetic Bearings." PhD Dissertation. Department of Mechanical Engineering, Texas A&M University, College Station.

APPENDIX A

STATIC PRESSURE MEASUREMENTS

Table A. 1. Static pressure versus cavity number without swirl brakes for 2.75 bar inlet pressure.

Target PR	Cavity	Pressure (bar)	± (bar)	Pressure (psia)	± (psia)
0.5	Pin	2.81	0.03	40.7	0.4
	1	2.77	0.00	40.1	0.0
	2	2.47	0.00	35.8	0.1
	3	2.20	0.00	31.9	0.0
	4	2.00	0.00	29.0	0.0
	Pout	1.34	0.02	19.5	0.3
0.6	Pin	2.93	0.03	42.5	0.4
	1	2.81	0.00	40.7	0.1
	2	2.60	0.00	37.7	0.0
	3	2.39	0.00	34.7	0.0
	4	2.23	0.00	32.3	0.0
	Pout	1.77	0.01	25.6	0.2
0.7	Pin	2.95	0.02	42.8	0.3
	1	2.91	0.00	42.2	0.1
	2	2.72	0.00	39.4	0.1
	3	2.53	0.01	36.7	0.1
	4	2.39	0.00	34.6	0.0
	Pout	2.01	0.03	29.1	0.4
0.8	Pin	2.66	0.01	38.6	0.1
	1	2.66	0.00	38.6	0.1
	2	2.54	0.00	36.8	0.1
	3	2.43	0.00	35.2	0.0
	4	2.34	0.00	34.0	0.0
	Pout	2.06	0.02	29.8	0.2

Table A. 2. Static pressure versus cavity number without swirl brakes for 3.79 bar inlet pressure.

Target PR	Cavity	Pressure (bar)	± (bar)	Pressure (psia)	± (psia)
0.5	Pin	3.82	0.01	55.4	0.2
	1	3.70	0.01	53.7	0.1
	2	3.35	0.00	48.5	0.1
	3	2.99	0.00	43.4	0.1
	4	2.69	0.01	39.1	0.1
	Pout	1.79	0.01	26.0	0.2
0.6	Pin	3.53	0.01	51.2	0.2
	1	3.52	0.00	51.0	0.0
	2	3.26	0.00	47.3	0.1
	3	3.01	0.01	43.6	0.1
	4	2.81	0.00	40.7	0.0
	Pout	2.19	0.02	31.7	0.2
0.7	Pin	3.88	0.02	56.3	0.3
	1	3.93	0.00	57.0	0.1
	2	3.70	0.01	53.6	0.1
	3	3.47	0.01	50.4	0.1
	4	3.30	0.01	47.8	0.1
	Pout	2.71	0.02	39.4	0.3
0.8	Pin	3.73	0.03	54.1	0.4
	1	3.84	0.01	55.7	0.1
	2	3.66	0.01	53.1	0.1
	3	3.49	0.00	50.6	0.1
	4	3.36	0.01	48.7	0.1
	Pout	2.86	0.03	41.5	0.4

Table A. 3. Static pressure versus cavity number without swirl brakes for 4.83 bar inlet pressure.

Target PR	Cavity	Pressure (bar)	± (bar)	Pressure (psia)	± (psia)
0.5	Pin	4.73	0.06	68.6	0.8
	1	4.67	0.01	67.7	0.1
	2	4.21	0.01	61.1	0.1
	3	3.78	0.01	54.8	0.1
	4	3.41	0.00	49.5	0.1
	Pout	2.38	0.03	34.6	0.4
0.6	Pin	4.69	0.03	68.1	0.4
	1	4.65	0.01	67.5	0.1
	2	4.30	0.01	62.4	0.1
	3	3.95	0.01	57.3	0.1
	4	3.69	0.01	53.5	0.1
	Pout	2.87	0.02	41.6	0.3
0.7	Pin	5.3	0.2	76	3
	1	4.93	0.01	71.5	0.1
	2	4.75	0.01	68.9	0.1
	3	4.55	0.01	66.0	0.1
	4	4.41	0.01	64.0	0.2
	Pout	3.7	0.1	53	2
0.8	Pin	4.69	0.02	68.0	0.3
	1	4.76	0.01	69.1	0.1
	2	4.54	0.01	65.9	0.1
	3	4.32	0.00	62.6	0.1
	4	4.16	0.01	60.3	0.1
	Pout	3.58	0.03	51.9	0.4

Table A. 4. Static pressure versus cavity number with swirl brakes for 2.75 bar inlet pressure.

Target PR	Cavity	Pressure (bar)	± (bar)	Pressure (psia)	± (psia)
0.5	Pin	2.90	0.01	42.1	0.1
	1	2.86	0.00	41.5	0.1
	2	2.61	0.00	37.8	0.0
	3	2.37	0.00	34.3	0.0
	4	2.14	0.00	31.1	0.0
	Pout	1.51	0.00	21.9	0.1
0.6	Pin	2.93	0.01	42.4	0.2
	1	2.91	0.00	42.3	0.1
	2	2.71	0.00	39.3	0.1
	3	2.51	0.00	36.4	0.0
	4	2.32	0.01	33.6	0.1
	Pout	1.80	0.01	26.1	0.1
0.7	Pin	3.03	0.01	44.0	0.2
	1	3.06	0.00	44.4	0.1
	2	2.90	0.00	42.0	0.0
	3	2.73	0.00	39.6	0.1
	4	2.58	0.00	37.4	0.0
	Pout	2.13	0.01	30.9	0.1
0.8	Pin	2.93	0.01	42.5	0.1
	1	2.98	0.00	43.3	0.1
	2	2.85	0.00	41.3	0.1
	3	2.71	0.01	39.3	0.1
	4	2.59	0.00	37.5	0.1
	Pout	2.20	0.01	31.9	0.1

Table A. 5. Static pressure versus cavity number with swirl brakes for 3.79 bar inlet pressure.

Target PR	Cavity	Pressure (bar)	± (bar)	Pressure (psia)	± (psia)
0.5	Pin	3.72	0.02	53.9	0.3
	1	3.65	0.00	52.9	0.1
	2	3.32	0.00	48.1	0.1
	3	2.99	0.00	43.4	0.0
	4	2.68	0.00	38.9	0.0
	Pout	1.84	0.01	26.7	0.1
0.6	Pin	3.66	0.02	53.1	0.3
	1	3.64	0.00	52.8	0.0
	2	3.37	0.00	48.9	0.1
	3	3.11	0.00	45.1	0.1
	4	2.87	0.01	41.7	0.1
	Pout	2.22	0.01	32.3	0.1
0.7	Pin	4.0	0.1	58	1
	1	3.83	0.00	55.6	0.0
	2	3.68	0.01	53.3	0.1
	3	3.54	0.01	51.4	0.1
	4	3.40	0.00	49.3	0.1
	Pout	2.76	0.05	40.0	0.7
0.8	Pin	3.75	0.02	54.4	0.3
	1	3.81	0.01	55.2	0.1
	2	3.62	0.00	52.5	0.1
	3	3.43	0.00	49.8	0.1
	4	3.27	0.00	47.4	0.1
	Pout	2.78	0.01	40.3	0.2

Table A. 6. Static pressure versus cavity number with swirl brakes for 4.83 bar inlet pressure.

Target PR	Cavity	Pressure (bar)	± (bar)	Pressure (psia)	± (psia)
0.5	Pin	5.0	0.1	73	2
	1	4.76	0.01	69.1	0.1
	2	4.59	0.01	66.6	0.1
	3	4.11	0.00	59.7	0.1
	4	3.67	0.00	53.3	0.1
	Pout	2.48	0.05	36.0	0.7
0.6	Pin	5.0	0.1	72	2
	1	4.77	0.01	69.2	0.1
	2	4.42	0.00	64.2	0.1
	3	4.08	0.00	59.1	0.1
	4	3.85	0.01	55.8	0.1
	Pout	3.04	0.07	44.0	1.0
0.7	Pin	5.0	0.1	72	2
	1	4.81	0.01	69.8	0.1
	2	4.53	0.00	65.8	0.1
	3	4.26	0.01	61.8	0.1
	4	4.14	0.01	60.0	0.1
	Pout	3.5	0.1	51	1
0.8	Pin	4.92	0.05	71.3	0.7
	1	4.94	0.01	71.7	0.1
	2	4.69	0.01	68.0	0.1
	3	4.42	0.01	64.2	0.1
	4	4.20	0.01	60.9	0.1
	Pout	3.60	0.04	52.1	0.5

APPENDIX B
DYNAMIC PRESSURE PHASE AND AMPLITUDE MEASUREMENTS

Legend entries indicate pressure sensor number, and the location of the sensors are seen in Figs. 15-16.

B.1 Without Swirl Brakes

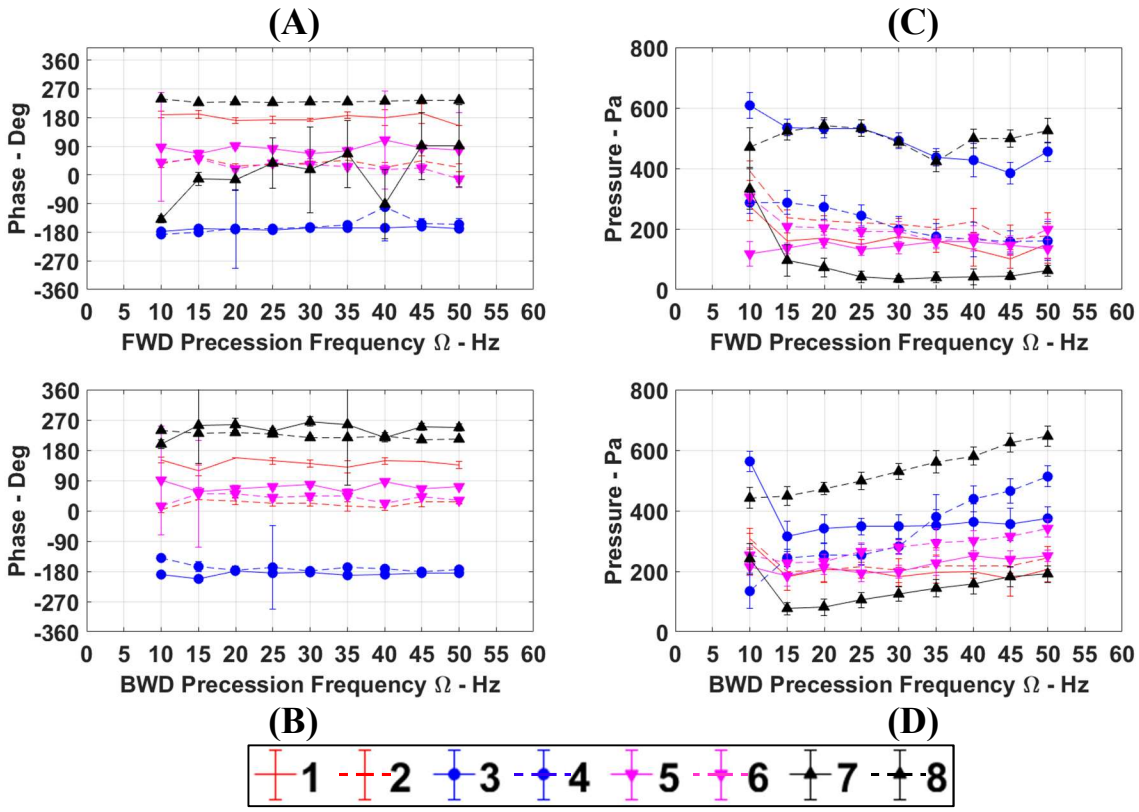

Figure B. 1. Dynamic pressure phase versus forward (A) and backward (B) precession frequency and dynamic pressure amplitude versus forward (C) and backward (D) precession frequency for each sensor at 2.75 bar inlet pressure and a 0.5 pressure ratio.

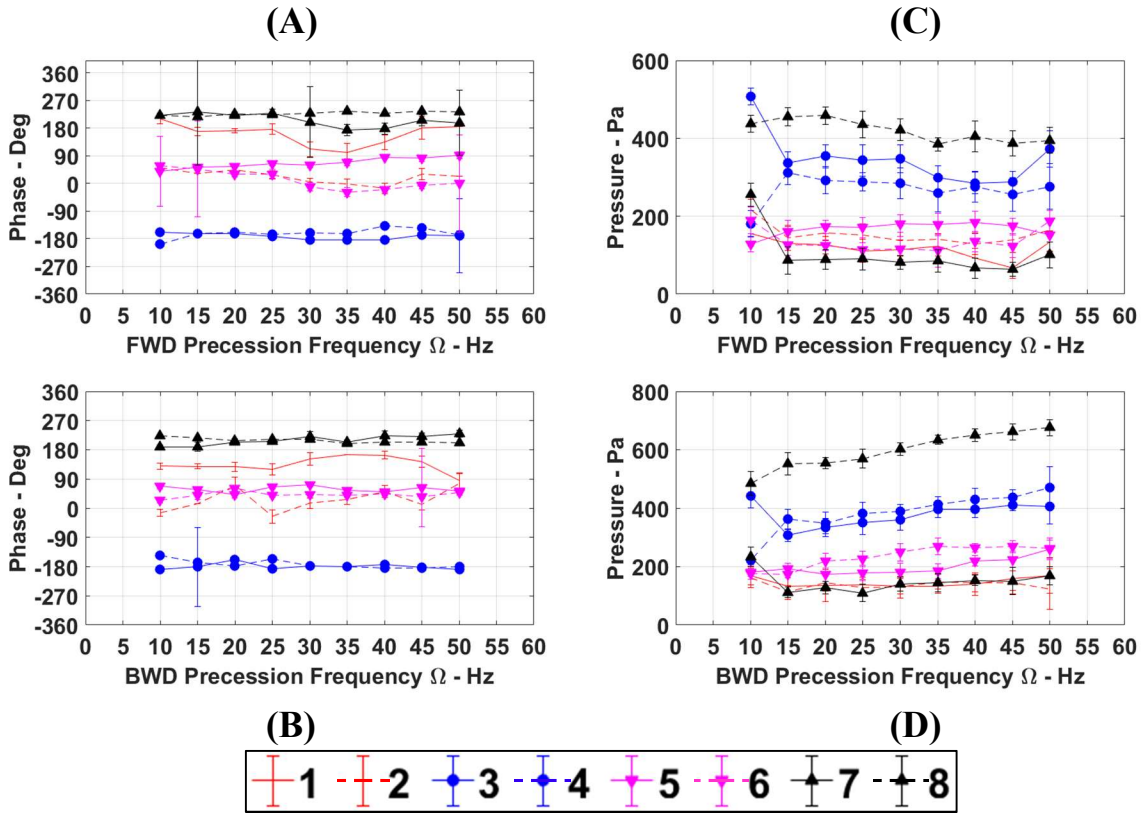

Figure B. 2. Dynamic pressure phase versus forward (A) and backward (B) precession frequency and dynamic pressure amplitude versus forward (C) and backward (D) precession frequency for each sensor at 2.7 5 bar inlet pressure and a 0.6 pressure ratio.

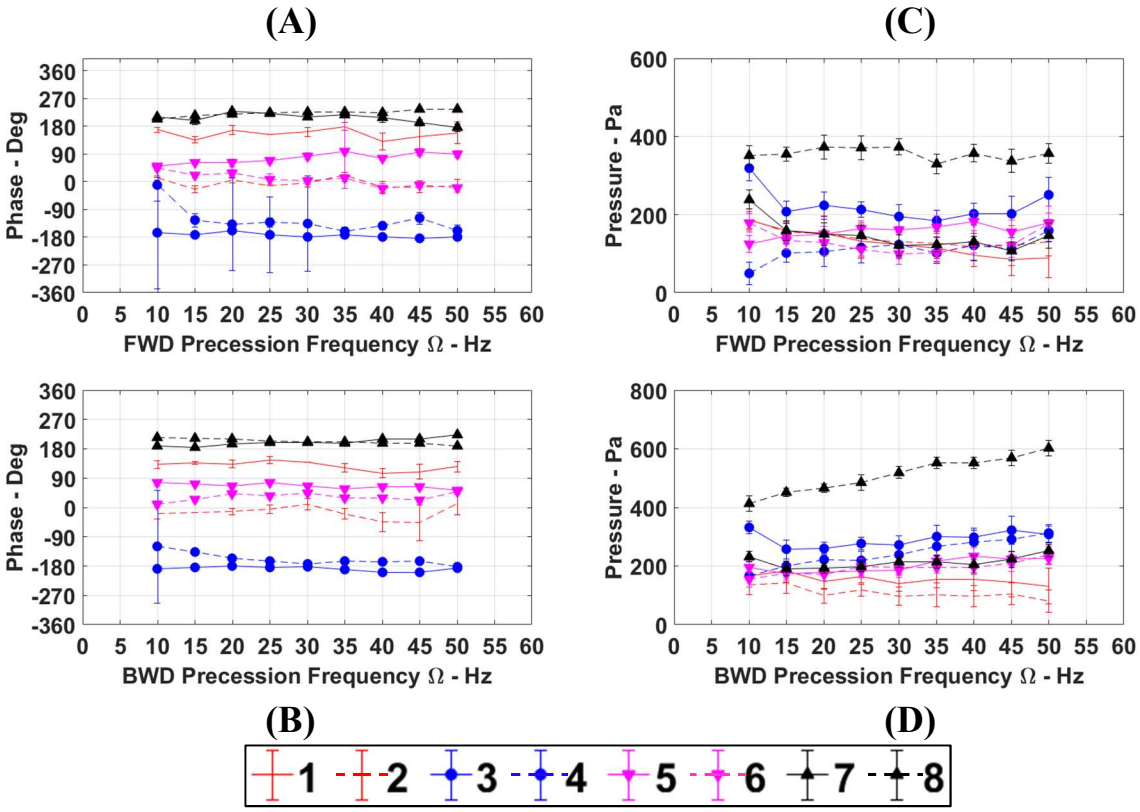

Figure B. 3. Dynamic pressure phase versus forward (A) and backward (B) precession frequency and dynamic pressure amplitude versus forward (C) and backward (D) precession frequency for each sensor at 2.75 bar inlet pressure and a 0.7 pressure ratio.

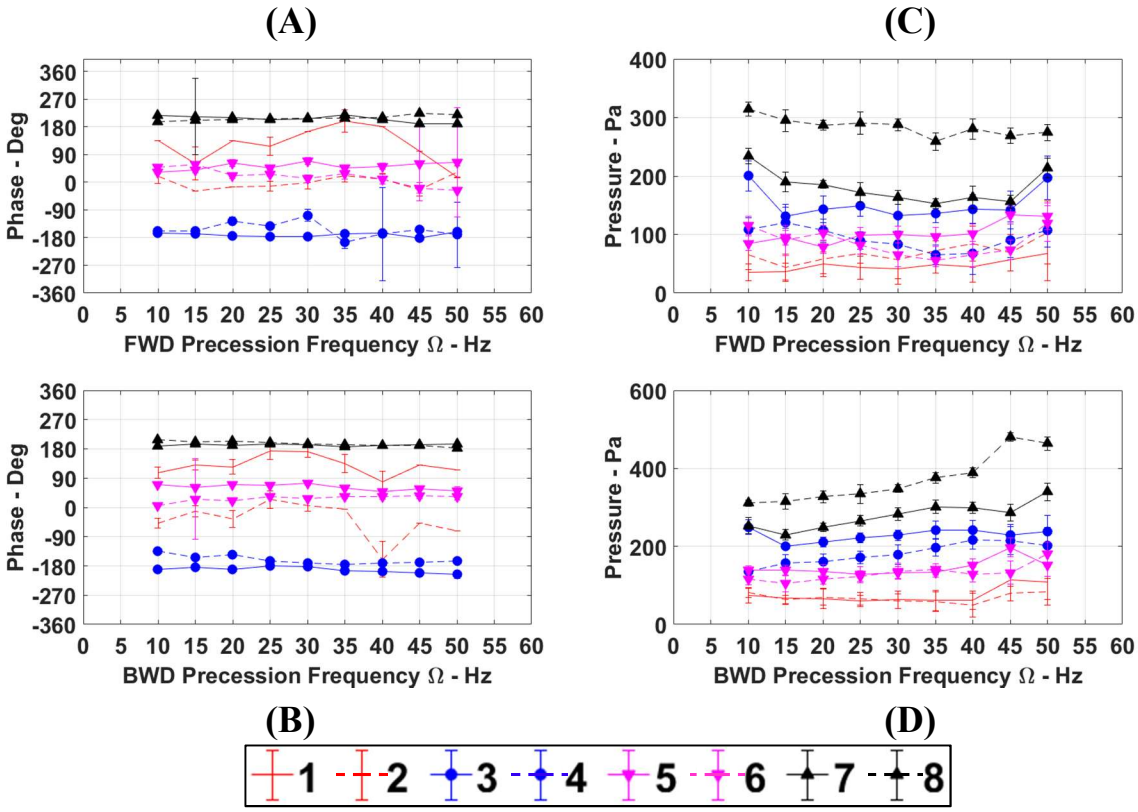

Figure B. 4. Dynamic pressure phase versus forward (A) and backward (B) precession frequency and dynamic pressure amplitude versus forward (C) and backward (D) precession frequency for each sensor at 2.75 bar inlet pressure and a 0.8 pressure ratio.

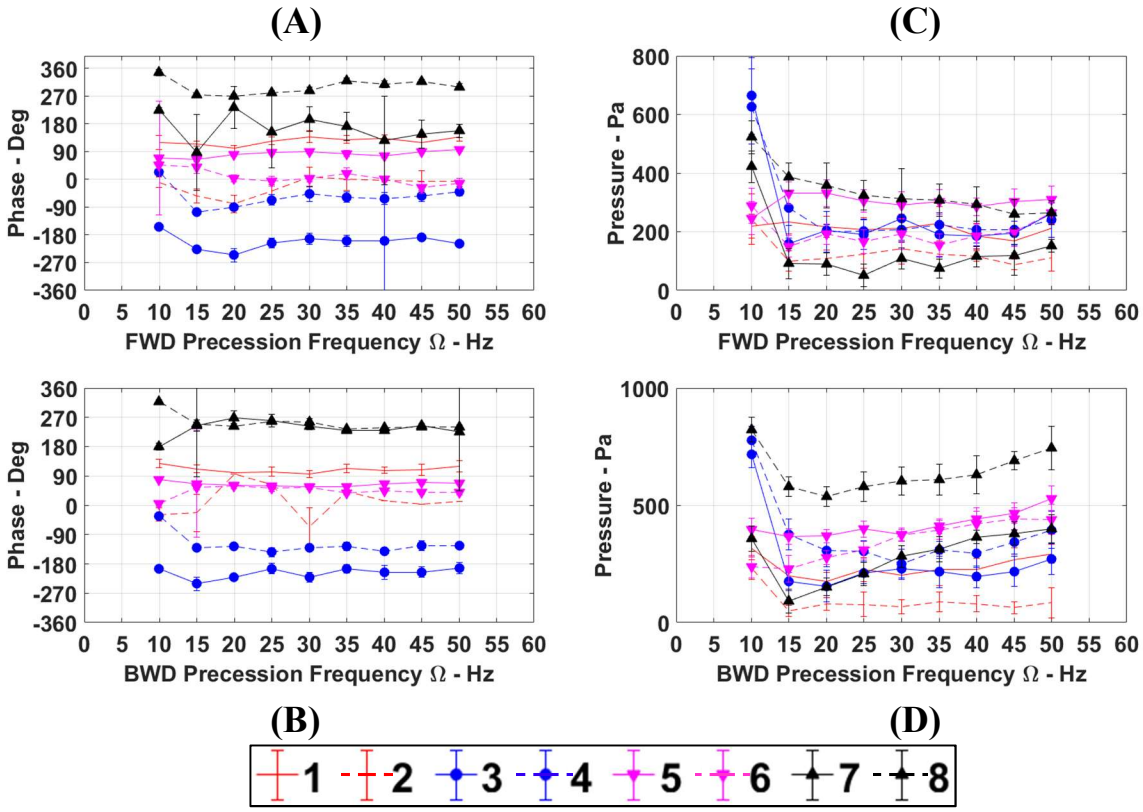

Figure B. 5. Dynamic pressure phase versus forward (A) and backward (B) precession frequency and dynamic pressure amplitude versus forward (C) and backward (D) precession frequency for each sensor at 3.79 bar inlet pressure and a 0.5 pressure ratio.

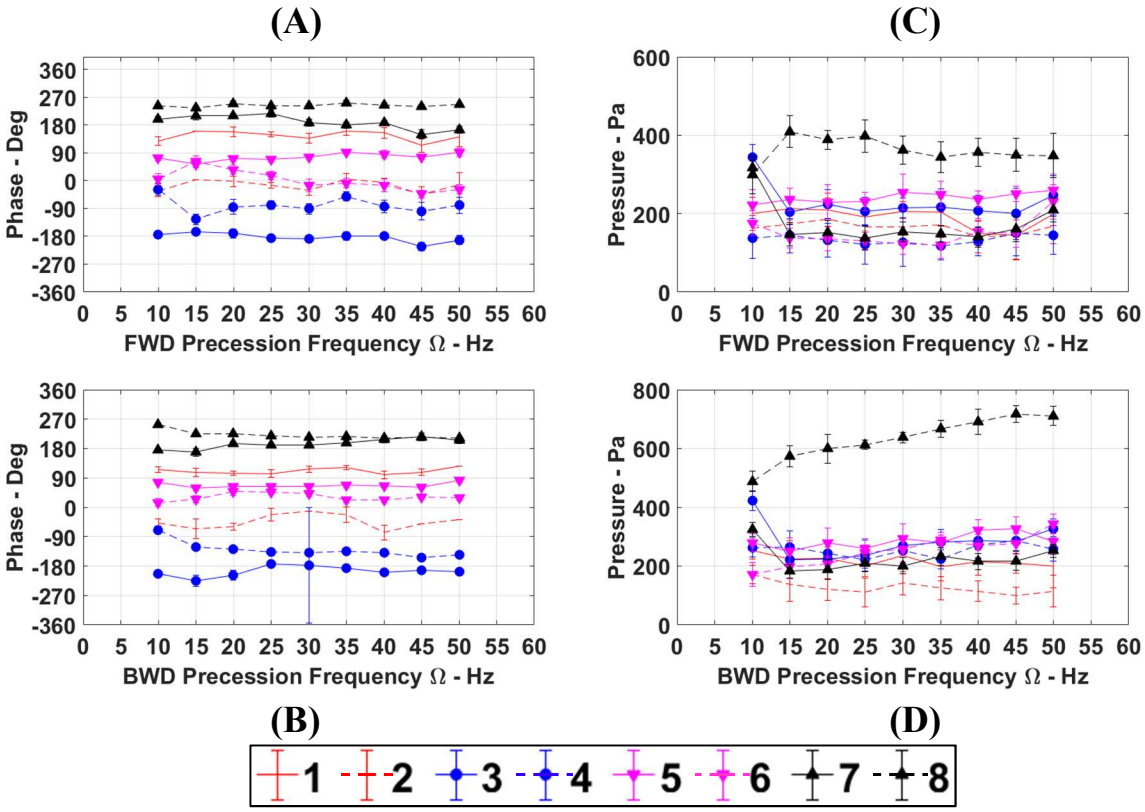

Figure B. 6. Dynamic pressure phase versus forward (A) and backward (B) precession frequency and dynamic pressure amplitude versus forward (C) and backward (D) precession frequency for each sensor at 3.79 bar inlet pressure and a 0.6 pressure ratio.

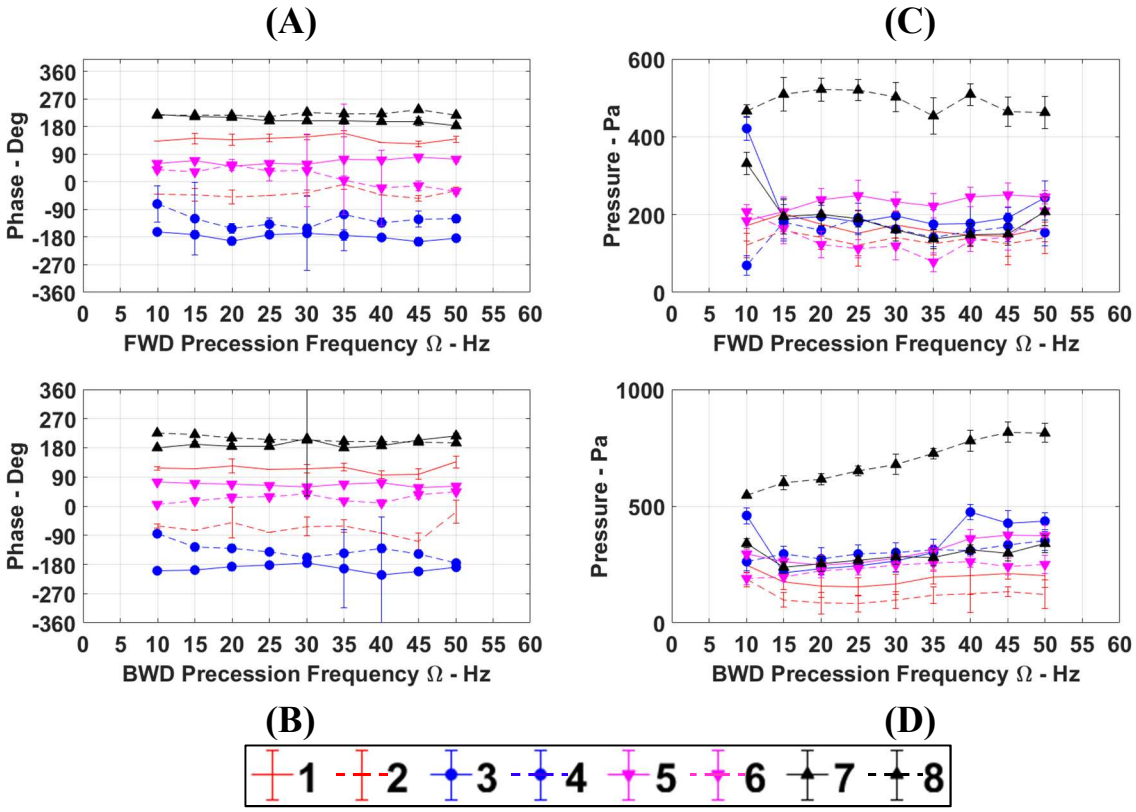

Figure B. 7. Dynamic pressure phase versus forward (A) and backward (B) precession frequency and dynamic pressure amplitude versus forward (C) and backward (D) precession frequency for each sensor at 3.79 bar inlet pressure and a 0.7 pressure ratio.

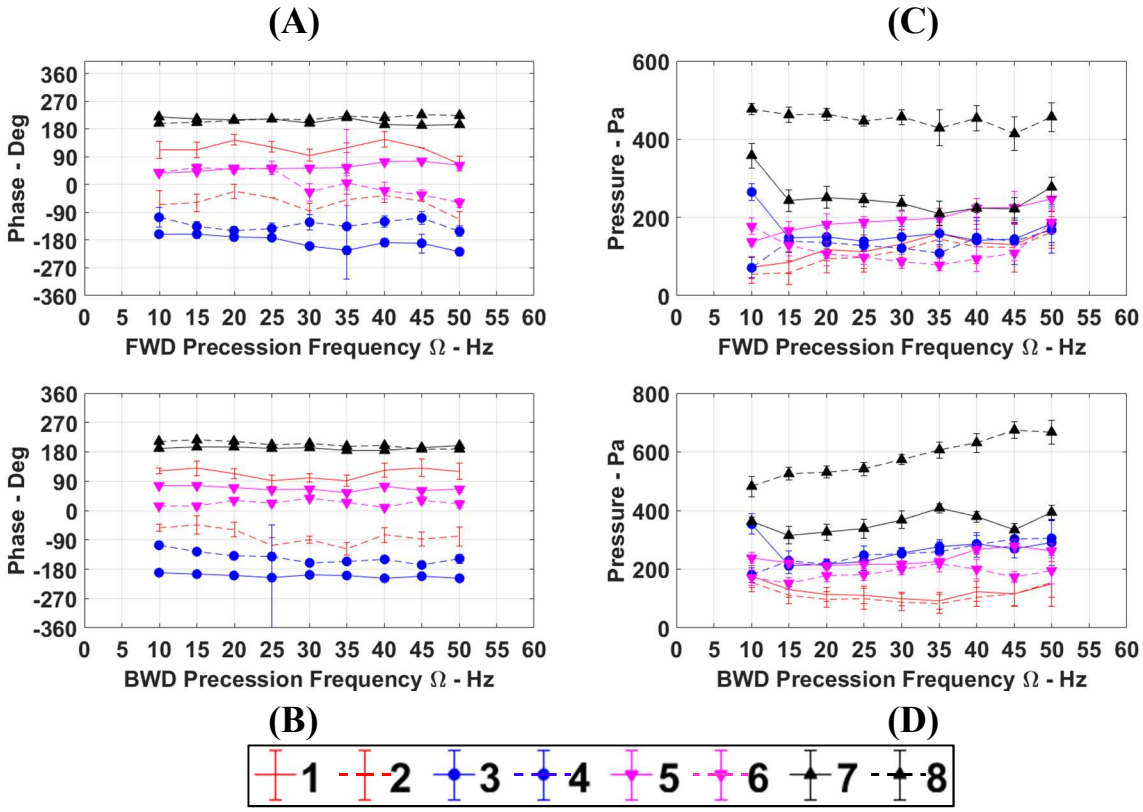

Figure B. 8. Dynamic pressure phase versus forward (A) and backward (B) precession frequency and dynamic pressure amplitude versus forward (C) and backward (D) precession frequency for each sensor at 3.79 bar inlet pressure and a 0.8 pressure ratio.

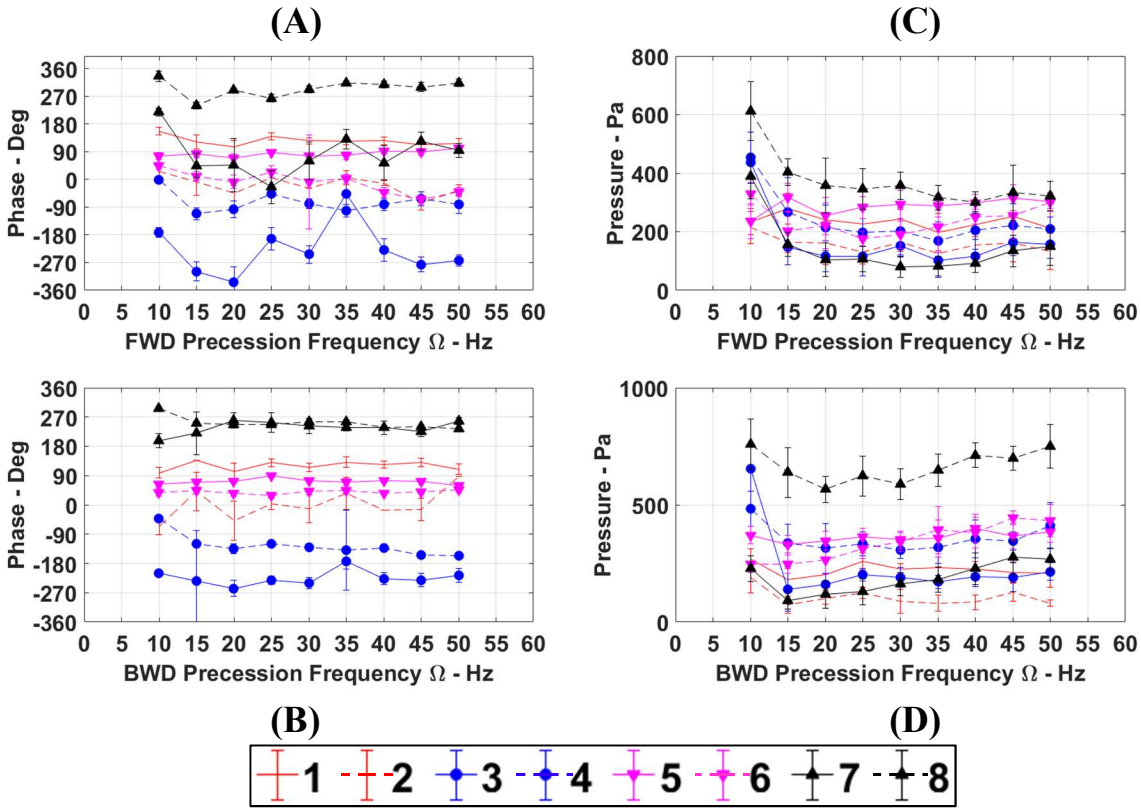

Figure B. 9. Dynamic pressure phase versus forward (A) and backward (B) precession frequency and dynamic pressure amplitude versus forward (C) and backward (D) precession frequency for each sensor at 4.83 bar inlet pressure and a 0.5 pressure ratio.

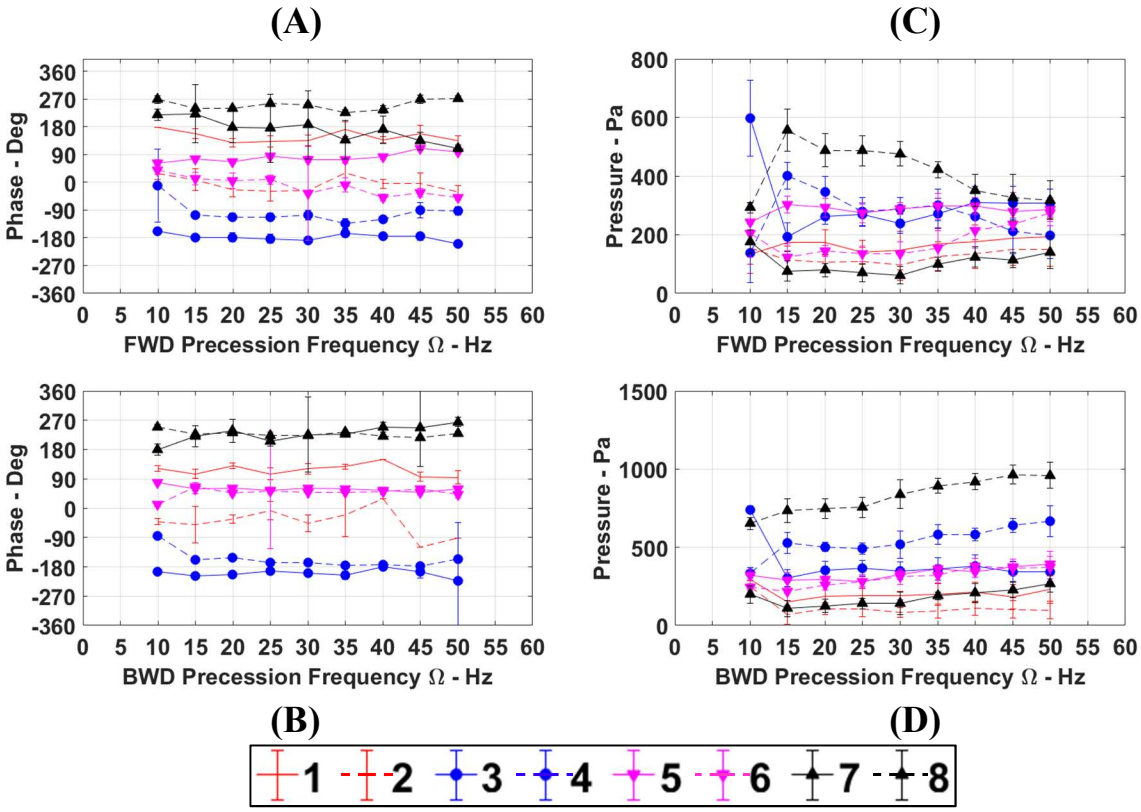

Figure B. 10. Dynamic pressure phase versus forward (A) and backward (B) precession frequency and dynamic pressure amplitude versus forward (C) and backward (D) precession frequency for each sensor at 4.83 bar inlet pressure and a 0.6 pressure ratio.

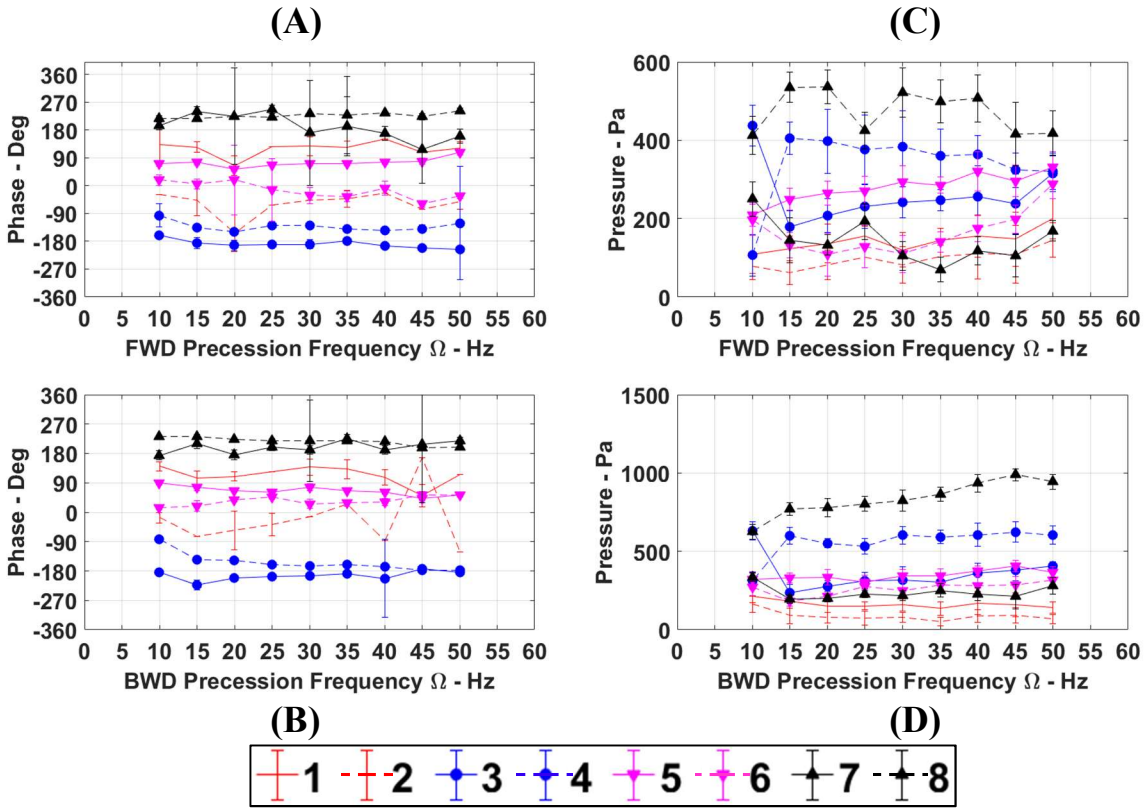

Figure B. 11. Dynamic pressure phase versus forward (A) and backward (B) precession frequency and dynamic pressure amplitude versus forward (C) and backward (D) precession frequency for each sensor at 4.83 bar inlet pressure and a 0.7 pressure ratio.

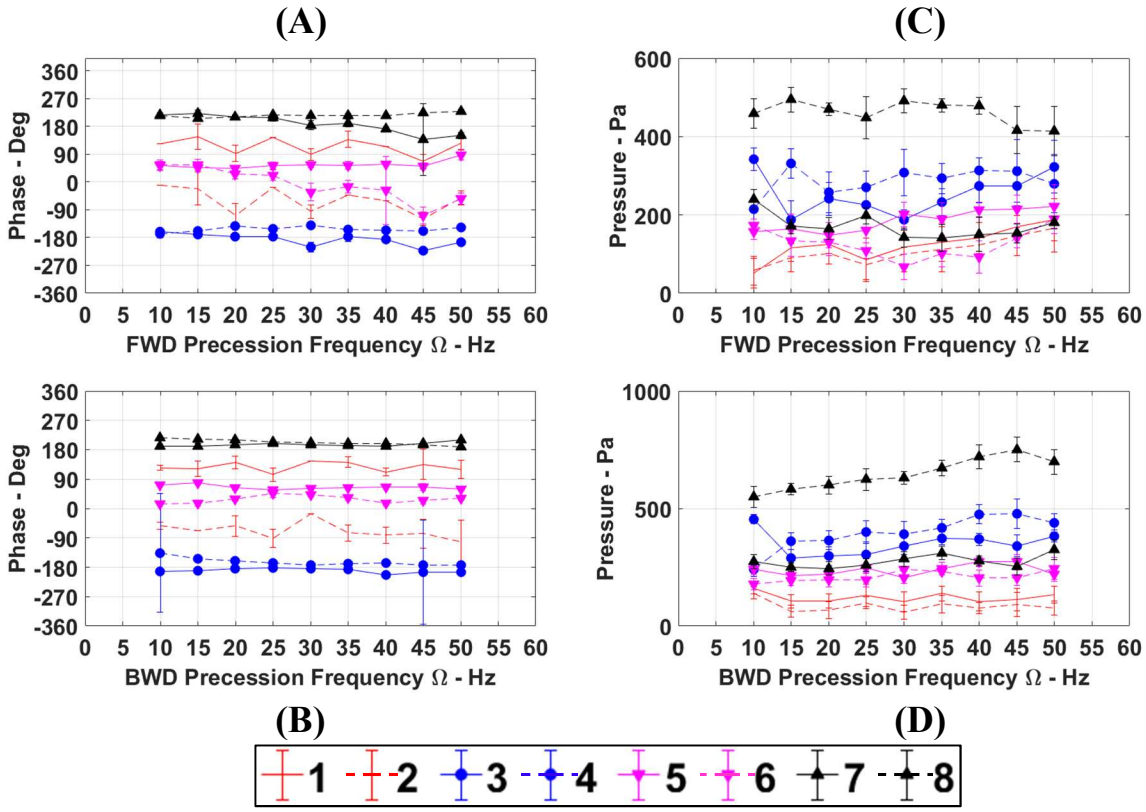

Figure B. 12. Dynamic pressure phase versus forward (A) and backward (B) precession frequency and dynamic pressure amplitude versus forward (C) and backward (D) precession frequency for each sensor at 4.83 bar inlet pressure and a 0.8 pressure ratio.

B.2 With Swirl Brakes

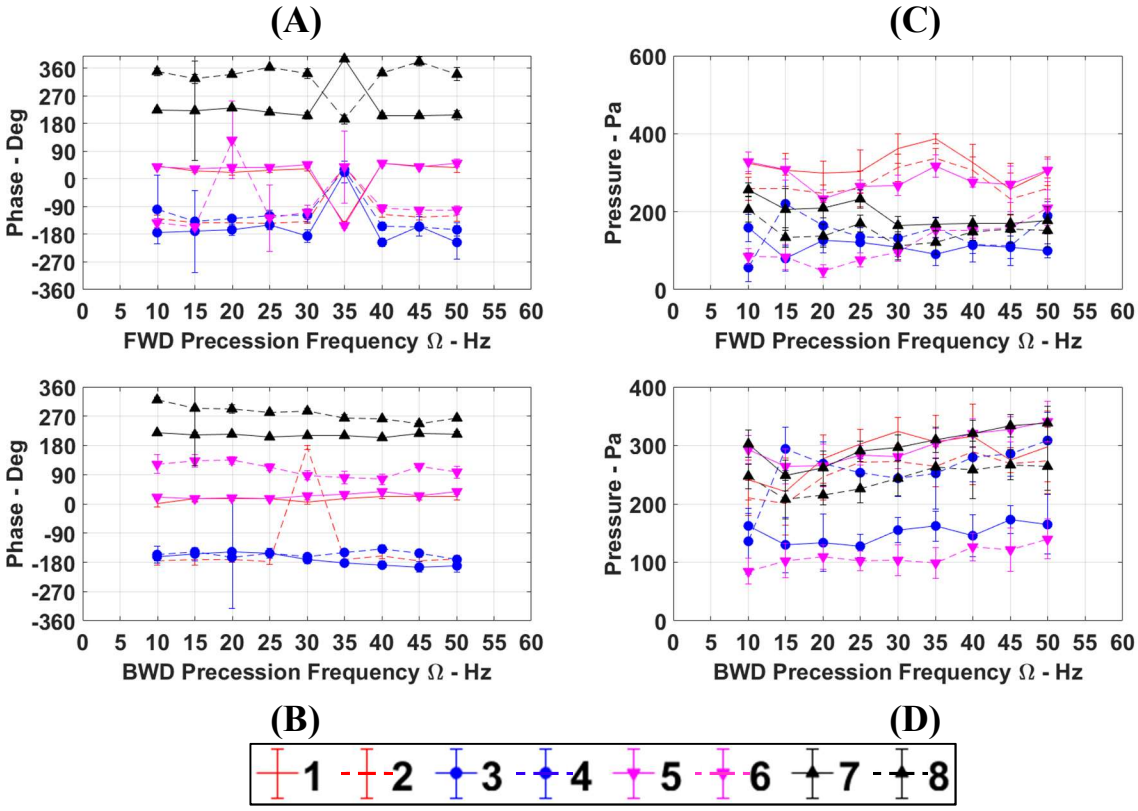

Figure B. 13. Dynamic pressure phase versus forward (A) and backward (B) precession frequency and dynamic pressure amplitude versus forward (C) and backward (D) precession frequency for each sensor at 2.75 bar inlet pressure and a 0.5 pressure ratio.

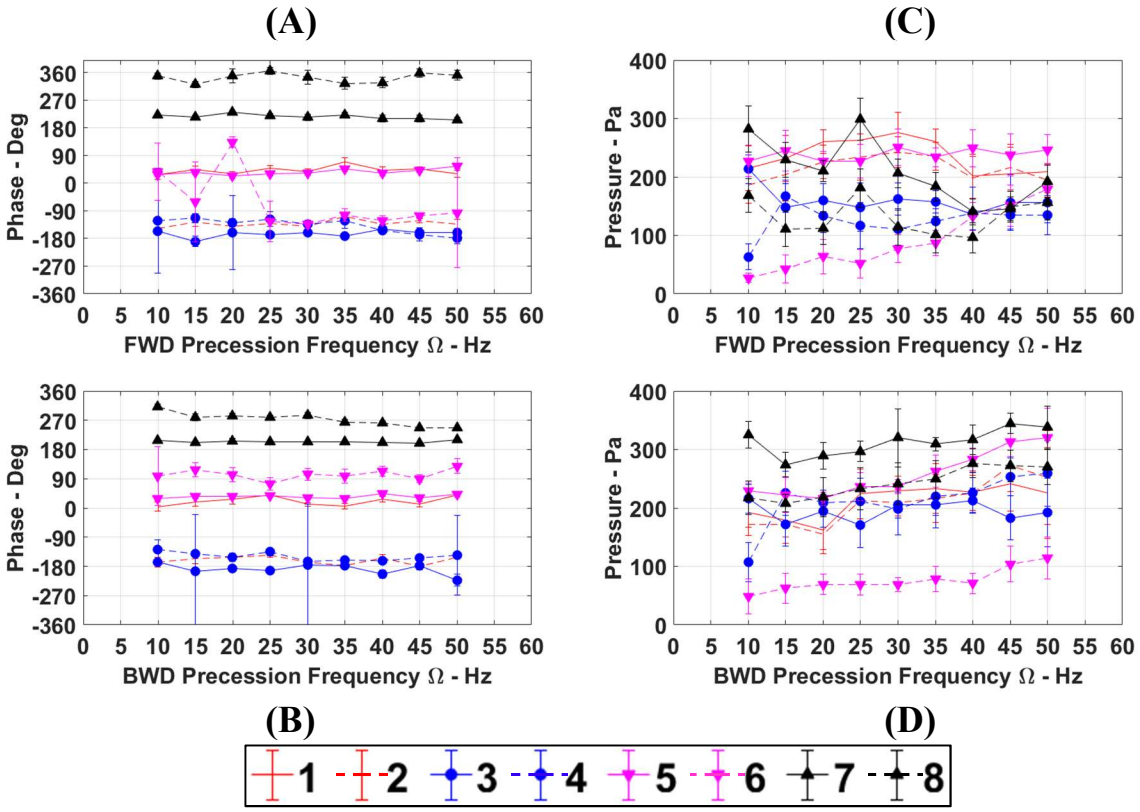

Figure B. 14. Dynamic pressure phase versus forward (A) and backward (B) precession frequency and dynamic pressure amplitude versus forward (C) and backward (D) precession frequency for each sensor at 2.75 bar inlet pressure and a 0.6 pressure ratio.

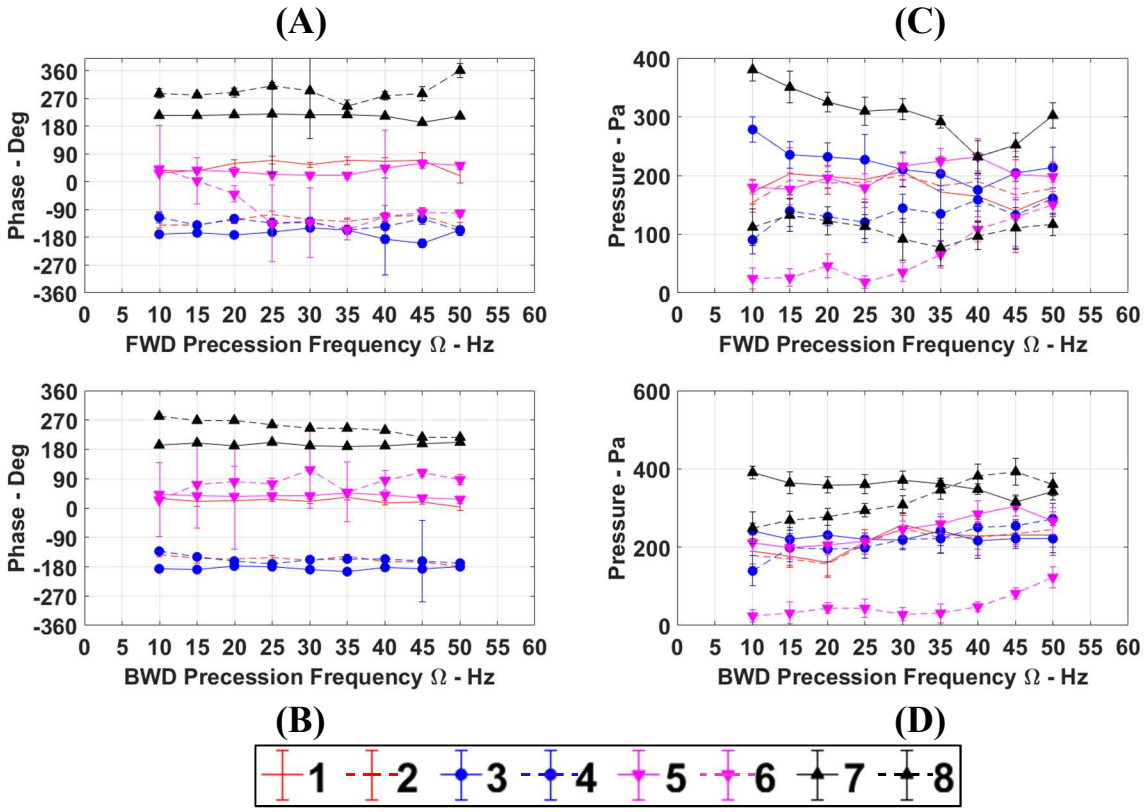

Figure B. 15. Dynamic pressure phase versus forward (A) and backward (B) precession frequency and dynamic pressure amplitude versus forward (C) and backward (D) precession frequency for each sensor at 2.75 bar inlet pressure and a 0.7 pressure ratio.

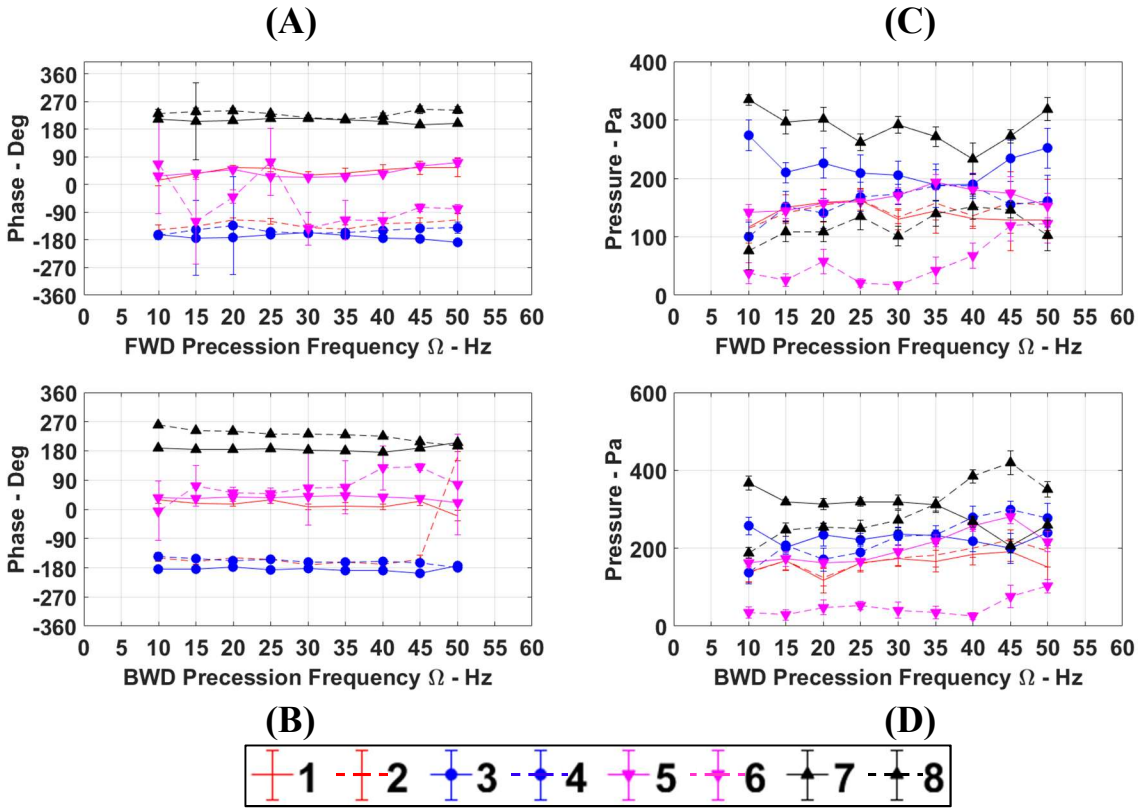

Figure B. 16. Dynamic pressure phase versus forward (A) and backward (B) precession frequency and dynamic pressure amplitude versus forward (C) and backward (D) precession frequency for each sensor at 2.75 bar inlet pressure and a 0.8 pressure ratio.

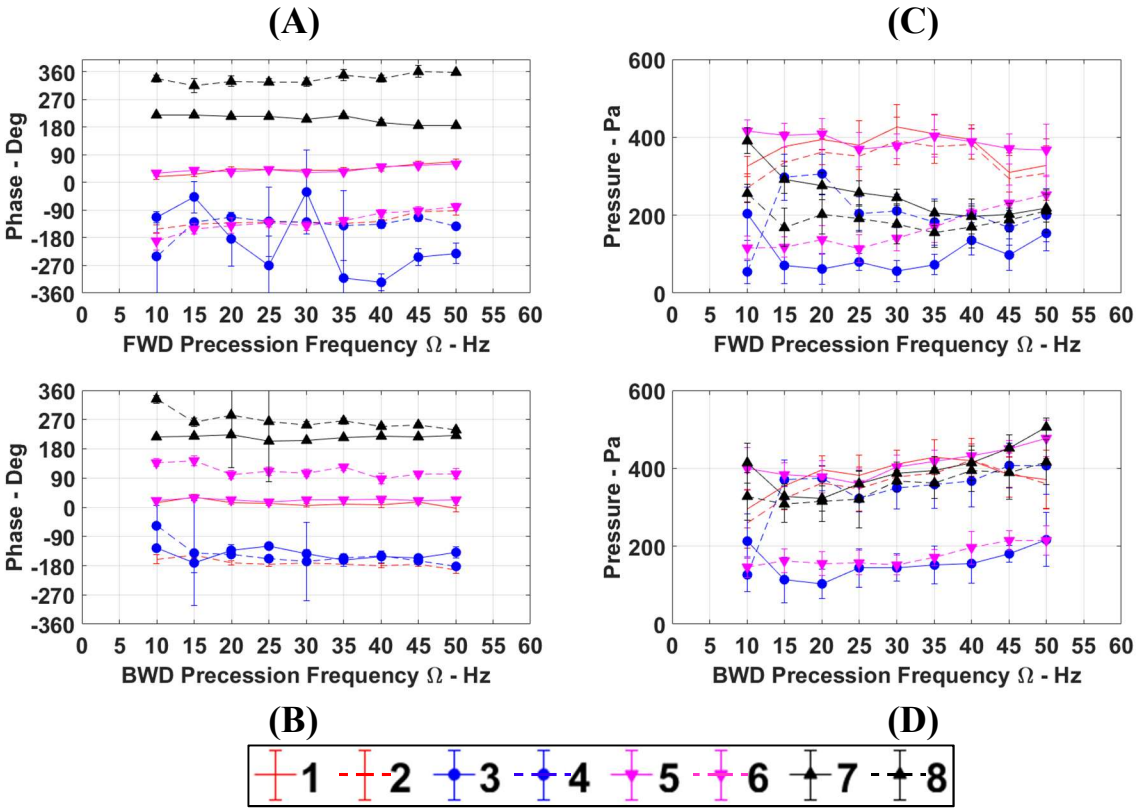

Figure B. 17. Dynamic pressure phase versus forward (A) and backward (B) precession frequency and dynamic pressure amplitude versus forward (C) and backward (D) precession frequency for each sensor at 3.79 bar inlet pressure and a 0.5 pressure ratio.

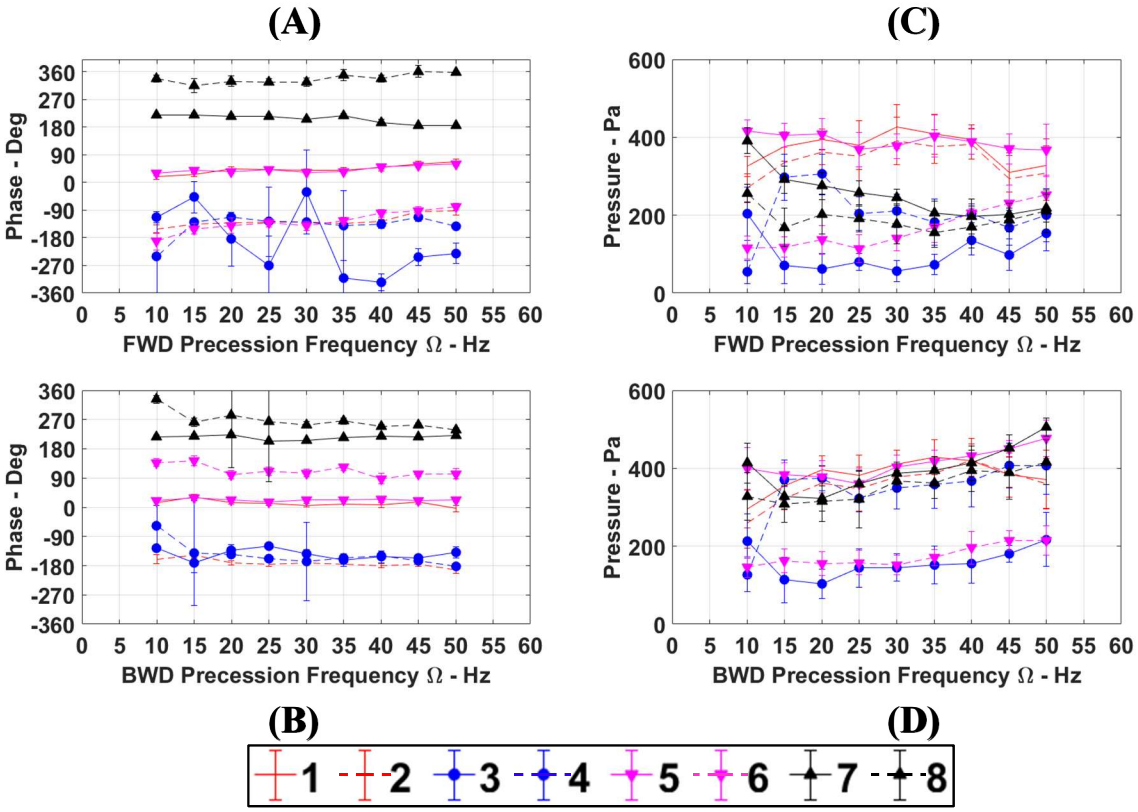

Figure B. 18. Dynamic pressure phase versus forward (A) and backward (B) precession frequency and dynamic pressure amplitude versus forward (C) and backward (D) precession frequency for each sensor at 3.79 bar inlet pressure and a 0.6 pressure ratio.

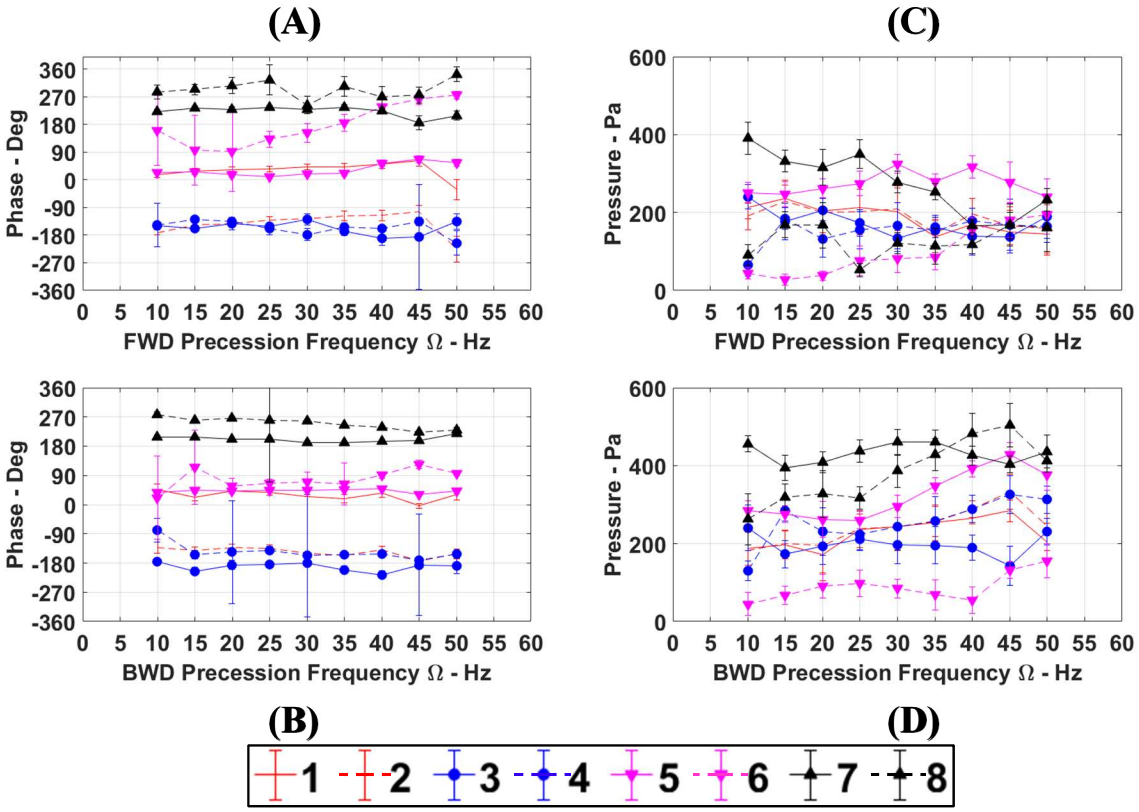

Figure B. 19. Dynamic pressure phase versus forward (A) and backward (B) precession frequency and dynamic pressure amplitude versus forward (C) and backward (D) precession frequency for each sensor at 3.79 bar inlet pressure and a 0.7 pressure ratio.

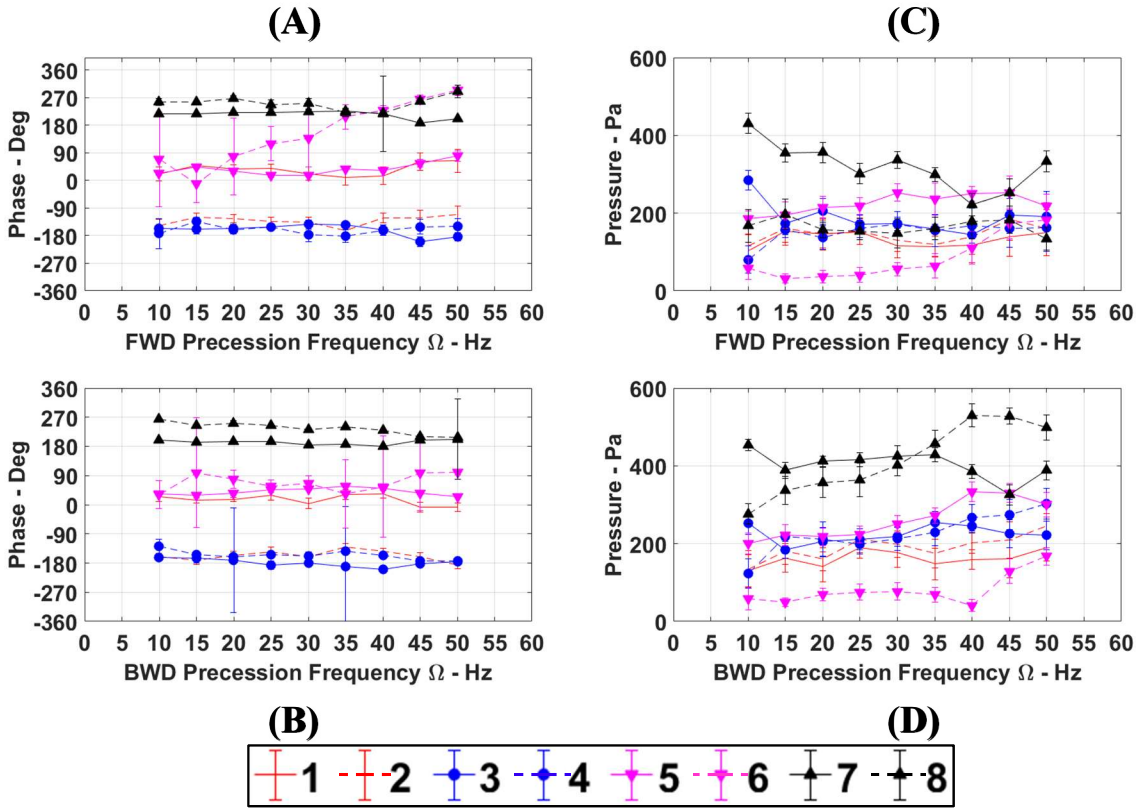

Figure B. 20. Dynamic pressure phase versus forward (A) and backward (B) precession frequency and dynamic pressure amplitude versus forward (C) and backward (D) precession frequency for each sensor at 3.79 bar inlet pressure and a 0.8 pressure ratio.

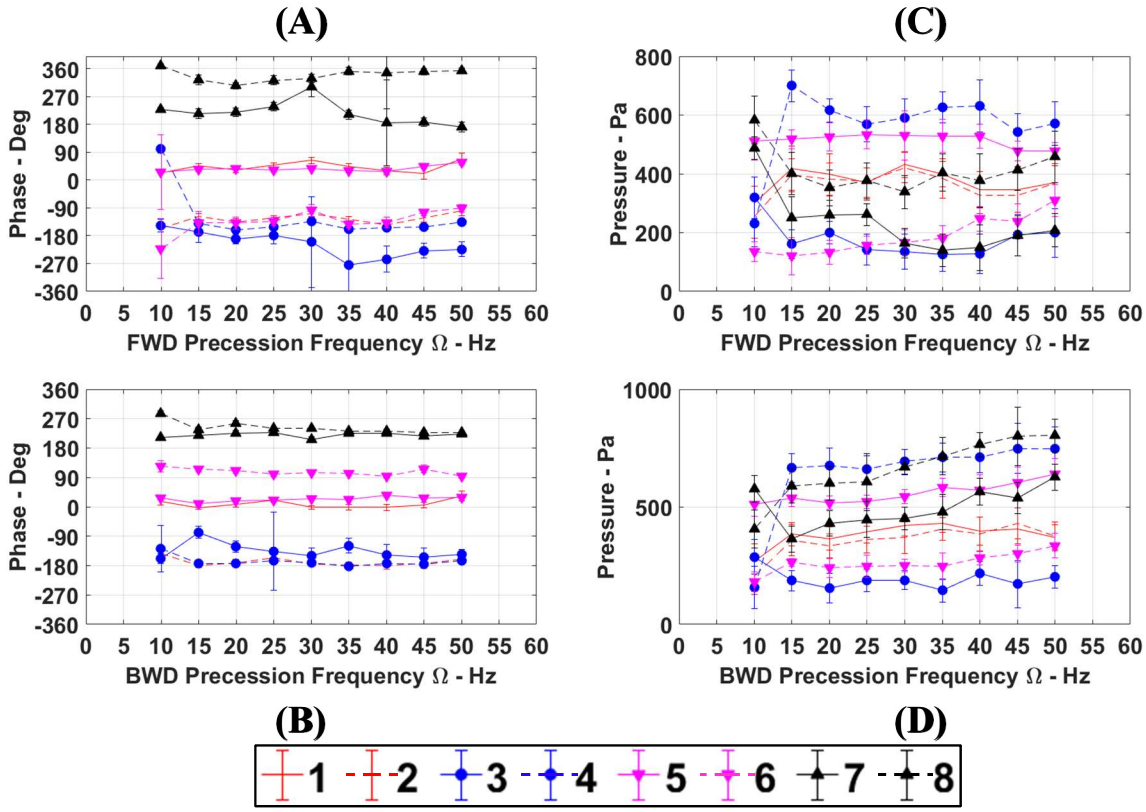

Figure B. 21. Dynamic pressure phase versus forward (A) and backward (B) precession frequency and dynamic pressure amplitude versus forward (C) and backward (D) precession frequency for each sensor at 4.83 bar inlet pressure and a 0.5 pressure ratio.

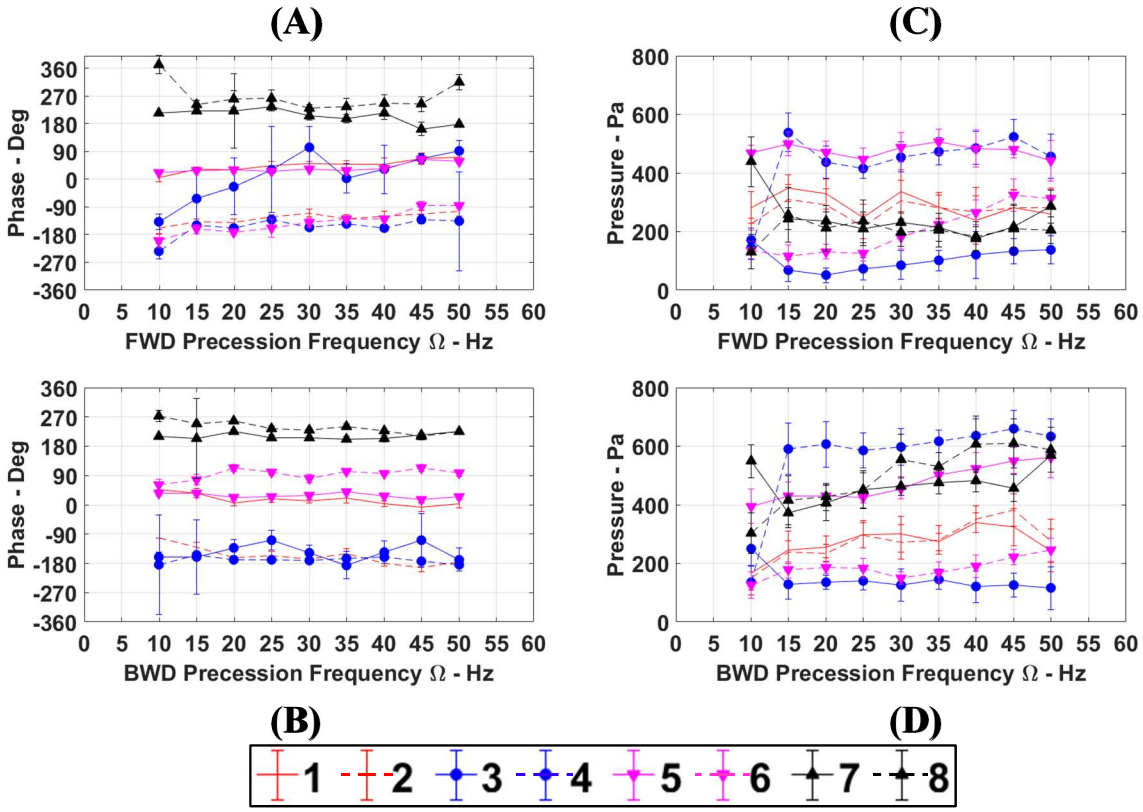

Figure B. 22. Dynamic pressure phase versus forward (A) and backward (B) precession frequency and dynamic pressure amplitude versus forward (C) and backward (D) precession frequency for each sensor at 4.83 bar inlet pressure and a 0.6 pressure ratio.

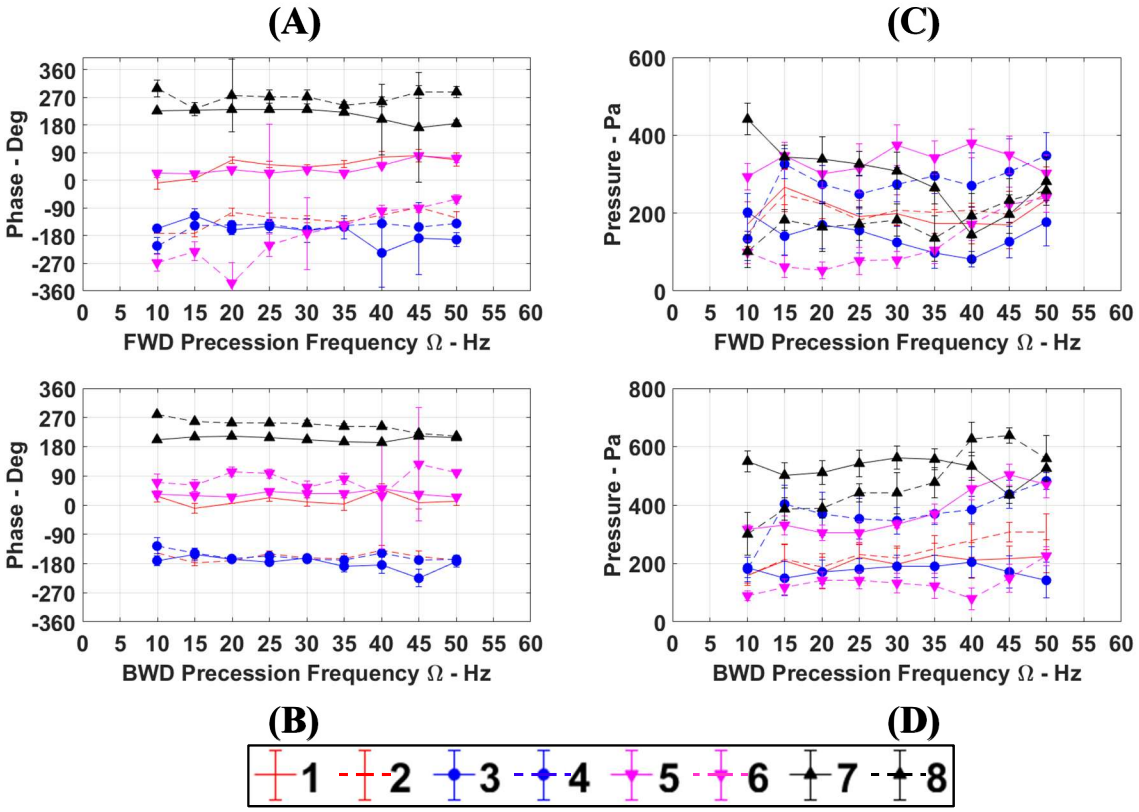

Figure B. 23. Dynamic pressure phase versus forward (A) and backward (B) precession frequency and dynamic pressure amplitude versus forward (C) and backward (D) precession frequency for each sensor at 4.83 bar inlet pressure and a 0.7 pressure ratio.

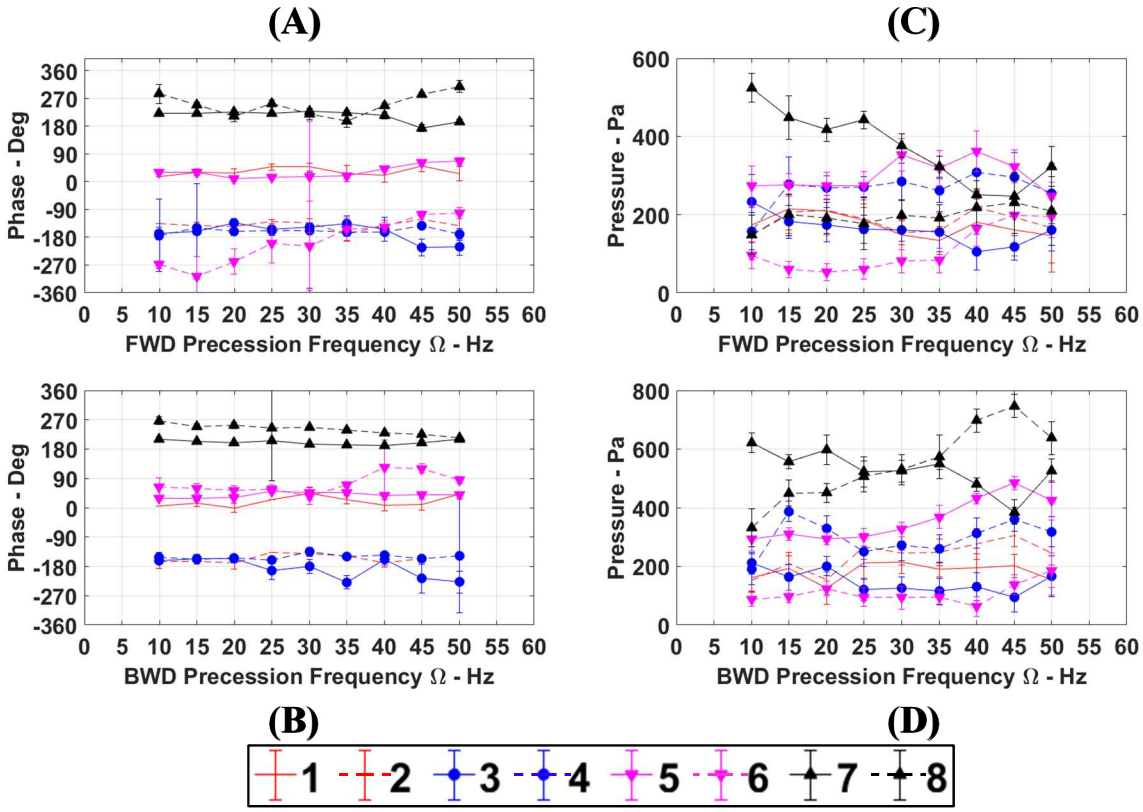

Figure B. 24. Dynamic pressure phase versus forward (A) and backward (B) precession frequency and dynamic pressure amplitude versus forward (C) and backward (D) precession frequency for each sensor at 4.83 bar inlet pressure and a 0.8 pressure ratio.

APPENDIX C

DYNAMIC FORCE VALUES

Table C. 1. F_θ/e_0 (kN/m) for each forward precession frequency at 3.79 bar inlet pressure without swirl brakes.

Cavity Number	Target PR	Precession Frequency (Hz)								
		10	15	20	25	30	35	40	45	50
Σ(1 - 4)	0.5	7 ± 21	-3 ± 12	2 ± 12	-3 ± 11	0 ± 19	4 ± 17	4 ± 10	6 ± 18	4 ± 11
	0.6	-4 ± 9	-7 ± 9	-7 ± 12	-6 ± 9	-3 ± 11	-3 ± 12	-7 ± 13	-3 ± 13	1 ± 20
	0.7	-10 ± 12	-9 ± 10	-4 ± 14	-6 ± 13	-8 ± 6	-8 ± 9	-9 ± 6	-10 ± 12	-8 ± 10
	0.8	-12 ± 15	-5 ±11	-5 ± 11	-8 ± 9	-7 ± 13	-8 ± 11	-8 ± 14	-9 ± 11	-12 ± 12
1	0.5	5 ± 7	4 ± 3	5 ± 2	3 ± 3	6 ± 6	4 ± 5	5 ± 2	5 ± 6	5 ± 3
	0.6	3 ± 2	2 ± 1	3 ± 4	2 ± 2	2 ± 3	3 ± 4	2 ± 3	3 ± 4	3 ± 9
	0.7	2 ± 0	1 ± 4	1 ± 5	0 ± 2	0 ± 2	2 ± 3	1 ± 0	0 ± 3	1 ± 3
	0.8	1 ± 8	1 ± 5	1 ± 5	1 ± 2	1 ± 5	1 ± 3	0 ± 5	0 ± 1	0 ± 4
2	0.5	-1 ± 7	-5 ± 4	1 ± 3	-5 ± 3	-3 ± 5	-5 ± 4	-4 ± 3	-7 ± 3	-1 ± 3
	0.6	-5 ± 3	-5 ± 3	-5 ± 3	-3 ± 3	-3 ± 3	-3 ± 3	-5 ± 4	-5 ± 4	-2 ± 5
	0.7	-6 ± 9	-5 ± 2	-1 ± 4	-4 ± 4	-4 ± 2	-5 ± 2	-4 ± 3	-1 ± 4	-5 ± 3
	0.8	-6 ± 4	-4 ± 3	-3 ± 3	-3 ± 3	-3 ± 3	1 ± 2	-3 ± 4	-4 ± 6	-2 ± 4
3	0.5	14 ± 3	13 ± 3	12 ± 3	10 ± 3	9 ± 2	10 ± 3	8 ± 2	8 ± 3	7 ± 3
	0.6	9 ± 2	10 ± 3	9 ± 3	10 ± 2	8 ± 3	8 ± 3	6 ± 4	6 ± 2	6 ± 4
	0.7	9 ± 2	9 ± 2	10 ± 3	8 ± 5	8 ± 1	6 ± 2	7 ± 1	7 ± 3	4 ± 2
	0.8	6 ± 2	7 ± 2	8 ± 2	7 ± 3	5 ± 4	5 ± 2	6 ± 4	6 ± 3	4 ± 2
4	0.5	-11 ± 4	-14 ± 2	-17 ± 4	-12 ± 2	-12 ± 6	-5 ± 5	-4 ± 3	-1 ± 6	-7 ± 2
	0.6	-12 ± 2	-14 ± 2	-14 ± 2	-15 ± 2	-10 ± 2	-10 ± 2	-10 ± 2	-7 ± 3	-6 ± 2
	0.7	-15 ± 1	-13 ± 2	-13 ± 2	-11 ± 2	-11 ± 1	-11 ± 2	-13 ± 2	-16 ± 2	-8 ± 2
	0.8	-13 ± 1	-9 ± 1	-11 ± 1	-13 ± 1	-10 ± 1	-15 ± 2	-11 ± 1	-11 ± 1	-14 ± 2

Table C. 2. F_θ/e_0 (kN/m) for each backward precession frequency at 3.79 bar inlet pressure without swirl brakes.

Cavity Number	Target PR	Precession Frequency								
		10	15	20	25	30	35	40	45	50
Σ(1 - 4)	0.5	-9 ± 15	0 ± 15	-3 ± 11	0 ± 11	-7 ± 20	-3 ± 13	-1 ± 14	-4 ± 15	-5 ± 16
	0.6	-4 ± 11	-3 ± 15	-1 ± 11	-1 ± 10	0 ± 8	-1 ± 12	-1 ± 13	0 ± 9	1 ± 10
	0.7	-6 ± 7	-8 ± 8	-1 ± 17	-4 ± 7	-4 ± 13	4 ± 11	7 ± 11	4 ± 17	6 ± 17
	0.8	-4 ± 9	-7 ± 12	-3 ± 8	-2 ± 9	-1 ± 7	1 ± 8	4 ± 11	6 ± 12	4 ± 18
1	0.5	5 ± 4	6 ± 7	7.5 ± 0.9	8 ± 2	10 ± 10	8 ± 3	8 ± 3	9 ± 3	9 ± 4
	0.6	4 ± 3	4 ± 6	3 ± 3	4 ± 4	4 ± 2	4 ± 5	4 ± 6	4 ± 2	4 ± 1
	0.7	1 ± 2	3 ± 1	0 ± 10	2 ± 1	2 ± 6	3 ± 5	3 ± 3	2 ± 8	3 ± 10
	0.8	1 ± 3	1 ± 7	0 ± 4	0 ± 5	0 ± 3	0 ± 3	1 ± 6	-1 ± 7	0 ± 9
2	0.5	-7 ± 4	-2 ± 4	-8 ± 4	-4 ± 5	-4 ± 4	-7 ± 4	-4 ± 4	-6 ± 6	-9 ± 5
	0.6	-3 ± 3	-5 ± 4	-2 ± 2	-5 ± 2	-5 ± 2	-4 ± 3	'-5 ± 3	-2 ± 2	-1 ± 4
	0.7	-5 ± 2	-7 ± 3	-5 ± 3	-6 ± 3	-4 ± 3	-3 ± 2	0 ± 3	-1 ± 3	2 ± 3
	0.8	-3 ± 2	-3 ± 2	-2 ± 2	-2 ± 1	0 ± 2	-1 ± 2	1 ± 2	1 ± 2	1 ± 4
3	0.5	14 ± 3	18 ± 2	19 ± 2	20 ± 3	21 ± 2	19 ± 3	21 ± 3	24 ± 3	24 ± 3
	0.6	11 ± 3	11 ± 3	14 ± 3	13 ± 2	14 ± 2	14 ± 2	14 ± 2	15 ± 2	15 ± 3
	0.7	11 ± 2	10 ± 2	12 ± 2	11 ± 2	12 ± 2	12 ± 2	15 ± 3	15 ± 4	15 ± 2
	0.8	9 ± 2	8 ± 2	11 ± 1	9 ± 2	10 ± 1	10 ± 2	10 ± 2	11 ± 2	10 ± 4
4	0.5	-21 ± 4	-22 ± 3	-20 ± 4	23 ± 4	-30 ± 4	-23 ± 3	-27 ± 4	-31 ± 3	-28 ± 4
	0.6	-15 ± 2	-13 ± 2	-16 ± 3	-14 ± 2	-13 ± 2	-16 ± 2	-15 ± 2	-18 ± 3	-17 ± 2
	0.7	-14 ± 1	-14 ± 2	-11 ± 2	-11 ± 2	-14 ± 2	-8 ± 2	-10 ± 2	-12 ± 2	-13 ± 2
	0.8	-11 ± 2	-14 ± 1	-13 ± 1	-10 ± 1	-11 ± 1	-7 ± 1	-7 ± 1	-6 ± 1	8 ± 1

Table C. 3. F_r/e_0 (kN/m) for each forward precession frequency at 3.79 bar inlet pressure without swirl brakes.

Cavity Number	Target PR	Precession Frequency (Hz)								
		10	15	20	25	30	35	40	45	50
Σ(1 - 4)	0.5	12 ± 20	4 ± 13	2 ± 20	5 ± 11	5 ± 12	7 ± 16	9 ± 9	4 ± 12	6 ± 12
	0.6	-13 ± 13	-15 ± 9	-10 ± 11	-10 ± 8	-11 ± 10	-10 ± 9	-10 ± 10	-11 ± 15	-14 ± 12
	0.7	-27 ± 6	-19 ± 11	-22 ± 10	-24 ± 12	-19 ± 8	-19 ± 8	-19 ± 7	-16 ± 11	-21 ± 11
	0.8	-26 ± 7	-22 ± 9	-24 ± 7	-21 ± 7	-20 ± 6	-16 ± 9	-24 ± 11	-18 ± 13	-22 ± 14
1	0.5	0 ± 7	-1 ± 3	-1 ± 5	0 ± 3	-2 ± 3	-1 ± 5	0 ± 2	0 ± 2	-1 ± 2
	0.6	0 ± 4	0 ± 2	1 ± 3	-1 ± 2	0 ± 2	-1 ± 2	1 ± 3	1 ± 6	0 ± 3
	0.7	0 ± 2	-1 ± 4	-1 ± 3	-1 ± 4	0 ± 2	0 ± 2	0 ± 1	0 ± 3	0 ± 3
	0.8	0 ± 3	0 ± 3	1 ± 2	0 ± 3	0 ± 2	0 ± 3	-1 ± 3	1 ± 4	0 ± 6
2	0.5	-1 ± 6	-5 ± 4	-3 ± 4	-3 ± 3	-3 ± 4	0 ± 4	-2 ± 3	-2 ± 3	-2 ± 3
	0.6	-6 ± 3	-9 ± 3	-8 ± 3	-6 ± 2	-6 ± 3	-7 ± 3	-7 ± 3	-9 ± 5	-9 ± 3
	0.7	-14 ± 2	-7 ± 3	-10 ± 3	-10 ± 3	-11 ± 2	-9 ± 2	-8 ± 2	-9 ± 3	-11 ± 3
	0.8	-9 ± 2	-8 ± 2	-9 ± 2	-8 ± 2	-6 ± 2	-4 ± 2	-9 ± 4	-8 ± 4	-9 ± 4
3	0.5	8 ± 3	9 ± 3	9 ± 2	7 ± 3	8 ± 3	5 ± 3	8 ± 2	7 ± 3	8 ± 3
	0.6	8 ± 4	6 ± 2	7 ± 3	7 ± 2	5 ± 3	5 ± 2	6 ± 2	7 ± 2	6 ± 3
	0.7	8 ± 1	8 ± 2	7 ± 2	7 ± 3	6 ± 2	5 ± 2	6 ± 2	7 ± 3	7 ± 2
	0.8	7 ± 1	6 ± 2	6 ± 2	6 ± 1	6 ± 1	6 ± 2	6 ± 2	6 ± 2	7 ± 3
4	0.5	5 ± 4	1 ± 3	-2 ± 9	1 ± 2	1 ± 2	3 ± 4	3 ± 2	-1 ± 4	1 ± 4
	0.6	-15 ± 2	-12 ± 2	-9 ± 2	-11 ± 2	-9 ± 2	-8 ± 2	-10 ± 2	-10 ± 2	-11 ± 3
	0.7	-20 ± 1	-18 ± 2	-18 ± 2	-20 ± 2	-14 ± 2	-15 ± 2	-17 ± 2	-14 ± 2	-17 ± 3
	0.8	-24 ± 1	-20 ± 2	-21 ± 1	-20 ± 1	-20 ± 1	-18 ± 2	-20 ± 2	-17 ± 3	-20 ± 1

Table C. 4. F_r/e_0 (kN/m) for each backward precession frequency at 3.79 bar inlet pressure without swirl brakes.

Cavity Number	Target PR	Precession Frequency								
		10	15	20	25	30	35	40	45	50
Σ(1 - 4)	0.5	15 ± 22	-10 ± 17	-8 ± 11	-4 ± 12	-8 ± 12	-13 ± 13	-16 ± 11	-17 ± 14	-21 ± 15
	0.6	-18 ± 11	-23 ± 13	-22 ± 11	-25 ± 9	-26 ± 10	-27 ± 10	-29 ± 10	-31 ± 9	-36 ± 12
	0.7	-31 ± 8	-29 ± 8	-30 ± 12	-35 ± 8	-37 ± 12	-40 ± 9	-44 ± 12	-46 ± 10	-51 ± 13
	0.8	-32 ± 9	-31 ± 9	30 ± 8	35 ± 8	39 ± 7	-42 ± 9	-40 ± 10	-42 ± 11	-41 ± 13
1	0.5	0 ± 10	-1 ± 8	-1 ± 2	0 ± 3	0 ± 2	-1 ± 3	1 ± 2	-1 ± 3	-1 ± 4
	0.6	1 ± 3	0 ± 5	0 ± 3	0 ± 3	0 ± 3	0 ± 3	-1 ± 3	0 ± 2	-1 ± 4
	0.7	0 ± 2	-2 ± 2	-2 ± 5	-2 ± 2	-1 ± 5	-2 ± 3	0 ± 5	-2 ± 2	-2 ± 5
	0.8	0 ± 3	0 ± 3	0 ± 4	-1 ± 3	-1 ± 2	-2 ± 5	-2 ± 5	-3 ± 5	-2 ± 5
2	0.5	-3 ± 3	-11 ± 4	-9 ± 4	-13 ± 3	-12 ± 4	-11 ± 4	-14 ± 5	-15 ± 5	-18 ± 5
	0.6	-11 ± 3	-12 ± 3	-12 ± 3	-12 ± 3	-14 ± 2	-14 ± 3	-17 ± 3	-18 ± 2	-18 ± 3
	0.7	-14 ± 3	-13 ± 2	-13 ± 3	-14 ± 3	-18 ± 3	-18 ± 2	-20 ± 3	-20 ± 3	-26 ± 3
	0.8	-12 ± 3	-12 ± 2	-12 ± 2	-13 ± 2	-17 ± 2	-17 ± 2	-16 ± 2	-17 ± 2	-17 ± 4
3	0.5	10 ± 4	10 ± 2	11 ± 2	13 ± 2	14 ± 2	17 ± 3	15 ± 2	16 ± 3	18 ± 3
	0.6	8 ± 3	9 ± 3	9 ± 3	10 ± 2	11 ± 3	12 ± 2	12 ± 2	13 ± 3	11 ± 3
	0.7	8 ± 2	10 ± 2	10 ± 2	11 ± 2	10 ± 2	13 ± 2	12 ± 2	13 ± 2	11 ± 3
	0.8	7 ± 2	8 ± 2	8 ± 1	9 ± 1	8 ± 1	11 ± 1	10 ± 2	10 ± 2	10 ± 3
4	0.5	7 ± 5	-8 ± 3	- 9 ± 3	-5 ± 4	-10 ± 4	-18 ± 3	-18 ± 2	-17 ± 3	-19 ± 3
	0.6	-16 ± 2	-20 ± 2	-20 ± 2	-23 ± 2	-24 ± 2	-25 ± 2	-23 ± 2	-26 ± 2	-29 ± 2
	0.7	-25 ± 1	-24 ± 2	-26 ± 2	-29 ± 1	-28 ± 2	-33 ± 2	-36 ± 2	-36 ± 3	-34 ± 2
	0.8	-27 ± 1	-27 ± 2	-26 ± 1	-30 ± 2	-28 ± 2	-34 ± 1	-32 ± 1	-32 ± 2	-32 ± 2

Table C. 5. F_θ/e_0 (kN/m) for each forward precession frequency at 3.79 bar inlet pressure with swirl brakes.

Cavity Number	Target PR	Precession Frequency (Hz)								
		10	15	20	25	30	35	40	45	50
Σ(1 - 4)	0.5	-15 ± 17	-18 ± 21	-17 ± 16	-11 ± 14	-13 ± 14	-6 ± 15	-7 ± 13	-2 ± 17	4 ± 21
	0.6	-5 ± 13	-19 ± 17	-11 ± 12	-9 ± 14	-8 ± 16	-6 ± 15	-12 ± 22	-10 ± 18	-5 ± 27
	0.7	-12 ± 8	-21 ± 12	-20 ± 13	-15 ± 18	-18 ± 18	-16 ± 16	-8 ± 16	-12 ± 18	-9 ± 27
	0.8	-20 ± 14	-20 ± 10	-16 ± 9	-15 ± 16	-18 ± 11	-12 ± 15	-12 ± 13	-7 ± 16	-11 ± 24
1	0.5	-1 ± 4	-2 ± 3	1 ± 3	-2 ± 5	-2 ± 5	-1 ± 4	-1 ± 3	-3 ± 3	-2 ± 6
	0.6	-1 ± 4	-1 ± 3	1 ± 3	1 ± 2	-1 ± 4	0 ± 4	0 ± 4	-1 ± 5	1 ± 6
	0.7	2 ± 2	-1 ± 4	0 ± 3	-1 ± 3	-2 ± 3	-1 ± 3	-3 ± 4	-1 ± 5	0 ± 10
	0.8	-1 ± 5	-1 ± 3	-1 ± 3	-1 ± 3	-1 ± 3	0 ± 5	-2 ± 5	-2 ± 5	-1 ± 9
2	0.5	-9 ± 4	-10 ± 9	-13 ± 2	-6 ± 3	-9 ± 3	-2 ± 4	-4 ± 4	-1 ± 7	4 ± 5
	0.6	-1 ± 2	-11 ± 4	-9 ± 4	-8 ± 4	-5 ± 3	-3 ± 4	-7 ± 8	-7 ± 6	-5 ± 11
	0.7	-7 ± 1	-7 ± 3	-7 ± 4	-6 ± 4	-6 ± 5	-5 ± 4	-2 ± 4	-4 ± 3	-5 ± 9
	0.8	-6 ± 6	-8 ± 2	-5 ± 3	-6 ± 3	-5 ± 3	-3 ± 3	-4 ± 3	0 ± 4	-1 ± 6
3	0.5	10 ± 6	8 ± 4	5 ± 6	7 ± 3	5 ± 3	4 ± 4	4 ± 2	2 ± 3	3 ± 5
	0.6	8 ± 4	4 ± 9	6 ± 7	6 ± 4	5 ± 4	4 ± 3	3 ± 3	1 ± 3	0 ± 4
	0.7	5 ± 1	6 ± 2	5 ± 1	5 ± 4	5 ± 5	3 ± 4	6 ± 3	3 ± 4	1 ± 3
	0.8	6 ± 1	5 ± 2	6 ± 1	5 ± 8	5 ± 2	6 ± 5	2 ± 3	2 ± 4	2 ± 5
4	0.5	-15 ± 3	-14 ± 5	-10 ± 5	-10 ± 3	-7 ± 3	-7 ± 3	-6 ± 4	-1 ± 4	-1 ± 4
	0.6	-11 ± 3	-12 ± 1	-9 ± 2	-8 ± 4	-7 ± 5	-7 ± 4	8 ± 7	-3 ± 4	-2 ± 6
	0.7	-12 ± 4	-18 ± 3	-17 ± 5	-12 ± 7	-16 ± 5	-13 ± 5	-10 ± 5	-10 ± 6	-6 ± 5
	0.8	-19 ± 2	-17 ± 3	-16 ± 2	-13 ± 2	-17 ± 3	-14 ± 2	-8 ± 2	-8 ± 3	-11 ± 4

Table C. 6. F_θ/e_0 (kN/m) for each backward precession frequency at 3.79 bar inlet pressure with swirl brakes.

Cavity Number	Target PR	Precession Frequency								
		10	15	20	25	30	35	40	45	50
Σ(1 - 4)	0.5	-19 ± 24	-23 ± 14	-23 ± 13	-17 ± 14	-16 ± 13	-15 ± 14	-18 ± 17	-12 ± 14	-14 ± 19
	0.6	-10 ± 17	-15 ± 11	-16 ± 17	-18 ± 14	-10 ± 14	-14 ± 13	-11 ± 15	-9 ± 17	-9 ± 19
	0.7	-17 ± 16	-16 ± 11	-16 ± 15	-13 ± 11	-12 ± 12	-7 ± 26	-8 ± 11	-10 ± 11	-13 ± 21
	0.8	-17 ± 17	-13 ± 8	-16 ± 11	-13 ± 12	-9 ± 12	-14 ± 8	-6 ± 9	-7 ± 11	-6 ± 11
1	0.5	-1 ± 4	0 ± 3	2 ± 3	2 ± 4	-1 ± 3	2 ± 1	2 ± 4	3 ± 4	3 ± 4
	0.6	-2 ± 4	-1 ± 3	0 ± 5	-1 ± 3	0 ± 4	-1 ± 3	'-1 ± 4	'-2 ± 6	-1 ± 7
	0.7	0 ± 6	-2 ± 4	-2 ± 5	-1 ± 3	-1 ±1	-1 ± 4	-3 ± 3	-2 ± 3	0 ± 7
	0.8	0 ± 4	1 ± 3	-1 ± 3	-1 ± 4	-2 ± 4	-1 ± 5	-2 ± 4	-3 ± 5	0 ± 4
2	0.5	-10 ± 14	-11 ± 5	-13 ± 4	-12 ± 4	-7 ± 4	-8 ± 6	-8 ± 6	-8 ± 4	-6 ± 7
	0.6	-2 ± 7	-6 ± 2	-7 ± 5	-6 ± 4	-4 ± 3	-3 ± 4	0 ± 5	-4 ± 6	0 ± 5
	0.7	-7 ± 7	-2 ± 4	-3 ± 4	-4 ± 3	-4 ± 2	-1 ± 4	2 ± 3	-2 ± 2	-4 ± 8
	0.8	-6 ± 5	-6 ± 3	-4 ± 1	-2 ± 3	-3 ± 3	-4 ± 1	0 ± 3	-1 ± 3	-2 ± 3
3	0.5	11 ± 3	12 ± 3	11 ± 3	9 ± 3	14 ± 3	14 ± 3	14 ± 4	15 ± 2	18 ± 5
	0.6	10 ± 4	9 ± 3	9 ± 4	11 ± 3	12 ± 4	13 ± 4	14 ± 4	15 ± 2	18 ± 4
	0.7	8 ± 1	11 ± 1	11 ± 3	12 ± 3	11 ± 6	14 ± 14	14 ± 2	14 ± 4	15 ± 3
	0.8	6 ± 7	7 ± 1	8 ± 5	10 ± 3	11 ± 3	10 ± 1	13 ± 1	13 ± 1	11 ± 3
4	0.5	-19 ± 3	-23 ± 3	-23 ± 3	-17 ± 3	-22 ± 3	-22 ± 4	-26 ± 3	-22 ± 4	-30 ± 3
	0.6	-17 ± 2	-17 ± 3	-18 ± 3	-22 ± 4	-18 ± 3	-23 ± 2	-24 ± 2	-18 ± 3	-25 ± 3
	0.7	-18 ± 2	-22 ± 2	-22 ± 3	-19 ± 2	-18 ± 3	-19 ± 2	-22 ± 3	-20 ± 2	-24 ± 3
	0.8	-17 ± 1	-14 ± 1	-18 ± 2	-20 ± 2	-15 ± 2	-20 ± 1	-16 ± 1	-16 ± 2	-15 ± 1

Table C. 7. F_r/e_0 (kN/m) for each forward precession frequency at 3.79 bar inlet pressure with swirl brakes.

Cavity Number	Target PR	Precession Frequency (Hz)								
		10	15	20	25	30	35	40	45	50
Σ(1 - 4)	0.5	9 ± 15	5 ± 17	3 ± 15	4 ± 10	2 ± 12	11 ± 10	3 ± 18	8 ± 16	8 ± 18
	0.6	-3 ± 15	-5 ± 16	-7 ± 13	-6 ± 13	1 ± 15	-5 ± 18	-8 ± 21	-9 ± 22	-4 ± 20
	0.7	-11 ± 11	-6 ± 10	-4 ± 14	-9 ± 14	-10 ± 14	-9 ± 11	-13 ± 14	-17 ± 18	-12 ± 17
	0.8	-24 ± 13	-19 ± 16	-15 ± 10	-15 ± 9	-17 ± 11	-20 ± 10	-17 ± 13	-23 ± 20	-20 ± 16
1	0.5	4 ± 3	5 ± 3	3 ± 3	2 ± 3	4 ± 3	2 ± 3	1 ± 3	4 ± 5	4 ± 5
	0.6	2 ± 5	2 ± 4	1 ± 3	1 ± 2	2 ± 5	0 ± 4	1 ± 5	0 ± 5	-1 ± 7
	0.7	1 ± 3	-1 ± 3	1 ± 5	1 ± 5	0 ± 5	1 ± 3	0 ± 4	2 ± 5	1 ± 5
	0.8	0 ± 4	1 ± 2	1 ± 3	1 ± 3	1 ± 4	1 ± 3	1 ± 4	-2 ± 8	0 ± 5
2	0.5	-4 ± 4	-5 ± 7	-7 ± 4	-7 ± 1	-5 ± 2	-3 ± 0	-3 ± 7	-3 ± 4	-6 ± 8
	0.6	-7 ± 2	-9 ± 4	-12 ± 4	-10 ± 4	-12 ± 4	-7 ± 7	-11 ± 7	-10 ± 9	-8 ± 5
	0.7	-11 ± 3	-9 ± 3	-9 ± 3	-14 ± 3	-8 ± 4	-15 ± 3	-13 ± 4	-14 ± 4	-14 ± 4
	0.8	-14 ± 4	-12 ± 4	-13 ± 3	-12 ± 2	-13 ± 4	-13 ± 2	-12 ± 3	-14 ± 6	-13 ± 5
3	0.5	11 ± 5	9 ± 3	9 ± 4	9 ± 3	9 ± 3	10 ± 3	8 ± 4	9 ± 4	9 ± 3
	0.6	11 ± 6	10 ± 5	10 ± 4	9 ± 3	8 ± 3	10 ± 3	7 ± 4	8 ± 3	6 ± 5
	0.7	8 ± 2	11 ± 1	10 ± 2	9 ± 3	10 ± 3	6 ± 2	5 ± 3	4 ± 4	4 ± 4
	0.8	8 ± 2	6 ± 9	7 ± 2	8 ± 2	8 ± 1	6 ± 3	5 ± 3	5 ± 4	4 ± 3
4	0.5	-1 ± 3	-3 ± 4	-2 ± 4	0 ± 3	-6 ± 4	2 ± 4	-3 ± 4	-1 ± 3	2 ± 2
	0.6	-8 ± 2	-7 ± 3	-6 ± 2	-5 ± 4	2 ± 3	-8 ± 4	-4 ± 6	-8 ± 5	-2 ± 3
	0.7	9 ± 3	-6 ± 3	-6 ± 4	-5 ± 3	-11 ± 2	-2 ± 3	-5 ± 3	-8 ± 5	-3 ± 4
	0.8	-17 ± 3	-15 ± 1	-11 ± 2	-11 ± 2	-13 ± 2	-14 ± 2	-11 ± 3	-12 ± 2	-11 ± 3

Table C. 8. F_r/e_0 (kN/m) for each backward precession frequency at 3.79 bar inlet pressure with swirl brakes.

Cavity Number	Target PR	Precession Frequency								
		10	15	20	25	30	35	40	45	50
Σ(1 - 4)	0.5	8 ± 19	-14 ± 18	-12 ± 13	-20 ± 14	-25 ± 13	-21 ± 13	-20 ± 18	-26 ± 14	-37 ± 19
	0.6	-3 ± 14	-15 ± 11	-17 ± 12	-18 ± 13	-23 ± 14	-27 ± 15	-29 ± 15	-36 ± 15	-34 ± 18
	0.7	-14 ± 14	-26 ± 11	-23 ± 12	-25 ± 12	-31 ± 14	-28 ± 15	-36 ± 13	-43 ± 12	-37 ± 15
	0.8	-23 ± 12	-30 ± 9	-31 ± 9	-28 ± 13	-38 ± 13	-40 ± 10	-39 ± 8	-44 ± 11	-46 ± 9
1	0.5	2 ± 5	0 ± 4	1 ± 3	0 ± 4	1 ± 3	2 ± 3	-1 ± 4	0 ± 4	0 ± 6
	0.6	2 ± 4	-1 ± 3	-1 ± 3	2 ± 2	0 ± 4	1 ± 5	-2 ± 4	-3 ± 4	-1 ± 6
	0.7	0 ± 4	2 ± 3	-1 ± 3	1 ± 3	1 ± 4	0 ± 4	-1 ± 4	0 ± 3	-1 ± 5
	0.8	0 ± 4	0 ± 3	-1 ± 3	0 ± 4	0 ± 4	1 ± 3	-2 ± 2	-1 ± 4	-2 ± 3
2	0.5	-5 ± 6	-15 ± 6	-17 ± 4	-16 ± 4	-21 ± 3	-21 ± 5	-15 ± 6	-23 ± 4	-25 ± 6
	0.6	-11 ± 4	-13 ± 3	-17 ± 4	-20 ± 4	-16 ± 3	-18 ± 4	-18 ± 4	-19 ± 4	-23 ± 5
	0.7	-10 ± 4	-19 ± 3	-14 ± 3	-15 ± 4	-19 ± 4	-14 ± 5	-17 ± 4	-20 ± 4	-21 ± 3
	0.8	-13 ± 3	-16 ± 2	-17 ± 3	-13 ± 3	'-17 ± 3	-20 ± 3	-17 ± 2	-20 ± 3	-23 ± 3
3	0.5	13 ± 3	12 ± 4	11 ± 4	11 ± 3	14 ± 4	12 ± 2	15 ± 5	15 ± 3	15 ± 4
	0.6	9 ± 3	12 ± 2	11 ± 2	9 ± 5	13 ± 4	11 ± 2	15 ± 3	12 ± 3	13 ± 4
	0.7	10 ± 2	8 ± 2	11 ± 4	10 ± 3	9 ± 3	12 ± 3	11 ± 3	11 ± 2	10 ± 4
	0.8	9 ± 3	7 ± 2	7 ± 2	9 ± 4	8 ± 4	8 ± 2	10 ± 2	10 ± 2	9 ± 2
4	0.5	-2 ± 5	-12 ± 4	-8 ± 2	-15 ± 3	-19 ± 3	-13 ± 3	-19 ± 3	-18 ± 3	-26 ± 3
	0.6	-3 ± 3	-13 ± 3	-10 ± 3	-9 ± 2	-19 ± 3	-21 ± 4	-24 ± 4	-26 ± 4	-23 ± 3
	0.7	-15 ± 4	-17 ± 3	-19 ± 2	-20 ± 2	-21 ± 3	-26 ± 3	-29 ± 2	-34 ± 3	-25 ± 3
	0.8	-18 ± 2	-21 ± 2	-21 ± 2	-23 ± 2	-29 ± 2	-29 ± 2	-30 ± 2	-32 ± 2	-30 ± 2

APPENDIX D

ROTORDYNAMIC COEFFICIENTS FROM SLOPE AND INTERCEPT OF DYNAMIC FORCES

Table D. 1. *k*, *C*, *K*, and *c* for the entire seal at each test condition.

Configuration	Inlet Pressure (bar)	Target PR	k (kN/m)	C (Ns/m)	R^2	K (kN/m)	c (Ns/m)	R^2
Without Swirl Brakes	2.75	0.5	-1.4	25	0.88	-26	11	0.20
		0.6	-3.1	23	0.85	-31	31	0.92
		0.7	-1.8	23	0.90	-24	34	0.90
		0.8	-1.6	18	0.86	-22	31	0.93
	3.79	0.5	-0.55	-14	0.45	-1.7	41	0.66
		0.6	-2.8	6.4	0.27	-19	38	0.88
		0.7	-4.1	22	0.66	-29	47	0.89
		0.8	-4.3	22	0.76	-29	40	0.90
	4.83	0.5	0.35	-11	0.41	1.6	57	0.75
		0.6	-8.1	15	0.32	-30	66	0.87
		0.7	-8.1	23	0.50	-40	66	0.91
		0.8	-4.6	22	0.62	-43	44	0.83
With Swirl Brakes	2.75	0.5	-7.6	-8.3	0.18	-6.6	35	0.79
		0.6	-8.9	2.4	0.06	-11	33	0.71
		0.7	-12	12	0.46	-22	35	0.76
		0.8	-9.4	17	0.88	-27	20	0.61
	3.79	0.5	-13	-22	0.42	-6.2	66	0.81
		0.6	-11	-5.6	0.09	-14	47	0.74
		0.7	-13	4.2	0.05	-20	48	0.74
		0.8	-13	7.5	0.11	-27	43	0.80
	4.83	0.5	-20	-33	0.47	-20.5	110	0.80
		0.6	-16	-6.5	0.04	-23	70	0.79
		0.7	-17	-2.0	0.01	-26	53	0.73
		0.8	-19	-9.1	0.11	-29	36	0.77

Table D. 2. *k*, *C*, *K*, and *c* for cavity (1) at each test condition.

Configuration	Inlet Pressure (bar)	Target PR	k (kN/m)	C (Ns/m)	R^2	K (kN/m)	c (Ns/m)	R^2
Without Swirl Brakes	2.75	0.5	5.4	5.0	0.87	1.1	-1.5	0.25
		0.6	3.4	2.9	0.72	0.89	1.2	0.36
		0.7	2.2	3.6	0.70	0.43	1.4	0.19
		0.8	0.93	0.17	0.02	0.80	3.6	0.85
	3.79	0.5	6.0	-6.3	0.62	-0.65	-0.32	0.01
		0.6	3.3	3.3	0.62	0.085	0.64	0.06
		0.7	1.6	4.0	0.70	-1.0	2.9	0.53
		0.8	0.52	-1.2	0.20	-0.55	3.6	0.56
	4.83	0.5	6.0	4.7	0.48	-0.52	1.5	0.10
		0.6	4.2	4.0	0.50	-0.67	0.63	0.03
		0.7	4.2	3.0	0.27	-1.1	1.7	0.16
		0.8	1.1	1.4	0.32	-1.2	4.8	0.55
With Swirl Brakes	2.75	0.5	0.54	7.6	0.80	1.6	2.0	0.06
		0.6	0.17	2.4	0.25	0.63	3.1	0.45
		0.7	-0.04	0.73	0.05	0.11	1.1	0.12
		0.8	-0.59	0.71	0.06	0.094	1.9	0.30
	3.79	0.5	-0.04	7.7	0.71	1.8	5.9	0.51
		0.6	-0.55	-2.5	0.31	0.31	2.9	0.17
		0.7	-1.0	-1.1	0.04	0.38	2.9	0.34
		0.8	-1.1	-0.28	0.00	-0.17	2.6	0.25
	4.83	0.5	-0.96	3.2	0.19	2.4	4.1	0.23
		0.6	-1.0	1.1	0.02	0.86	5.0	0.25
		0.7	-1.2	-1.7	0.12	-0.61	2.9	0.22
		0.8	-1.3	-1.9	0.09	-0.89	6.1	0.45

Table D. 3. *k*, *C*, *K*, and *c* for cavity (2) at each test condition.

Configuration	Inlet Pressure (bar)	Target PR	k (kN/m)	C (Ns/m)	R^2	K (kN/m)	c (Ns/m)	R^2
Without Swirl Brakes	2.75	0.5	-2.2	12	0.81	-23	6.5	0.11
		0.6	-3.0	10	0.69	-22	14	0.68
		0.7	-2.0	5.6	0.40	-13	17	0.71
		0.8	-1.2	5.0	0.45	-11	13	0.83
	3.79	0.5	-4.5	-5.6	0.19	-7.0	25	0.84
		0.6	-3.8	0.40	0.00	-11	17	0.79
		0.7	-3.6	2.9	0.07	-14	21	0.76
		0.8	-2.0	5.5	0.31	-11	18	0.82
	4.83	0.5	-3.8	1.0	0.00	-6.1	31	0.89
		0.6	-5.5	20	0.57	-23	41	0.89
		0.7	-5.5	11	0.40	-25	35	0.85
		0.8	-3.0	8.9	0.41	-24	16	0.53
With Swirl Brakes	2.75	0.5	-4.0	-4.9	0.10	-11	21	0.54
		0.6	-4.3	3.6	0.19	-13	13	0.66
		0.7	-4.0	8.5	0.52	-15	10	0.56
		0.8	-3.6	7.2	0.84	-16	8.5	0.55
	3.79	0.5	-7.4	-11	0.25	-11	34	0.81
		0.6	-4.8	7.0	0.24	-13	20	0.76
		0.7	-4.1	5.8	0.25	-14	11	0.36
		0.8	-3.7	2.3	0.05	-15	12	0.64
	4.83	0.5	-8.8	-2.7	0.02	-28	22	0.37
		0.6	-7.3	2.5	0.02	-19	33	0.73
		0.7	-6.2	3.1	0.04	-18	15	0.46
		0.8	-6.1	1.6	0.01	-17	-5.1	0.14

Table D. 4. *k*, *C*, *K*, and *c* for cavity (3) at each test condition.

Configuration	Inlet Pressure (bar)	Target PR	k (kN/m)	C (Ns/m)	R^2	K (kN/m)	c (Ns/m)	R^2
Without Swirl Brakes	2.75	0.5	10	14	0.95	8.0	-8.6	0.79
		0.6	8.4	12	0.98	7.6	-8.6	0.84
		0.7	7.6	9.7	0.94	6.9	-7.4	0.84
		0.8	4.8	7.7	0.93	5.2	-4.7	0.83
	3.79	0.5	15	27	0.96	11	-17	0.82
		0.6	11	15	0.95	8.4	-11	0.85
		0.7	9.9	14	0.92	8.8	-11	0.84
		0.8	7.9	10	0.88	7.6	-7.3	0.80
	4.83	0.5	16	30	0.95	11	-19	0.89
		0.6	14	30	0.96	11	-17	0.90
		0.7	14	23	0.90	11	-13	0.80
		0.8	9.0	15	0.86	8.9	-9.1	0.79
With Swirl Brakes	2.75	0.5	6.3	17	0.80	7.7	-11	0.35
		0.6	5.9	16	0.96	7.7	-6.4	0.73
		0.7	5.3	15	0.97	7.1	-5.3	0.50
		0.8	4.4	9.9	0.92	6.3	-4.4	0.52
	3.79	0.5	9.2	21	0.92	11	-10	0.81
		0.6	8.2	23	0.94	10	-8.8	0.70
		0.7	8.2	20	0.92	8.8	-9.4	0.61
		0.8	7.0	15	0.87	7.5	-6.4	0.65
	4.83	0.5	13	33	0.92	15	-13	0.68
		0.6	11	27	0.91	14	-10	0.59
		0.7	9.7	21	0.88	11	-13	0.61
		0.8	9.0	20	0.88	10	-12	0.64

Table D. 5. *k*, *C*, *K*, and *c* for cavity (4) at each test condition.

Configuration	Inlet Pressure (bar)	Target PR	k (kN/m)	C (Ns/m)	R^2	K (kN/m)	c (Ns/m)	R^2
Without Swirl Brakes	2.75	0.5	-15	-6.9	0.25	-13	15	0.64
		0.6	-12	-1.7	0.08	-17	24	0.92
		0.7	-9.6	3.7	0.33	-18	23	0.91
		0.8	-6.1	5.4	0.72	-17	19	0.91
	3.79	0.5	-17	-42	0.91	-4.7	33	0.67
		0.6	-13	-12	0.64	-17	31	0.91
		0.7	-12	0.95	0.01	-24	35	0.91
		0.8	-11	7.4	0.38	-25	26	0.92
	4.83	0.5	-18	-47	0.91	-2.7	43	0.74
		0.6	-21	-39	0.86	-17	41	0.87
		0.7	-21	-14	0.34	-25	42	0.92
		0.8	-12	-3.0	0.07	-26	33	0.87
With Swirl Brakes	2.75	0.5	-10	-28	0.85	-4.8	24	0.76
		0.6	-11	-19	0.90	-6.6	23	0.78
		0.7	-13	-12	0.57	-14	29	0.88
		0.8	-9.6	-0.37	0.01	-17	14	0.78
	3.79	0.5	-15	-40	0.92	-8.0	36	0.79
		0.6	-14	-33	0.94	-11	33	0.70
		0.7	-17	-21	0.75	-15	43	0.88
		0.8	-15	-10	0.35	-19	35	0.91
	4.83	0.5	-23	-66	0.92	-10	94	0.90
		0.6	-18	-37	0.66	-19	42	0.79
		0.7	-19	-25	0.70	-19	48	0.89
		0.8	-20	-29	0.69	-22	47	0.94

APPENDIX E

ROTORDYNAMIC COEFFICIENTS AT EACH PRECESSION FREQUENCY

Table E. 1. *k*, *C*, *K*, and *Ceff* for the entire seal at 3.79 bar inlet pressure and 0.5 pressure ratio.

Configuration	Precession Frequency	k	±	C	±	K	±	Ceff	±
	(Hz)	(kN/m)	(kN/m)	(Ns/m)	(Ns/m)	(kN/m)	(kN/m)	(Ns/m)	(Ns/m)
Without Swirl Brakes	10	-1	13	-130	200	13	15	-120	310
	15	-1	10	15	100	-3	11	30	150
	20	-0.4	8.1	-17	65	-3	6	-13	79
	25	-1.6	7.8	10	50	0.3	8.1	20	72
	30	-3	14	-20	73	-1.5	8.5	-1	86
	35	0	11	-17	49	-3	10	-20	68
	40	1.5	8.6	-12	34	-3.7	7.1	-18	44
	45	1	12	-17	41	-6.5	9.2	-21	53
	50	0	10	-14	31	-7	10	-13	43
With Swirl Brakes	10	-17	15	-34	230	8	12	230	300
	15	-20	13	-28	130	-5	12	190	190
	20	-20	10	-25	82	-4	10	140	110
	25	-14	10	-20	63	-7.7	8.6	71	83
	30	-15	10	-9	51	-11.6	8.8	70	69
	35	-10	10	-21	47	-4.6	8.2	25	60
	40	-13	11	-23	43	-8	13	26	66
	45	-7	11	-16	39	-9	11	9	54
	50	-5	14	-30	45	-14	13	-13	61

Table E. 2. *k*, *C*, *K*, and *Ceff* for the entire seal at 3.79 bar inlet pressure and 0.6 pressure ratio.

Configuration	Precession Frequency	k	±	C	±	K	±	Ceff	±
	(Hz)	(kN/m)	(kN/m)	(Ns/m)	(Ns/m)	(kN/m)	(kN/m)	(Ns/m)	(Ns/m)
Without Swirl Brakes	10	-3.6	7.1	-2	110	-15.4	8.5	56	180
	15	-5.1	8.7	19	93	-19.2	7.9	73	130
	20	-4.0	8.1	22	65	-16.0	7.8	54	90
	25	-3.8	6.7	15	43	-17.5	6.0	39	57
	30	-1.8	6.8	9	36	-18.6	7.1	18	52
	35	-1.9	8.5	3	39	-18.6	6.7	12	49
	40	-4.0	9.2	11	37	-19.4	7.1	26	46
	45	-1.8	7.9	5	28	-21.1	8.7	11	42
	50	1	11	0	36	-25.1	8.5	-3	45
With Swirl Brakes	10	-8	11	-38	170	-3	10	82	240
	15	-17	10	23	100	-10.0	9.7	200	150
	20	-13	10	-19	83	-11.9	8.8	88	110
	25	-13.4	9.9	-28	63	-11.9	9.2	57	86
	30	-9	11	-5	56	-11	10	43	78
	35	-9.7	9.9	-18	45	-16	12	26	70
	40	-11	13	3	53	-18	13	49	74
	45	-10	12	2	44	-22	13	37	64
	50	-7	17	-5	53	-19	13	17	68

Table E. 3. *k*, *C*, *K*, and *Ceff* for the entire seal at 3.79 bar inlet pressure and 0.7 pressure ratio.

Configuration	Precession Frequency	k	±	C	±	K	±	Ceff	±
	(Hz)	(kN/m)	(kN/m)	(Ns/m)	(Ns/m)	(kN/m)	(kN/m)	(Ns/m)	(Ns/m)
Without Swirl Brakes	10	-8.0	6.9	29	110	-28.9	5.0	160	140
	15	-8.5	6.4	1	68	-24.3	6.8	92	99
	20	-3	11	10	88	-25.7	7.8	32	107
	25	-5.2	7.4	8	47	-29.5	7.2	41	66
	30	-6.0	7.2	9	38	-28.3	7.2	41	54
	35	-2.2	7.1	28	32	-29.5	6.0	38	42
	40	-1.0	6.3	33	25	-31.4	6.9	37	37
	45	-3	10	24	37	-31.1	7.4	34	45
	50	-0.9	9.9	21	31	-35.9	8.5	24	41
With Swirl Brakes	10	-14.5	8.9	-34	140	-13.0	8.9	200	200
	15	-18.1	8.1	27	86	-15.8	7.4	220	120
	20	-17.9	9.9	13	79	-13.6	9.2	160	110
	25	-14	11	6	67	-16.9	9.2	94	89
	30	-15	11	16	57	-20.5	9.9	96	78
	35	-11	15	21	69	-18.5	9.3	72	81
	40	-8.1	9.7	-1	39	-24.3	9.6	31	54
	45	-11	11	4	37	-30	11	44	53
	50	-11	17	-7	54	-24	11	29	65

Table E. 4. *k*, *C*, *K*, and *Ceff* for the entire seal at 3.79 bar inlet pressure and 0.8 pressure ratio.

Configuration	Precession Frequency	k	±	C	±	K	±	Ceff	±
	(Hz)	(kN/m)	(kN/m)	(Ns/m)	(Ns/m)	(kN/m)	(kN/m)	(Ns/m)	(Ns/m)
Without Swirl Brakes	10	-8.3	8.7	62	140	-28.8	5.7	190	170
	15	-6.3	8.1	-11	86	-26.4	6.4	55	110
	20	-4.3	6.8	8	54	-26.8	5.3	43	69
	25	-4.7	6.4	20	41	-28.2	5.3	50	53
	30	-3.9	7.4	15	39	-29.0	4.6	36	46
	35	-3.5	6.8	21	31	-28.7	6.4	36	42
	40	-2.0	8.9	23	35	-31.7	7.4	31	46
	45	-1.6	8.1	26	29	-29.7	8.5	32	42
	50	-4	11	25	34	-31.4	9.6	38	46
With Swirl Brakes	10	-19	11	22	180	-23.6	8.8	320	230
	15	-16.6	6.4	38	68	-24.6	9.2	210	120
	20	-16.0	7.1	1	57	-23.4	6.7	130	78
	25	-14	10	8	64	-21.1	7.9	97	81
	30	-13.5	8.1	24	43	-28.0	8.5	96	62
	35	-13.2	8.5	-5	39	-30.1	7.1	55	50
	40	-8.9	7.9	12	31	-28.1	7.6	48	44
	45	-7	10	0	34	-33	11	26	53
	50	-8	13	8	42	-33.1	9.2	35	51

Table E. 5. *k*, *C*, *K*, and *Ceff* for cavity (1) at 3.79 bar inlet pressure and 0.5 pressure ratio.

Configuration	Precession Frequency	k	±	C	±	K	±	Ceff	±
	(Hz)	(kN/m)	(kN/m)	(Ns/m)	(Ns/m)	(kN/m)	(kN/m)	(Ns/m)	(Ns/m)
Without Swirl Brakes	10	7.0	3.8	25	61	-0.8	6.1	-86	110
	15	6.2	4.0	26	43	-1.3	4.2	-39	61
	20	6.4	1.2	11.6	9.7	-0.2	2.6	-39	23
	25	5.9	2.1	16	13	-0.6	2.4	-22	20
	30	5.5	6.5	-1	34	-0.8	2.0	-31	36
	35	6.0	3.1	8	14	-0.7	2.7	-20	19
	40	6.0	1.7	6.0	6.6	-0.7	1.4	-18.0	8.6
	45	5.6	3.4	0	12	-0.4	1.8	-19	14
	50	5.0	2.4	0.1	7.7	-0.3	2.1	-16	10
With Swirl Brakes	10	-0.9	2.9	0	45	3.0	3.0	13	65
	15	-1.2	1.9	13	20	2.7	2.4	26	32
	20	1.4	2.1	4	17	1.9	2.0	-7	23
	25	0.2	3.1	12	20	1.3	2.4	11	25
	30	-1.4	2.8	4	15	2.1	1.9	12	18
	35	0.4	2.1	7	10	2.1	2.3	5	14
	40	0.5	2.6	6	10	-0.1	2.6	4	14
	45	0.3	2.6	10.5	9.3	2.1	3.0	9	14
	50	0.3	4.0	7	13	1.6	3.7	7	17

Table E. 6. *k*, *C*, *K*, and *Ceff* for cavity (1) at 3.79 bar inlet pressure and 0.6 pressure ratio.

Configuration	Precession Frequency	k	±	C	±	K	±	Ceff	±
	(Hz)	(kN/m)	(kN/m)	(Ns/m)	(Ns/m)	(kN/m)	(kN/m)	(Ns/m)	(Ns/m)
Without Swirl Brakes	10	3.7	1.9	4	31	-0.2	2.6	-55	51
	15	3.4	3.0	11	32	0.0	2.6	-25	42
	20	3.5	2.4	7	19	0.1	2.1	-21	25
	25	3.3	2.5	7	16	-0.2	2.0	-14	20
	30	2.6	1.9	5	10	-0.1	1.9	-9	14
	35	3.7	3.1	3	14	-0.4	2.1	-14	17
	40	2.6	3.3	2	13	0.5	2.1	-8	16
	45	3.5	2.3	2.0	8.3	0.5	3.0	-11	13
	50	3.3	4.5	1	14	0.6	2.6	-10	17
With Swirl Brakes	10	-1.5	2.7	-9	43	2.0	2.9	14	63
	15	-1.0	2.2	-4	23	0.4	2.5	6	35
	20	0.3	3.1	-3	25	0.0	2.0	-5	29
	25	0.3	1.9	-6	12	1.1	1.3	-8	15
	30	-0.6	2.8	2	15	1.0	3.2	5	23
	35	-0.3	2.5	-2	11	0.8	3.3	-1	19
	40	-0.8	2.9	-3	11	-0.6	3.3	1	17
	45	-1.5	4.0	-1	14	-1.1	3.4	4	19
	50	0.1	4.7	-3	15	-0.7	4.6	-4	21

Table E. 7. *k*, *C*, *K*, and *Ceff* for cavity (1) at 3.79 bar inlet pressure and 0.7 pressure ratio.

Configuration	Precession Frequency	k	±	C	±	K	±	Ceff	±
	(Hz)	(kN/m)	(kN/m)	(Ns/m)	(Ns/m)	(kN/m)	(kN/m)	(Ns/m)	(Ns/m)
Without Swirl Brakes	10	2.1	1.1	8	17	-1.4	1.7	-26	32
	15	1.5	2.0	8	21	-1.9	2.2	-8	31
	20	1.7	5.3	9	42	-0.7	3.0	-4	49
	25	1.7	1.0	8.2	6.5	-1.5	2.2	-3	15
	30	1.1	3.1	5	16	-0.6	2.6	-1	21
	35	1.8	3.1	1	14	-1.0	1.6	-7	16
	40	1.9	1.4	5.2	5.5	-0.6	2.7	-2	12
	45	1.4	4.3	4	15	-0.9	1.8	-1	17
	50	1.2	5.3	1	17	-0.1	3.0	-3	19
With Swirl Brakes	10	0.9	3.0	-9	48	0.8	2.3	-24	60
	15	-1.5	2.6	-3	27	0.6	2.1	13	35
	20	-1.2	3.1	-8	24	-0.1	2.9	1	33
	25	-1.0	2.2	0	14	1.1	2.9	7	23
	30	-1.1	1.4	2.4	7.4	0.3	3.3	8	19
	35	-1.1	2.7	0	12	0.8	2.4	5	16
	40	-2.5	2.4	0	10	-0.4	2.8	10	15
	45	-1.6	2.8	-2	10	0.6	2.8	4	14
	50	0.1	6.2	-1	20	-0.1	3.4	-2	22

Table E. 8. *k*, *C*, *K*, and *Ceff* for cavity (1) at 3.79 bar inlet pressure and 0.8 pressure ratio.

Configuration	Precession Frequency	k	±	C	±	K	±	Ceff	±
	(Hz)	(kN/m)	(kN/m)	(Ns/m)	(Ns/m)	(kN/m)	(kN/m)	(Ns/m)	(Ns/m)
Without Swirl Brakes	10	0.6	4.1	-10	65	-1.4	2.1	-20	74
	15	0.2	4.2	-12	44	-1.4	2.2	-13	50
	20	0.7	2.9	0	23	-0.7	2.3	-6	29
	25	0.3	2.8	-2	18	-0.6	2.0	-4	22
	30	0.6	2.9	-3	15	-0.4	1.6	-6	17
	35	0.8	2.1	-1.6	9.6	-0.6	3.1	-5	17
	40	0.3	3.9	0	16	-0.1	3.1	-1	20
	45	0.6	3.5	1	12	0.3	3.1	-1	17
	50	0.6	4.8	1	15	0.0	3.8	-1	20
With Swirl Brakes	10	-0.3	3.2	9	51	-0.2	2.7	14	67
	15	0.0	2.2	6	23	0.5	1.7	6	30
	20	-1.3	2.3	2	18	0.1	2.2	12	25
	25	-0.8	2.4	-1	15	0.3	2.5	4	22
	30	-1.6	2.6	-1	14	0.1	3.1	8	21
	35	-0.9	3.6	-2	16	1.0	2.1	2	19
	40	-2.0	3.3	-1	13	-0.8	2.3	6	16
	45	-2.3	3.6	-3	13	-1.6	4.3	6	20
	50	-0.4	5.1	2	16	-1.0	3.0	4	19

Table E. 9. *k*, *C*, *K*, and *Ceff* for cavity (2) at 3.79 bar inlet pressure and 0.5 pressure ratio.

Configuration	Precession Frequency	k	±	C	±	K	±	Ceff	±
	(Hz)	(kN/m)	(kN/m)	(Ns/m)	(Ns/m)	(kN/m)	(kN/m)	(Ns/m)	(Ns/m)
Without Swirl Brakes	10	-4.1	3.9	-53	62	-1.9	3.2	13	80
	15	-3.8	2.8	15	30	-8.1	2.9	55	43
	20	-3.6	2.4	-37	19	-5.9	3.0	-9	30
	25	-4.4	3.1	1	20	-7.8	2.3	29	25
	30	-3.2	3.3	-2	17	-7.5	2.6	15	22
	35	-6.0	2.8	-7	13	-5.5	2.9	21	18
	40	-4.0	2.3	1.0	9.2	-7.8	3.0	17	15
	45	-6.2	3.3	1	12	-8.7	2.9	23	16
	50	-4.9	3.1	-13	10	-10.1	3.1	3	14
With Swirl Brakes	10	-9.4	7.1	-14	110	-4.7	3.4	140	130
	15	-10.6	5.1	-8	54	-10.2	4.8	110	74
	20	-13.2	2.1	2	17	-11.5	2.9	110	28
	25	-8.8	2.4	-19	15	-11.8	2.0	37	20
	30	-8.2	2.3	5	12	-12.7	1.9	48	16
	35	-5.2	3.4	-15	15	-12.1	2.4	9	19
	40	-5.8	3.6	-9	14	-8.7	4.8	15	24
	45	-4.4	3.9	-11	14	-13.2	3.1	5	18
	50	-0.7	4.3	-15	14	-15.8	4.9	-13	21

Table E. 10. *k*, *C*, *K*, and *Ceff* for cavity (2) at 3.79 bar inlet pressure and 0.6 pressure ratio.

Configuration	Precession Frequency	k	±	C	±	K	±	Ceff	±
	(Hz)	(kN/m)	(kN/m)	(Ns/m)	(Ns/m)	(kN/m)	(kN/m)	(Ns/m)	(Ns/m)
Without Swirl Brakes	10	-4.0	2.1	9	33	-8.3	2.3	74	49
	15	-4.9	2.6	-4	27	-10.5	2.2	49	36
	20	-3.4	2.7	9	21	-9.8	2.1	37	27
	25	-4.1	1.9	-7	12	-8.9	1.8	19	16
	30	-4.5	1.5	-5.4	8.2	-10.0	1.8	18	13
	35	-3.2	2.1	-1.8	9.4	-10.5	1.9	13	13
	40	-4.7	2.3	-0.5	9.0	-11.9	1.9	18	12
	45	-3.2	2.5	4.8	9.0	-13.6	2.8	16	13
	50	-1.6	3.2	1	10	-13.2	2.1	6	12
With Swirl Brakes	10	-1.4	3.7	-2	58	-9.0	2.1	21	67
	15	-8.6	2.1	23	22	-11.0	2.7	114	36
	20	-8.0	3.1	10	25	-14.2	2.7	73	33
	25	-6.9	3.0	5	19	-14.8	2.9	49	27
	30	-4.2	2.2	3	12	-13.9	2.5	25	18
	35	-3.0	3.0	2	13	-12.7	4.2	15	23
	40	-3.4	4.8	14	19	-14.6	4.2	28	25
	45	-5.1	4.3	5	15	-14.5	5.1	24	24
	50	-2.5	6.3	7	20	-15.4	3.7	14	23

Table E. 11. *k*, *C*, *K*, and *Ceff* for cavity (2) at 3.79 bar inlet pressure and 0.7 pressure ratio.

Configuration	Precession Frequency	k	±	C	±	K	±	Ceff	±
	(Hz)	(kN/m)	(kN/m)	(Ns/m)	(Ns/m)	(kN/m)	(kN/m)	(Ns/m)	(Ns/m)
Without Swirl Brakes	10	-5.3	4.5	10	72	-14.1	1.6	94	76
	15	-6.1	1.9	-10	20	-10.2	1.6	55	26
	20	-3.3	2.4	-15	19	-11.1	1.9	12	25
	25	-5.4	2.2	-6	14	-12.1	1.9	28	19
	30	-4.2	1.7	-1.0	9.0	-14.6	1.8	21	13
	35	-3.9	1.2	3.6	5.5	-13.7	1.5	21.4	8.9
	40	-2.0	2.0	6.2	7.8	-14.2	1.7	14	10
	45	-1.0	2.4	0.6	8.6	-14.9	2.4	4	12
	50	-1.6	2.0	9.9	6.3	-18.4	1.8	14.9	8.6
With Swirl Brakes	10	-6.9	3.8	1	60	-10.5	2.2	110	69
	15	-4.4	2.5	27	26	-14.0	2.0	74	34
	20	-5.1	3.0	17	24	-11.5	2.2	57	30
	25	-5.3	2.5	7	16	-14.7	2.5	40	22
	30	-4.9	2.8	6	15	-13.6	3.0	32	22
	35	-2.8	2.7	9	12	-14.4	2.7	21	17
	40	-0.1	2.8	7	11	-14.8	2.9	7	16
	45	-3.1	1.8	4.6	6.2	-17.0	2.8	16	12
	50	-4.2	5.9	1	19	-17.5	2.6	14	20

Table E. 12. *k*, *C*, *K*, and *Ceff* for cavity (2) at 3.79 bar inlet pressure and 0.8 pressure ratio.

Configuration	Precession Frequency	k	±	C	±	K	±	Ceff	±
	(Hz)	(kN/m)	(kN/m)	(Ns/m)	(Ns/m)	(kN/m)	(kN/m)	(Ns/m)	(Ns/m)
Without Swirl Brakes	10	-4.9	2.3	24	37	-10.4	1.6	102	45
	15	-3.6	1.8	9	19	-10.0	1.4	48	24
	20	-2.1	1.6	4	13	-10.7	1.4	21	17
	25	-2.3	1.7	4	11	-10.3	1.4	18	14
	30	-1.8	2.0	7	10	-11.7	1.3	17	12
	35	-0.2	1.4	-3.9	6.2	-10.4	1.3	-3.0	8.6
	40	-1.0	2.1	7.3	8.5	-12.5	2.1	11	12
	45	-1.4	3.1	10	11	-12.3	2.1	15	13
	50	-0.6	2.6	4.6	8.3	-13.1	2.9	6	12
With Swirl Brakes	10	-5.9	4.0	-6	63	-13.9	2.7	88	76
	15	-7.0	1.8	9	20	-13.8	2.2	83	30
	20	-4.6	1.7	3	14	-14.9	2.2	39	22
	25	-4.1	2.0	14	13	-12.5	1.9	40	18
	30	-3.9	2.0	5	10	-15.3	2.5	26	17
	35	-3.4	1.8	-1.0	8.1	-16.4	1.8	15	11
	40	-2.1	2.1	8.2	8.2	-14.5	2.0	17	11
	45	-0.6	2.7	-1.2	9.4	-17.1	3.2	1	15
	50	-1.7	3.1	-1.2	9.9	-18.0	3.1	4	14

Table E. 13. *k*, *C*, *K*, and *Ceff* for cavity (3) at 3.79 bar inlet pressure and 0.5 pressure ratio.

Configuration	Precession Frequency	k	±	C	±	K	±	Ceff	±
	(Hz)	(kN/m)	(kN/m)	(Ns/m)	(Ns/m)	(kN/m)	(kN/m)	(Ns/m)	(Ns/m)
Without Swirl Brakes	10	7.4	1.2	24	19	7.2	1.0	-94	25
	15	7.7	1.4	7	15	7.0	1.1	-75	19
	20	9.1	1.2	12.6	9.4	7.2	1.2	-60	13
	25	8.1	1.7	7	11	7.3	0.9	-45	13
	30	7.7	2.1	13	11	6.9	0.9	-27	12
	35	7.4	1.3	9.9	5.8	8.5	1.2	-23.6	8.0
	40	7.8	2.3	8.0	9.0	8.0	1.5	-23	11
	45	8.6	1.7	10.3	6.2	8.1	1.4	-20.0	8.0
	50	7.0	2.2	10.8	6.9	8.5	2.0	-11.5	9.3
With Swirl Brakes	10	5.7	3.4	2	54	8.3	1.8	-88	61
	15	5.7	1.3	9	14	6.7	4.4	-52	49
	20	6.9	2.7	6	22	7.1	1.3	-49	24
	25	7.4	4.1	16	26	8.2	2.1	-31	30
	30	7.8	1.9	15	10	8.1	2.0	-27	15
	35	7.9	2.6	11	12	6.8	1.9	-25	15
	40	7.3	1.3	21.1	5.2	7.5	1.6	-8.0	8.1
	45	7.6	2.0	19.1	6.9	7.7	2.2	-8	10
	50	6.6	2.8	13.1	8.9	6.7	2.0	-8	11

Table E. 14. *k*, *C*, *K*, and *Ceff* for cavity (3) at 3.79 bar inlet pressure and 0.6 pressure ratio.

Configuration	Precession Frequency	k	±	C	±	K	±	Ceff	±
	(Hz)	(kN/m)	(kN/m)	(Ns/m)	(Ns/m)	(kN/m)	(kN/m)	(Ns/m)	(Ns/m)
Without Swirl Brakes	10	10.3	1.8	18	29	7.7	2.2	-146	46
	15	10.1	2.1	6	23	7.6	1.8	-102	29
	20	11.6	1.9	19	15	7.9	1.9	-73	22
	25	11.4	1.2	11.9	7.9	8.6	1.6	-61	13
	30	11.3	1.9	17	10	8.2	2.0	-43	14
	35	10.6	1.8	13.9	8.1	8.9	1.5	-34	11
	40	10.0	2.2	15.1	8.8	9.0	1.6	-24	11
	45	10.4	1.4	16.2	5.0	9.8	1.7	-20.4	7.8
	50	10.5	2.3	15.5	7.3	8.2	2.0	-18	10
With Swirl Brakes	10	9.2	2.8	19	44	9.9	3.4	-130	70
	15	6.9	4.5	27	48	11.1	2.6	-46	55
	20	7.6	3.8	13	30	10.1	2.0	-48	34
	25	8.3	2.5	16	16	8.9	3.0	-37	25
	30	8.5	2.6	18	14	10.4	2.5	-27	19
	35	8.5	2.7	20	12	10.4	2.0	-19	15
	40	8.5	2.3	23.0	9.3	10.9	2.4	-11	13
	45	7.6	1.9	25.0	6.6	9.9	1.9	-1.9	9.5
	50	9.2	2.9	28.7	9.1	9.3	3.4	0	14

Table E. 15. *k*, *C*, *K*, and *Ceff* for cavity (3) at 3.79 bar inlet pressure and 0.7 pressure ratio.

Configuration	Precession Frequency	k	±	C	±	K	±	Ceff	±
	(Hz)	(kN/m)	(kN/m)	(Ns/m)	(Ns/m)	(kN/m)	(kN/m)	(Ns/m)	(Ns/m)
Without Swirl Brakes	10	10.2	1.6	11	26	7.9	1.1	-151	31
	15	9.5	1.5	8	16	8.6	1.4	-93	22
	20	10.6	1.8	8	15	8.9	1.7	-76	20
	25	9.8	2.5	9	16	8.8	1.6	-53	19
	30	9.7	1.3	11.4	6.7	7.8	1.4	-40	10
	35	8.7	1.3	14.2	5.8	8.9	1.4	-25.2	8.6
	40	10.8	1.5	16.0	6.0	9.4	1.5	-26.9	8.4
	45	10.8	2.4	13.3	8.5	9.9	1.6	-25	10
	50	9.6	1.6	16.6	5.0	9.3	1.7	-14.0	7.4
With Swirl Brakes	10	6.24	0.69	21	11	8.9	1.5	-78	26
	15	8.3	1.2	25	13	9.4	1.1	-63	18
	20	7.9	1.9	25	15	10.2	2.3	-38	24
	25	8.3	2.6	22	16	9.2	2.2	-31	22
	30	8.0	4.0	14	21	9.2	1.9	-28	24
	35	8.7	7.2	25	33	9.2	2.0	-14	34
	40	10.2	1.8	16.5	7.1	8.1	1.9	-24	10
	45	8.8	2.8	19	10	7.5	2.4	-12	13
	50	7.8	2.3	22.5	7.4	7.3	2.7	-2	11

Table E. 16. *k*, *C*, *K*, and *Ceff* for cavity (3) at 3.79 bar inlet pressure and 0.8 pressure ratio.

Configuration	Precession Frequency	k	±	C	±	K	±	Ceff	±
	(Hz)	(kN/m)	(kN/m)	(Ns/m)	(Ns/m)	(kN/m)	(kN/m)	(Ns/m)	(Ns/m)
Without Swirl Brakes	10	7.4	1.2	24	19	7.2	1.0	-94	25
	15	7.7	1.4	7	15	7.0	1.1	-75	19
	20	9.1	1.2	12.6	9.4	7.2	1.2	-60	13
	25	8.1	1.7	7	11	7.27	0.92	-45	13
	30	7.7	2.1	13	11	6.94	0.92	-27	12
	35	7.4	1.3	9.9	5.8	8.5	1.2	-23.6	8.0
	40	7.8	2.3	8.0	9.0	8.0	1.5	-23	11
	45	8.6	1.7	10.3	6.2	8.1	1.4	-20.0	8.0
	50	7.0	2.2	10.8	6.9	8.5	2.0	-11.5	9.3
With Swirl Brakes	10	5.7	3.4	2	54	8.3	1.8	-88	61
	15	5.7	1.3	9	14	6.7	4.4	-52	49
	20	6.9	2.7	6	22	7.1	1.3	-49	24
	25	7.4	4.1	16	26	8.2	2.1	-31	30
	30	7.8	1.9	15	10	8.1	2.0	-27	15
	35	7.9	2.6	11	12	6.8	1.9	-25	15
	40	7.3	1.3	21.1	5.2	7.5	1.6	-8.0	8.1
	45	7.6	2.0	19.1	6.9	7.7	2.2	-8	10
	50	6.6	2.8	13.1	8.9	6.7	2.0	-8	11

Table E. 17. *k*, *C*, *K*, and *Ceff* for cavity (4) at 3.79 bar inlet pressure and 0.5 pressure ratio.

Configuration	Precession Frequency	k	±	C	±	K	±	Ceff	±
	(Hz)	(kN/m)	(kN/m)	(Ns/m)	(Ns/m)	(kN/m)	(kN/m)	(Ns/m)	(Ns/m)
Without Swirl Brakes	10	-16.0	2.8	-76	44	5.8	3.3	180	68
	15	-17.8	1.8	-39	20	-3.6	1.9	150	28
	20	-18.5	2.9	-15	23	-5.6	4.9	130	45
	25	-17.6	2.5	-37	16	-2.0	2.2	75	21
	30	-20.8	3.6	-48	19	-4.3	2.9	62	24
	35	-14.1	3.2	-40	15	-7.2	2.6	24	19
	40	-15.3	2.2	-44.6	8.8	-7.3	1.7	16	11
	45	-15.9	3.4	-53	12	-8.9	2.5	3	15
	50	-17.5	2.3	-34.3	7.2	-9.4	2.7	22	11
With Swirl Brakes	10	-17.0	2.2	-34	36	-1.8	2.7	240	56
	15	-18.6	3.0	-50	32	-7.4	3.0	150	45
	20	-16.5	2.7	-51	21	-4.6	2.2	80	27
	25	-13.7	2.1	-22	13	-7.4	2.3	65	20
	30	-14.6	2.1	-41	11	-12.7	2.6	36	18
	35	-14.4	2.3	-34	11	-5.5	2.8	31	16
	40	-15.9	2.7	-40	11	-11.3	2.5	23	15
	45	-11.3	2.9	-37	10	-9.5	2.0	2	12
	50	-15.5	2.4	-46.0	7.7	-11.9	2.0	3	10

Table E. 18. *k*, *C*, *K*, and *Ceff* for cavity (4) at 3.79 bar inlet pressure and 0.6 pressure ratio.

Configuration	Precession Frequency	k	±	C	±	K	±	Ceff	±
	(Hz)	(kN/m)	(kN/m)	(Ns/m)	(Ns/m)	(kN/m)	(kN/m)	(Ns/m)	(Ns/m)
Without Swirl Brakes	10	-13.5	1.5	-31	24	-15.4	1.3	180	32
	15	-13.5	1.6	7	18	-16.0	1.6	150	24
	20	-15.1	1.6	-9	13	-14.5	1.2	110	16
	25	-14.3	1.4	3.7	9.2	-16.9	1.2	95	12
	30	-11.2	1.3	-7.7	7.1	-16.6	1.3	52	10
	35	-13.0	1.4	-11.7	6.4	-16.7	1.4	47.5	9.1
	40	-12.4	1.4	-8.7	5.4	-16.6	1.6	40.6	8.3
	45	-12.6	1.9	-18.9	6.6	-18.1	1.6	25.6	8.8
	50	-11.2	1.5	-17.6	4.7	-20.0	1.7	18.0	7.2
With Swirl Brakes	10	-13.9	1.6	-47	26	-5.9	1.6	170	37
	15	-14.4	1.6	-23	17	-10.4	1.9	130	27
	20	-13.4	1.5	-39	12	-7.9	1.9	68	19
	25	-15.0	2.6	-42	17	-7.0	2.2	53	22
	30	-12.7	3.0	-28	16	-8.3	2.2	39	20
	35	-14.8	2.2	-37.3	9.9	-14.2	2.7	30	16
	40	-15.6	3.5	-31	14	-14.0	3.3	31	19
	45	-10.6	2.8	-26.5	9.8	-16.9	3.3	11	15
	50	-13.7	3.5	-37	11	-12.2	2.0	6	13

Table E. 19. *k*, *C*, *K*, and *Ceff* for cavity (4) at 3.79 bar inlet pressure and 0.7 pressure ratio.

Configuration	Precession Frequency	k	±	C	±	K	±	Ceff	±
	(Hz)	(kN/m)	(kN/m)	(Ns/m)	(Ns/m)	(kN/m)	(kN/m)	(Ns/m)	(Ns/m)
Without Swirl Brakes	10	-14.37	0.80	10	13	-22.3	1.0	239	20
	15	-13.6	1.4	-6	15	-21.1	1.5	138	22
	20	-11.9	1.2	5	10	-22.2	1.4	100	15
	25	-10.7	1.3	0.3	8.5	-24.9	1.1	69	11
	30	-12.5	1.0	-5.9	5.5	-20.9	1.5	61	10
	35	-9.2	1.3	6.4	5.8	-23.6	1.6	48.3	9.1
	40	-11.5	1.2	6.8	4.8	-26.6	1.5	52.5	7.6
	45	-13.7	1.5	6.7	5.4	-25.0	1.7	55.2	8.1
	50	-10.7	1.4	-7.9	4.4	-25.8	1.8	26.0	7.2
With Swirl Brakes	10	-14.8	2.3	-47	36	-12.1	2.3	190	51
	15	-20.5	1.6	-22	17	-11.7	2.1	200	28
	20	-19.5	3.0	-20	24	-12.2	2.5	140	31
	25	-15.9	3.8	-23	25	-12.4	1.5	78	26
	30	-16.9	2.7	-6	14	-16.4	2.0	84	18
	35	-16.1	2.6	-12	12	-14.1	2.1	61	15
	40	-15.7	2.9	-25	12	-17.2	2.0	38	14
	45	-15.4	3.1	-18	11	-20.7	2.9	36	15
	50	-14.9	3.0	-29	10	-14.0	2.5	18	13

Table E. 20. *k*, *C*, *K*, and *Ceff* for cavity (4) at 3.79 bar inlet pressure and 0.8 pressure ratio.

Configuration	Precession Frequency	k	±	C	±	K	±	Ceff	±
	(Hz)	(kN/m)	(kN/m)	(Ns/m)	(Ns/m)	(kN/m)	(kN/m)	(Ns/m)	(Ns/m)
Without Swirl Brakes	10	-11.96	0.96	15	15	-25.45	0.89	210	21
	15	-11.53	0.82	-26.1	8.7	-23.2	1.1	96	15
	20	-11.88	0.82	-6.5	6.5	-23.7	1.0	88	10
	25	-11.10	0.65	9.8	4.1	-24.7	1.1	80.5	7.9
	30	-10.33	0.85	-2.2	4.5	-23.9	1.0	52.5	6.9
	35	-11.2	1.2	17.5	5.7	-26.0	1.1	68.5	7.5
	40	-9.27	0.88	7.2	3.5	-25.8	1.0	44.1	5.4
	45	-8.47	0.87	8.4	3.1	-24.7	1.5	38.3	6.1
	50	-10.6	1.1	9.4	3.5	-25.7	1.3	43.3	5.3
With Swirl Brakes	10	-18.3	1.2	18	19	-17.8	1.6	310	31
	15	-15.4	1.4	15	15	-17.9	1.4	180	21
	20	-16.9	1.2	-8.7	9.4	-15.7	1.5	130	15
	25	-16.4	1.6	-21	10	-17.1	1.4	84	14
	30	-15.9	1.6	5.2	8.4	-20.8	1.5	89	12
	35	-16.8	1.4	-13.3	6.3	-21.5	1.5	63.2	9.2
	40	-12.10	0.94	-15.5	3.7	-20.3	1.8	32.7	7.9
	45	-11.8	1.7	-15.0	6.0	-22.3	1.5	26.7	8.1
	50	-13.0	1.9	-6.4	6.1	-20.8	1.8	34.8	8.2